APPLICATIONS OF GOLD NANOMATERIALS FOR DETERMINATION OF PARATHYROID HORMONE, HYDROGEN PEROXIDE AND IODATE

AURACHAT LERT-ITTHIPORN

A THESIS SUBMITTED IN PARTIAL FULFILLMENT OF THE REQUIREMENT FOR
THE DEGREE OF DOCTOR OF PHILOSOPHY IN APPLIED CHEMISTRY
DEPARTMENT OF CHEMISTRY
FACULTY OF SCIENCE
KING MONGKUT'S INSTITUTE OF TECHNOLOGY LADKRABANG
2020

KMITL-2020-SC-D-010-050

APPLICATIONS OF GOLD NANOMATERIALS FOR DETERMINATION OF PARATHYROID HORMONE, HYDROGEN PEROXIDE AND IODATE

AURACHAT LERT-ITTHIPORN

A THESIS SUBMITTED IN PARTIAL FULFILLMENT OF THE REQUIREMENT FOR
THE DEGREE OF DOCTOR OF PHILOSOPHY IN APPLIED CHEMISTRY
DEPARTMENT OF CHEMISTRY
FACULTY OF SCIENCE
KING MONGKUT'S INSTITUTE OF TECHNOLOGY LADKRABANG
2020
KMITL-2020-SC-D-010-050

Thesis Title	Applications of gold nanomaterials for determination of parathyroid hormone, hydrogen peroxide and iodate
Student Name	Miss Aurachat Lert-itthiporn
Student ID	57605007
Degree	Doctor of Philosophy (Applied Chemistry)
Department	Chemistry
Year	2020
Thesis Advisor	Asst. Prof. Dr. Nathawut Choengchan

Abstract

This research work presents syntheses and characterizations of gold nanoparticles (AuNPs) and gold nanoclusters (AuNCs) for clinical diagnosis of hyperparathyroidism and for determination of hydrogen peroxide (H_2O_2) and iodate, respectively. For the first project, the AuNPs were prepared by the conventional Turkevich method and the as-prepared colloidal gold solution was applied for the determination of parathyroid hormone (PTH) in blood (biomarker for hyperparathyroidism). Detection principle is based on the reaction between PTH and the AuNPs, which results in aggregation of the nanoparticles and color changes from red wine to blue. This causes decreasing in the absorbances (521 nm) proportionally to the PTH concentrations. The as-prepared AuNPs were spherical (size: 25 nm) and monodispersed. Linearity range of standard PTH in concentrations of 10 - 1,000 pg/mL was obtained with good linearity (r^2 > 0.99). The method provided high precision (RSD: 2.05 % (10 pg/mL) and 2.52 % (100 pg/mL)) with high accuracy (Recovery: 98.36 – 104.94 %). Limit of detection ($y_B + 3S_B$) of 1.70 pg/mL was observed.

For the second project, the AuNPs was synthesized using bacterial cellulose nanopaper (BC) as both a reducing agent and a scaffold for the as-prepared AuNPs. The preparation process was started by putting the wet bare BC nanopaper (∅ 30 mm and 3 mm thickness) into 0.75 mmol L^{-1} $HAuCl_4$ (25.0 mL). This solution was vigorously and continuously stirred for 60 min at 90 °C. After the embedding process, color of the nanopaper was changed from milky-white to wine-red. The AuNPs-BC nanopaper was characterized by UV-visible spectrophotometer, FE-SEM and EDS. Absorption spectrum of the nanopaper showed the characteristic peak of Au^0 at 525 nm. The amount of 97.3 weight % of Au^0 was found. The spectrophotometric assay was carried out by dropping the aliquots of 100 µL of sample and 400 µL of 20 mmol L^{-1} citrate buffer (pH 6.0) onto the AuNPs-BC nanopaper. The nanopaper was

then kept in a plastic bag for 10 min. In the presence of H_2O_2, the wine-red color of the AuNPs-BC nanopaper was turned to pale red accordingly to oxidation of Au° to Au (III) by H_2O_2. Decreasing in the absorbance of the nanopaper at 525 nm was monitored using UV-visible spectrophotometer. Detection limit ($y_B + 3S_B$) of 0.79 % (v/v) was observed and this value was enough sensitive for the determination of H_2O_2 in wound cleaner and hair dye samples. The H_2O_2 contents in all samples were agreed well with the label values. Good analytical recovery (88.8 to 97.2 %) with high precision (RSD: 3.3 %) was obtained. These results confirmed that the as-prepared nanopaper was successfully synthesized and effectively applied as the two dimensional (2D)-microcuvette for the spectrophotometric determination of H_2O_2 in real samples.

For the last project, a new design of a paper-based analytical device (PAD) for membraneless gas-separation with subsequent determination of iodate is presented. The rectangular PAD was invented as the folded pattern, where two circular reservoirs: the donor reservoir and the acceptor reservoir were situated in a single paper for convenient use. The hydrophobic barrier of each reservoir was easily fabricated by painting with a permanent marker. The PAD was demonstrated for the quantitative analysis of iodate, based on the fluorescence quenching of the bovine serum albumin-stabilized gold nanoclusters (BSA-AuNCs). The BSA-AuNCs were fast prepared by a microwave-assisted approach. The nanoclusters solution was applied into the acceptor reservoir, while the sample, iodide and sulfuric acid were sequentially aliquoted into the donor reservoir. After folding the PAD, the donor and the acceptor were mounted together *via* a two-sided mounting tape. The headspace in between the two reservoirs allows membraneless gas-separation of free iodine from the donor to diffuse into the acceptor. Etching of gold core of the nanoclusters in the acceptor resulted in quenching of the red emission, was monitored by two methods, i.e. "fluorometric detection" (λ_{ex}: 490 nm, λ_{em}: 630 nm) and "image capture" of the acceptor under the UV irradiation by a smart phone's camera. Two calibrations were plotted accordingly to their detections and linear calibrations with good linearities ($r^2 > 0.98$) were observed from 0.005 to 0.1 mmol L^{-1} iodate. High accuracy (mean recovery: 95.1 ($\pm$ 4.6) %) and high precision (RSD < 3 %) was obtained. The lower limits of detection were 0.005 mmol L^{-1} (with fluorometric detection) and 0.01 mmol L^{-1} (with image capture). The method was effectively applied for the measurement of iodate in iodized salts and fish sauces without prior sample pre-treatment.

Keywords: Parathyroid hormone, Hydrogen peroxide, Iodate, Gold nanoparticles, Gold nanoclusters, Bacterial cellulose nanopaper, Paper based analytical device.

Acknowledgments

I would like to acknowledge all the thesis committees, Asst. Prof. Dr. Wiboon Praditweangkum, Asst. Prof. Dr. Nuanlaor Ratanawimarnwong, Assoc. Prof. Dr. Ekarat Detsri and Assoc. Prof. Dr. Saowapak Teerasong for their useful comments and suggestions which help improvement of thesis.

I would like to acknowledge Scientific Instrument Centre, KMITL for providing SEM and UV–Visible spectrometer for characterization of embedded gold nanoparticles bacterial cellulose nanopaper.

I also would like to acknowledge Mr. Pongpichet Srikritsadawong, Department of Chemistry, Faculty of Science, KMITL, for his kindness on validating of the method for the iodate determination.

Financial and Instrumental supports from Department of Chemistry, Faculty of Science, King Mongkut's Institute of Technology Ladkrabang (KMITL) and FIRST Lab @ KMITL as well as Applied Analytical Chemistry Research Unit are acknowledged.

Finally I would like to sincere acknowledge Asst. Prof. Dr. Nathawut Choengchan, my advisor, for all his supports of my work. I also appreciate all contributions from my colleagues.

Miss Aurachat Lert-itthiporn

Contents

List of Tables

List of Figures

Abbreviations / Symbols

AuNPs	Gold nanoparticles
AuNCs	Gold nanoclusters
PTH	Parathyroid hormone
BC	Bacterial cellulose nanopaper
H_2O_2	Hydrogen peroxide
KIO_3	Potassium iodate
KI	Potassium iodide
I_2	Iodine
PAD	Paper-based analytical device
SPR	Surface plasmon resonance
ng	Nanogram
mg	milligram

Chapter 1
Introduction

1.1 Research motivation

In recent years, nanomaterials have been many attractive for use as chemical sensors, biosensors and also clinical sensors due to their unique optical properties and their stability. Nano gold is the particles that are synthesized from gold salt to be smaller in the nanometer level. Nano-level of gold particles have different physical and chemical properties than normal gold, such as having a high surface area, speed up chemical reactions, good conductivity. The color and properties of nano gold can be changed according to particle size, shape and structure.

Nowadays, bio-material paper - based sensors have been widely using as analytical devices in many applications due to its simplicity, low cost, easy to use, biocompatibility and degradability. For optical sensing platform, bacterial cellulose (BC) nanopaper has attractive because of optical transparency, hydrophilicity, high porosity and high surface area.

Therefore, in this work, we aim to synthesis and use gold nanoparticle (AuNPs) to apply for clinical diagnosis of hyperparathyroidism, synthesis and embedded of AuNPs on nanopaper for quality control of hydrogen peroxide. And we also aim to synthesis gold nanoclusters (AuNCs) and apply for quality control of iodized table salts. All the researches in this work are summarized in the following issues:

1.1.1 Clinical diagnosis of hyperparathyroidism

Parathyroid hormone (PTH) is a hormone containing 84 amino acids that secreted from parathyroid glands and functioned with calcitonin hormone to regulate blood calcium levels. The amount of PTH for normal people is 10 - 65 pg mL^{-1}. Abnormal level of PTH can be separated into 2 types as 'hypoparathyroidism' and 'hyperparathyroidism'. Hypoparathyroidism occurs when insufficient PTH is produced resulting in low blood calcium. Hyperparathyroidism is caused by secretion of PTH is exorbitant occur with fragile bones and kidney stones. For patients which hyperparathyroidism they need to be parathyroid surgery.

Common analytical methods for monitoring the amount of blood PTH is chromatography which can determine within 20 min. Although this technique was rapid but it consumes a lot of solvent for use as carrier and complicated in operation of instruments.

This work, the simple immunoassay method for the PTH determination based on aggregation of antibody conjugated AuNPs in the presence of PTH was developed. Color of the particles was changed from red wine to purple in direct proportional to the concentration of PTH, resulted in changing of surface plasmon band measured by using uv – vis spectrophotometer.

1.1.2 Quality control of hydrogen peroxide

Hydrogen peroxide usually used as bleaching agent, and antiseptic. For antiseptic property, is a mild disinfectant that applied to local wound which may cause danger from cytotoxic effect. Over doses of hydrogen peroxide (more than 3%) can cause irritation, blistering, vomiting and several deaths. Therefore, this substance should only be used if necessary. Although there have applications about hydrogen peroxide but these method needs to use enzyme which suffered from its stability.

Bacterial cellulose nanopaper (BC) is a multipurpose material that has many features such as biocompatibility, biodegradability, optical transparency, heat resistance, high porosity, which is attractive for optical determination. Plasmonic or photoluminescent properties of embedded nanoparticles on BC can be utilized for many optical measurement applications.

In this research, the AuNPs embedded BC nanopaper for hydrogen peroxide determination was synthesized and applied. Detection reaction is based on bleaching of AuNPs by hydrogen peroxide and resulted in decreasing of absorbance which can be measured by using uv – vis spectrophotometer.

1.1.3 Quality control of iodized table salts

Iodine deficiency disorder (IDD) is a lack of iodine in human body resulting in increasing in size of thyroid gland and stunted of physical and mental growth. This situation still appears in many developing countries. For preventing IDD, adding iodine as KIO_3 in iodized table salt is performed. According to WHO, recommended minimum levels of iodine at consumption is 20 mg I per kg of salt.

Iodometric titration is a well-known method for the measurement of iodine content in edible salt. Although this method is very simple, it suffers from precision and accuracy. In addition, it consumes a lot of reagents volumes and time.

Nowadays, a paper-based analytical device (PAD) is widely used in many applications due to it allows liquid to pass through its hydrophilic fiber without any pump and consumes small amounts of samples and reagents. A PAD is easy to fabricate and low cost which makes it possible to use for portable test kit applications.

With attractive features of the membraneless gas-liquid separation PAD, in this work, a PAD for the iodate determination based on the redox reaction of tri-iodide and AuNCs was therefore developed. The intensity of AuNCs was decreased when tri-iodide was presence.

1.2 Objective of the study

1. To Synthesis of the AuNPs and to apply for the determination of PTH in blood.
2. To Synthesis of the AuNPs embedded BC and to apply for the quantitative analysis of hydrogen peroxide in wound cleaner samples.
3. To synthesis of the AuNCs and to fabricate a PAD for the detection of iodate.

1.3 Scopes of the study

1.3.1 Clinical diagnosis of hyperparathyroidism

Firstly, AuNPs was synthesized accordingly to Turkevich's method and the as-prepared AuNPs were characterized by UV–Visible spectrophotometer and transmission electron microscope (TEM). Secondly, AuNPs was conjugate with anti-PTH and then reacted with PTH. Next, effects of chemical and physical parameters affecting sensitivity of the method were investigated for the optimal condition. Then, the developed method was applied to determination of PTH in blood samples. Finally, analytical performances of this method were evaluated.

1.3.2 Quality control of hydrogen peroxide

Hydrogen peroxide can be detected by bleaching reaction of AuNPs. Firstly, BC nanopaper was-prepared by culturing of '*Acetobacter xylinum*' in Hestrin-Schramm culture medium. BC was then used as both a reducing agent and a substrate for synthesizing and embedding of AuNPs by using tetrachlorouric acid as a precursor. Optimization parameters for embedding of AuNPs were also studied. Next, the AuNPs embedded BC nanopaper was applied to determine hydrogen peroxide content in wound cleaner samples. Finally, analytical performances of this method were investigated.

1.3.3 Quality control of iodized table salts

The detection reaction of iodate is based on quenching effect of AuNCs by tri-iodide. The AuNCs were synthesized using bovine serum albumin (BSA) as reducing agent by exploiting microwave as a heating source. Optimal conditions

for AuNCs synthesis were also investigated. A foldable microfluidic paper-based analytical device (PAD) with circular hydrophobic barrier painting by permanent pen for acceptor and donor were assigned at left and right sides of the PAD, respectively. Generated tri-iodide from iodate and iodide in acidic medium was diffused from the donor side and further reacted with AuNCs on the acceptor side. Optimization parameters of using a PAD were studied. This method was then applied for the determination of iodate in iodized table salts. Then, results were validate against the iodometric titration.

1.4 Benefits of the study

1.4.1 A method for clinical diagnosis of hyperparathyroidism was achieved.

1.4.2 Embedding AuNPs on BC nanopaper was accomplished and applicable for hydrogen peroxide determination.

1.4.3 A PAD was successfully developed for the determination of iodate in eatable salts and fish sauces.

Chapter 2
Theory and Literature Reviews

2.1 Nanomaterials [1]

Nanotechnology is an interdisciplinary study that allows development of new materials with new, interesting and useful properties. These new materials are nanomaterials made from ultra-small particles. Nanomaterials can occur spontaneously and are caused by synthesis by modifying the arrangement of atoms or molecules. According to the European Commission, a nanomaterial is defined as a natural, incidental, or manufactured material containing particles, in an unbound state or as an aggregate or as an agglomerate and where, for 50% or more of the particles in the number size distribution, one or more external dimensions is in the size range 1–100 nm.

2.1.1 Gold nanoparticles [2-3]

Nanoparticles synthesized by the reduction of gold in aqueous phase tend to have quasi-sphere morphology as this shape presents the smallest surface area if compared to other morphologies. Typically, the suspension of spherical gold nanoparticles presents a ruby red color due to the scattering of light by the nanomaterial, but the increase in size, as well as a change in the environment surrounding the nanoparticles, may modify the optical properties of the colloid. Gold nanoparticles have physical and chemical properties that are different from normal gold, such as having a high ratio of surface area to volume and there helps to accelerate the reaction of electricity.

Optical properties of gold nanoparticles can be explained by the surface plasmon resonance (SPR). It is an optical phenomenon that is caused by the interaction of electromagnetic waves and electrons in nanoscale metals. When an electromagnetic wave from the outside hits the metal, the electron cloud that is restricted to nanoscale particles will collective oscillation and when the external electromagnetic waves have the same wavelengths that the electrons oscillate in the nanoparticles will cause resonance. The interaction between light and metal can occur in two ways: The light will hit and reflect with the same wavelength in every direction, which is called scattering. Some photons will be absorbed and transformed into oscillating energy, which is called absorption. It is a phenomenon that occurs at the junction of metal to dielectric substances, such as between gold particles and air or solutions. The wave size and amplitude of the resonant

spectrum of various materials depend on the size, shape, type of material and the environment around that material.

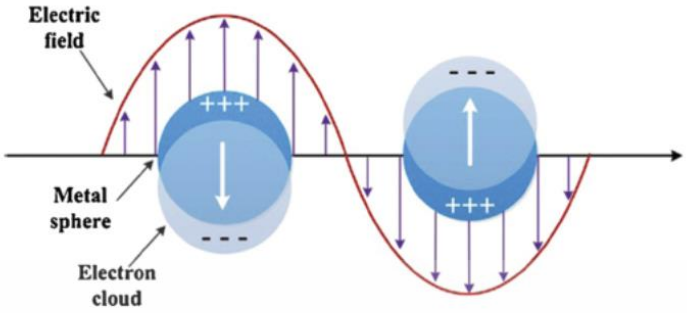

Figure 2.1 Illustration of the excitation of localized surface plasmon resonance. [3]

From the unique properties of gold nanoparticles, it can be used for a variety of uses especially applied in the field of chemical analysis.

2.1.2 Gold nanoclusters [4-5]

Gold nanoclusters (AuNCs) are a specific type of gold nanomaterials consisting of few to several Au atoms with ultra-small size (< 3 nm). In general, the solution of AuNCs is yellowish-brown and when exposed to UV light it occur red emission. AuNCs do not exhibit surface plasmon resonance (SPR) absorption in the visible region but have fluorescence in the visible to near-infrared (NIR) region.

Protein usually acts as a stabilizer and reducing agent to reduce gold solution to become AuNCs. Its stability depends on protein structure, temperature and optimal basic condition. There are many types of protein that used as stabilizer such as bovine serum albumin (BSA), lysosome, etc.

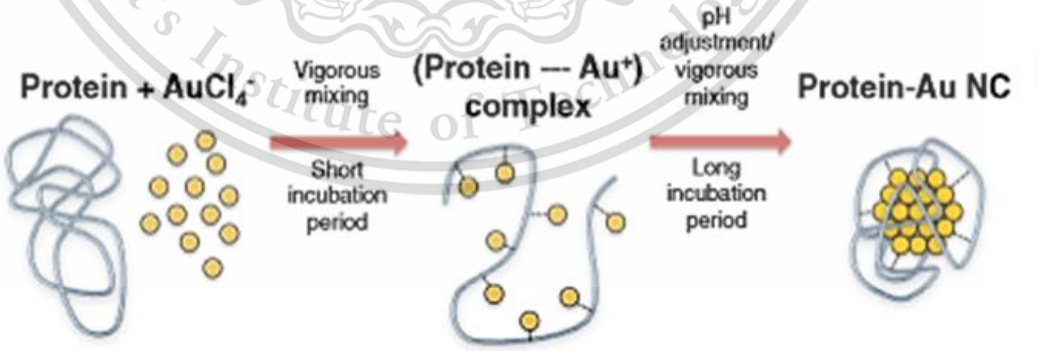

Figure 2.2 Synthesis of protein stabilized AuNCs. [5]

Characteristics of AuNPs and AuNCs are compared and shown in Table 2.1.

Table 2.1. Characteristics of AuNPs and AuNCs.

Charateristic	AuNPs	AuNCs
Size	5 – 50 nm	< 3 nm
SPR peak	✓	✘
Luminescent	✘	✓
Color	red	yellowish brown
Reducing agent	citrate	protein
Quencher ability	through fluorescence resonance energy transfer (FRET)	✘
Separate	centrifugation	dialysis, gel electrophoresis, HPLC

2.2 Theory and literature reviews for clinical diagnosis of hyperparathyroidism

2.2.1 Concepts and theories

2.2.1.1 Parathyroid hormone (PTH)

Parathyroid hormone (PTH) is a protein polymer made of 84 amino acids with a molecular weight 9500 Da.. It is a hormone secreted from 4 parathyroid glands that buried behind the thyroid glands [6]. The position of the parathyroid gland and the structure of the parathyroid hormone are shown in Figure 2.3 and 2.4 respectively.

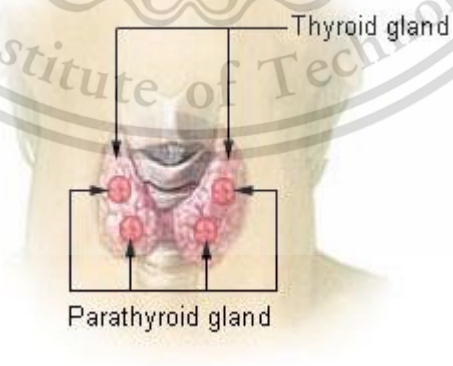

Figure 2.3 The position of the parathyroid gland **[7]**

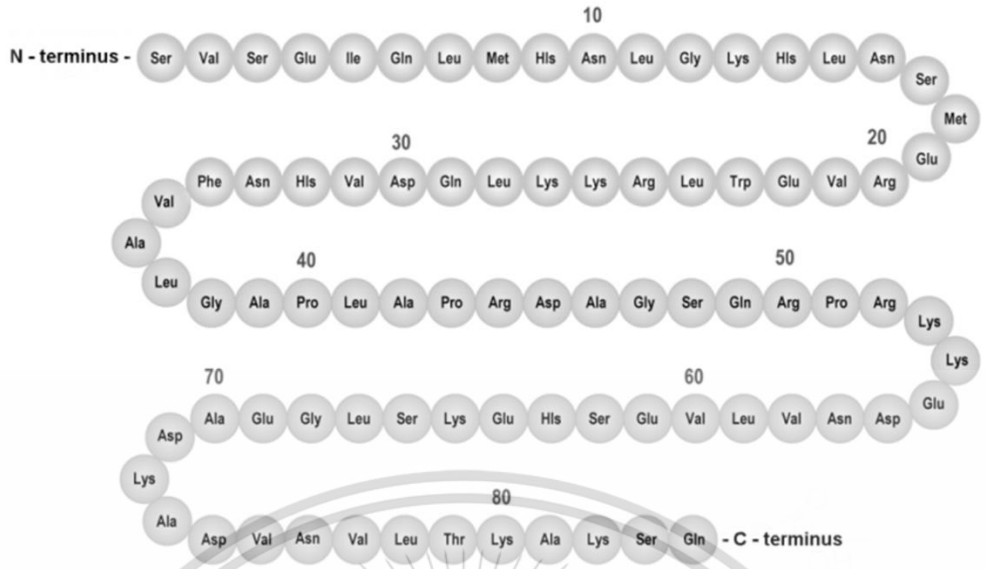

Figure 2.4 The structural formula of the parathyroid hormone. [8]

An important role of PTH is to maintain the balanced level of calcium in blood by working with calcitonin hormone which secreted from thyroid gland. In patients with goiter, the parathyroid gland may be obscured by the thyroid gland. The surgery of the thyroid gland to treat goiter must be careful not to cut the parathyroid gland because it can cause life threatening due to the lack of parathyroid hormones. The pathway of PTH was shown in Figure 2.5

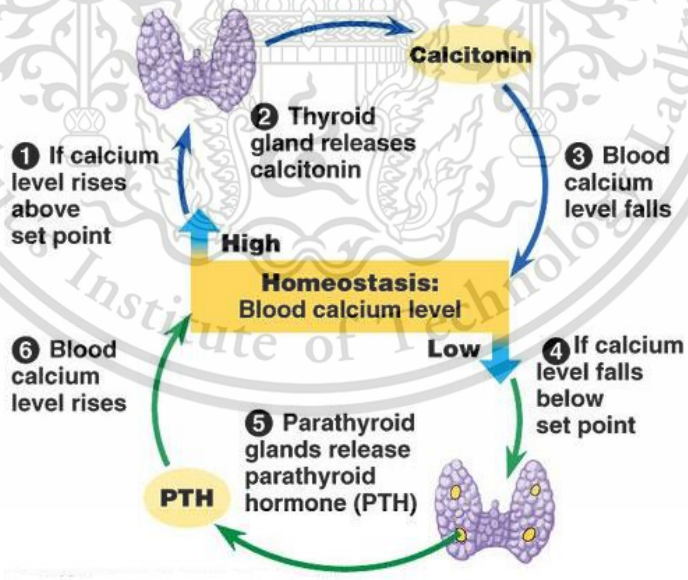

Figure 2.5 The PTH pathway. [9]

PTH disorders can be summarized as follows:

1. Hypoparathyroidism occurs when not enough PTH is produced and results in low blood calcium. The effect of low calcium levels causing tense muscles and

twitching. Hypoparathyroidism can treat by injecting calcium solution or PTH solution into blood vessels with providing vitamin D to increase the absorption of calcium from the intestines [10].

2. Hyperparathyroidism is caused by secretion of PTH is exorbitant occur with fragile bones and kidney stones. In addition, calcium will accumulate in various organs, including heart and spleen. Treatment of hypoparathyroidism is giving calcitonin hormone due to it is a hormone that causes blood calcium to drop rapidly [6].

2.2.1.2 Immunoassay

Immunological methods are the application of antigen-antibody interaction for diagnosis analytes in biological liquids such as serum or urine for medical and research purposes with details as follows: [12].

2.2.1.2.1 Antigen [13]

Antigen is a protein polymer. It is a foreign object that can specifically react to various products that are responded by the immune system. Antigens stimulate the production of antibodies that are specific to that antigen in which the antigen must have two characteristics, which are

1. Immunogenicity is the ability to stimulate the production of specific immune. Substances that stimulate a specific immune response are called immunogens.

2. Specific reactivity or antigenicity is the antigen that able to produce specific reactions to antibodies that are activated on the antigen. 1 molecule of antigen consists of small sub-locations that stimulate the body's immune system, called an antigenic determinant or epitope. Each antigen contains many different antigenic determinants.

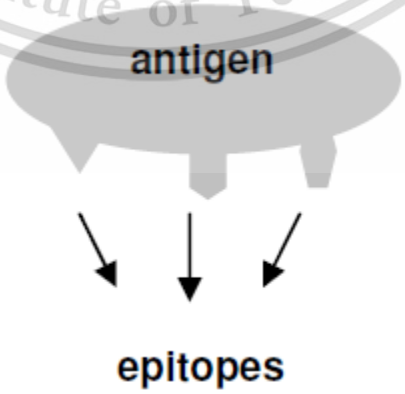

Figure 2.6 Image of an antigen and an epitope.

2.2.1.2.2 Antibody

Antibodies or immunoglobulin is a body immune protein. It is responsible for detecting and destroying foreign matters, such as bacteria and viruses with acting specifically on the target antigens.

The molecular structure of the antibody is in the Y shape. It consists of 4 polypeptide chains, 2 heavy chains and 2 light chains. The base of the Y shape of the antibody molecule called the constant region that indicates type of antibody such as IgG, IgA, IgM, IgD, IgE, etc. The tip of the Y is the position that binds to the antigen which has different varieties in each antibody. In this end it is called the variable region.

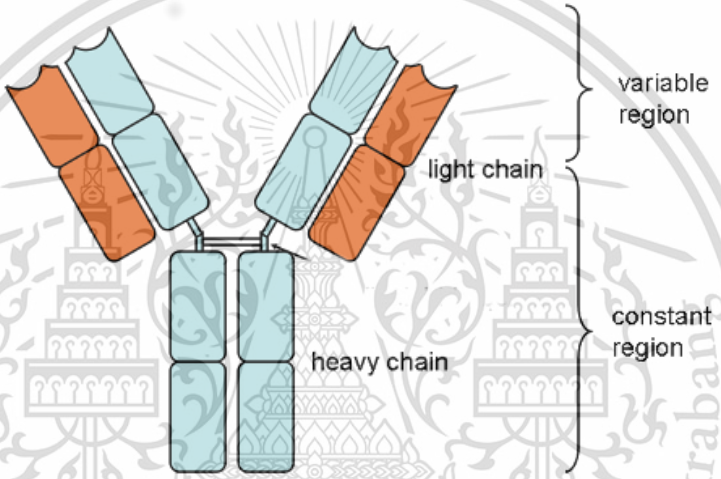

Figure 2.7 Visualize structures of antibodies.

2.2.1.2.3 Antigen and antibody reaction [14-15]

Antibodies have at least 2 combining sites that can attach to the antigen. Antigens have a position that can attach to the antibody in many ways or in many epitopes. When the antigens attack to body, it responds to antigens by creating immunity. Specific properties and ability of antibodies to bind to foreign antigens causing the antigens become ineffective. From this specific antigen-antibody reaction ability therefore, these properties can be used to diagnose various diseases.

The reaction between antigens and antibodies is caused by a non-covalent bond, which is a weak force. In which these forces are:

1. Electrostatic force (Coulombic force) is the force that occurs due to the different charges between antigens and antibodies.

2. Hydrogen bonding is the force that occurs between hydrophilic groups such as -OH, -NH_2, -COOH etc. This force depends greatly on the molecular intimacy.

3. Hydrophobic force is a force arising from the integration of non-polar substances by bringing the hydrophobic group together.

4. Van der Waals force is a force between molecules that are close to each other and then react between external electron clouds to give the attraction of the charge to a balanced state.

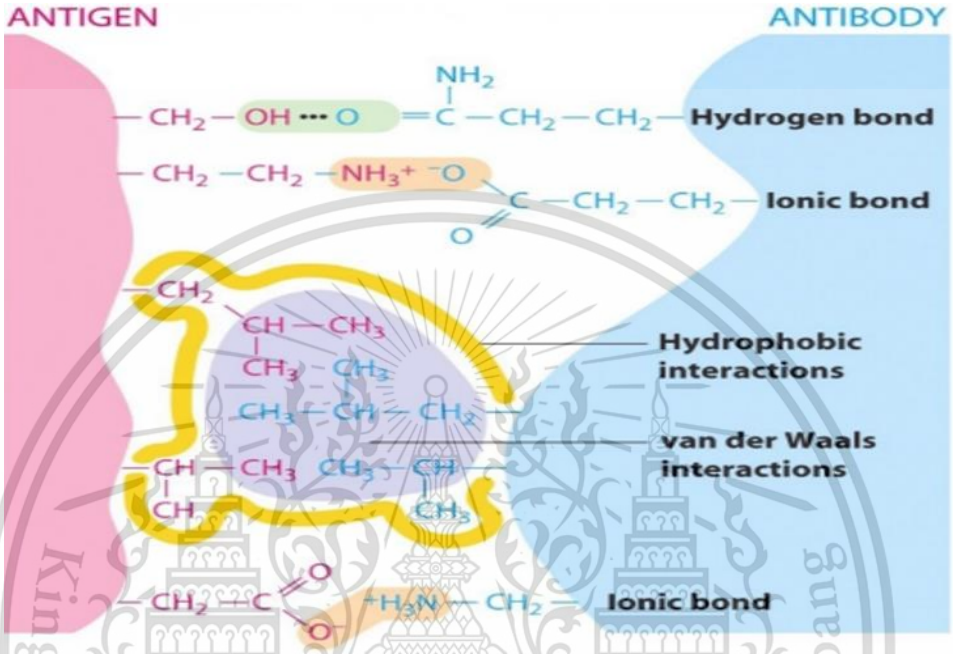

Figure 2.8 Reactions between antibodies and antigens. [15]

In addition to the four mentioned forces, the structure of antigens and antibodies also has an important part to strengthen the binding. The molecular structure of antigens and antibodies that are complementary such as the lock and key the grip will be more stable. In addition, environments also affect the interaction between antigens and antibodies which including:

1. pH: Antigens and antibodies react quite well at pH 7.2 - 7.4. At very high or lower pH, the reaction will be decreased.

2. Temperature: The optimum temperature for the reaction between antigens and antibodies is in the range of 4 – 40 °C. At too high temperature, antigens and antibodies may be denaturing.

3. Ionic strength: The concentration of ion or salt also affects the binding of antigens and antibodies. The appropriate salt concentration commonly used in research studies on the interaction between antibodies and antigens is 0.15 M NaCl (0.9% NaCl, isotonic solution) that is a physiological salt solution or normal saline solution (NSS).

2.2.1.3 UV – Visible spectrometer [16]

The instrument used in ultraviolet–visible spectroscopy is called UV–Vis–NIR Spectrophotometer. The device works by passing a beam of light through a sample and measuring the wavelength of light reaching a detector. The analysis data can be revealed in terms of transmittance, absorbance or reflectance of energy. A UV–Vis–NIR spectrophotometer measures absorbance or transmittance from the UV to the visible wavelength range. A basic principle of quantitative analysis is called the Lambert–Beer's law.

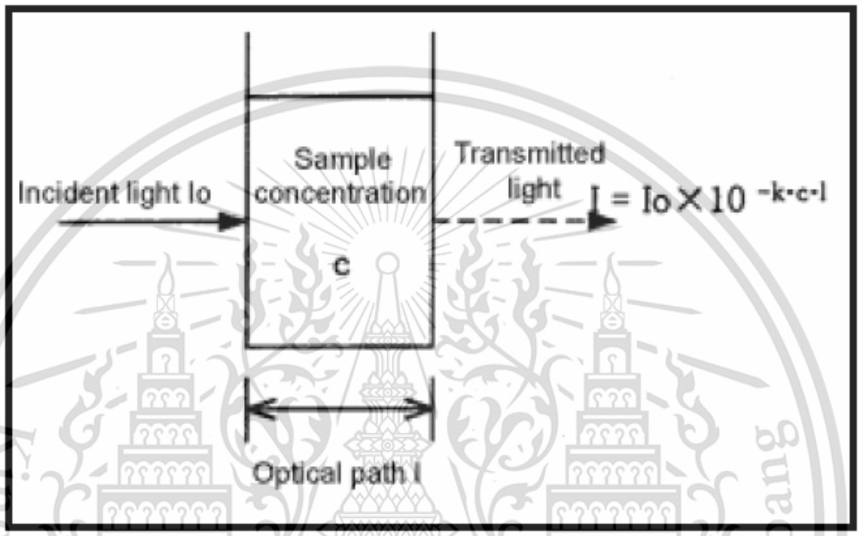

Figure 2.9 Lambert–Beer's law.

1) **Lambert's Law.**

The proportion of incident light absorbed by a transparent medium is independent of the intensity of the light (provided that there is no other physical or chemical change to the medium). Therefore successive layers of equal thickness will transmit an equal proportion of the incident energy. Lambert's law is expressed by equation.

$$T = \frac{I}{I_0}$$

Where I is the intensity of the transmitted light, I_0 is the intensity of the incident light, and T is the Transmittance.

It is customary to express transmittance as a percentage:

$$\%T = \frac{I}{I_0} \times 100$$

2) Beer's Law.

The absorption of light is directly proportional to both the concentration of the absorbing medium and the thickness of the medium in the light path. A combination of the two laws (known jointly as the Beer-Lambert Law) defines the relationship between absorbance (A) and transmittance (T).

$$A = -\log \frac{I}{I_0} = \log \frac{1}{T} = \varepsilon bc$$

Where A is absorbance (no unit of measurement), ε is molar absorptivity (L^{-1} mol^{-1} cm^{-1}), b is path length (cm) and c is molar concentration (mol L^{-1})

Spectrophotometers consist of several components: Light sources (UV and VIS), monochromator (wavelength selector), sample holder, detector, signal processor and readout. The radiation source used is often a tungsten filament, a deuterium arc lamp which is continuous over the ultraviolet region, and more recently light emitting diodes (LED) and xenon arc lamps for the visible wavelengths. The detector is typically a photodiode or a CCD. The containers for the sample and reference solution must be transparent to the radiation which will pass through them. Quartz or fused silica cuvettes are required for spectroscopy in the UV–Vis–NIR region. Figure 2.10 shows a schematic diagram of UV–Vis Spectrophotometer.

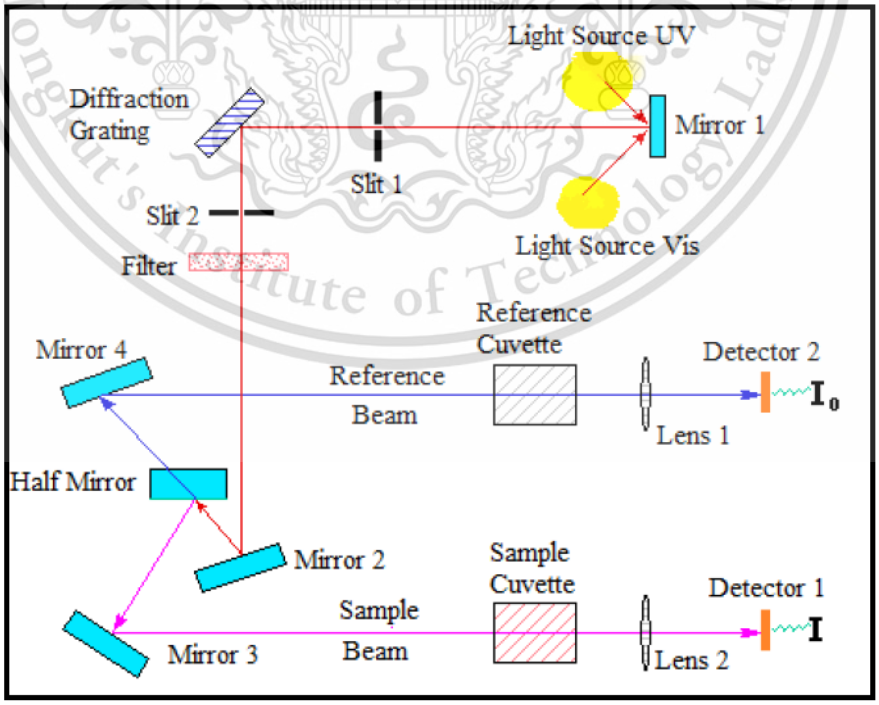

Figure 2.10 Schematic diagram of UV–Vis Spectrophotometer.

2.2.2 Detection principle

Detection principle is based on the reaction of gold nanoparticles with parathyroid hormones resulting in purple product due to aggregation. Intensity of purple color is proportional to the amount of parathyroid hormone in the blood. The measurement mechanism is shown in Figure 2.11.

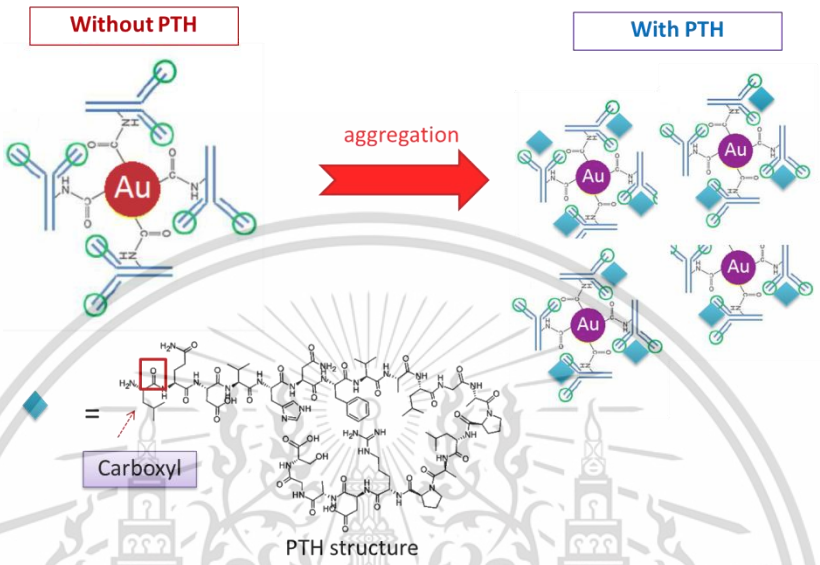

Figure 2.11 The mechanism for measuring of PTH proposed in this research.

2.2.3 Literature Reviews

2.2.3.1 Literature reviews based on immunology

Immunology for analysis of PTH is based on specific reaction between PTH antigen and antibody. There are many publications study on the development of analytical methods for measurement of PTH, For example:

M. T. Julían *et. al*. [17] measured parathyroid hormone levels after thyroid surgery to predict long-term performance of the parathyroid glands. This method was examining calcium and parathyroid hormones in the 24 hours and 6 months postoperative period. Parathyroid hormone testing is performed on an automated electrochemiluminescent immunoassay analyzer, and for the determination of calcium levels, it depends on the reaction with o-cresolphthalein to produced colored product. The results have shown that patients with PTH and calcium levels below 5.8 $pgmL^{-1}$ and 1.95 $mmolL^{-1}$, respectively are risk of permanent hypoparathyroidism.

E. P. García-Santos *et. al*. [18] measured parathyroid hormones during surgery for patients with higher levels of hormones. The measurements used immunochemiluminescence in combination with STAT system for processing. The measurements were performed during surgery and 5 and 10 minutes after the

surgery, respectively. Objective of this measurement is to evaluate and remedy the patients to reducing pain and shot time recuperating in hospital. From the measurement of 91 patients, 39 patients were required to undergo anesthesia, while another 52 were able to undergo cervical block surgery.

V. Cote *et al.* [19] determined parathyroid hormone levels for patients undergoing thyroid surgery for 1 hour. The measurements used Roche Elecsys System 2010 electrochemiluminescence immunoassay combined with blood calcium levels determination. They were found that 43% of patients have low blood calcium and parathyroid hormone levels are lower than the cut-off values (8 ng L^{-1}). 2.2% of patients with parathyroid hormones level below 15 ng L^{-1} have not developed into low blood calcium levels.

W.U. Dittmer *et al.* [20] conducted parathyroid hormone determination using labeled magnetic particles together with resistance measurement. The particles that labeled with conjugated antibodies are then activated and attached to target analytes. The particles are then sent to the surface of the sensor and have captured by immobilized antibody which causes GMR signal changed. This method has a detection limit at 10 pM and 0.8 pM with 15 minutes analysis time for 300 and 500 nm particles respectively.

C. S. Simsek *et al.* [21] developed the measurements using gold electrode modified with 6-mercaptohexanol and silane. PTH was measured using cyclic voltammetry and impedance measurements. The developed method was able to determination of PTH the level of concentrations of 10 - 50 pg/mL.

In addition, this principle was applied to point of care (POC) testing by V. Jarrige *et al.* [22] using the motion of magnetic particles to measure parathyroid hormone content. Parathyroid hormone is captured by a magnetic particle attached to an antibody (anti-N-terminal-PTH). The particles then move with a magnetic force and are attached to the surface of the sensor (anti-C-terminal-PTH). This developed devices that can be measured at the level of picomolar by measuring time less than 10 minutes.

2.2.3.2 Literature reviews based on other techniques

M. Kamberi *et al.* [23] used size exclusion chromatography to measure hPTH using hydrophobic and electrostatic reacted with the substance contained in the column and used 0.1% TFA in 0.2 M sodium chloride/acetone in the ratio of 80:20 by volume as mobile phase with injection volume 40 µL. It was found that separation of hPTH was completely within 7 minutes.

S.S. Rane *et al.* [24] measured parathyroid hormone levels using reversed phase high performance liquid chromatography (RP-HPLC) and ultra

performance liquid chromatography (RP-UPLC). Trifluoroacetic acid in water and trifluoroacetic acid in acetylene were used as mobile phase. The analysis time took 17 minutes and 2 minutes for HPLC and UPLC, respectively. Linearity ranges are 100 -300 μg mL^{-1} and 50 – 300 μg mL^{-1} for HPLC and UPLC, consequently.

E. E. Chambers *et al.* [25] determined parathyroid hormone content using the LC-MS/MS hybrid column containing particles smaller than 2 microns due to it is more effective than the C18 column. With formic acid as a mobile phase, there took 6 minutes for analysis and can be analyzed in the range of 15 - 500 pg mL^{-1}.

2.3 Theory and literature reviews for quality control of hydrogen peroxide content in wound cleaner samples.

2.3.1 Concepts and theories

2.3.1.1 Bacterial cellulose nanopaper (BC nanopaper) [26, 27]

Bacterial cellulose (BC) nanopaper is defined as a sheet of cellulose with its fibers below 50 nm which offer many attractive properties such as biological compatibility, biodegradability, optical transparency, flexibility, hydrophillicity, high porosity and high surface area, etc.

BC can be synthesized by specific non-pathogenic gram-negative bacteria, *Acetobacter xylinum*, which usually found in fruits. The production from the fermentation of this bacteria is polysaccharide which also known as "coconut jelly". This jelly sheet is cellulose with is a long chain glucose polymer with beta-1,4 glycosidic bonds. The structure of BC is shown in Figure 2.12.

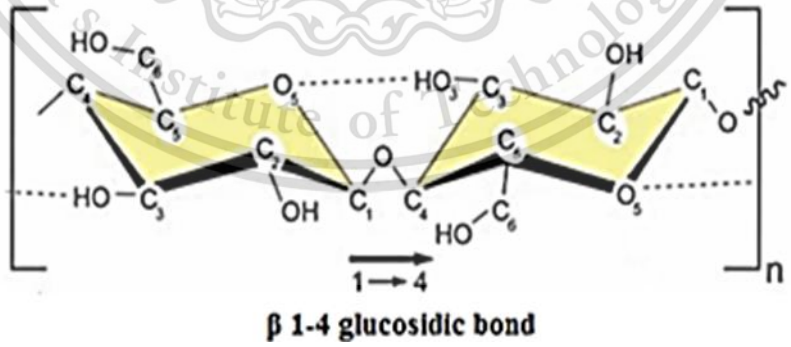

Figure 2.12 Molecule structure of cellulose unit connected with beta (β, 1-4) type of glycosidic bond [26].

Coconut juice is considered as a suitable substrate for producing starter bacterial cellulose because it contains carbon and nitrogen sources for producing a good quality BC [27]. Culture bacteria from coconut juice can

produce BC in culture medium by fermentation in acidic medium with an aerobic atmosphere. After fermentation for 2 weeks, the product becomes an opaque sheet floating on the surface of the media. There are many factors affecting the production process as follows:

1. Carbon source

Glucose is a popular source of carbon and there are also fructose, sucrose, lactose, mannitol that can be used as a carbon source.

2. Nitrogen source

Without nitrogen, it will stop growing of nano-cellulose bacteria. Nitrogen source which can be used is inorganic substances such as ammonium sulfate ($(NH_4)_2SO_4$) and ammonium phosphate ($(NH_4)_3PO_4$) and organic substances such as yeast extract, malt extract and peptone, etc.

3. pH

A suitable pH of culture medium will increase the growth rate of cellulose nano-paper and also helps to prevent the contamination of mold.

4. Temperature

The suitable temperature for the growing of bacterial cellulose is in the range of 28 -32 degrees Celsius. At temperature is higher than 45 degrees Celsius, it will stop growing of nano-cellulose bacteria.

5. Aeration

Acetobacter xylinum is a bacterium that requires air for growing. Therefore, in the production of cellulose bacteria, a wide surface container should be used to provide space for air permeability.

2.3.1.2 Hydrogen peroxide [28, 29]

Hydrogen peroxide is a chemical compound with the formula H_2O_2. In its pure form, it is a very pale blue liquid, slightly more viscous than water. It is used as an oxidizer, bleaching agent, and antiseptic. Hydrogen peroxide is unstable and slowly decomposes in the presence of light. Hydrogen peroxide is found in biological systems including the human body. Enzymes that use or decompose hydrogen peroxide are classified as peroxidases. The boiling point of H_2O_2 has been extrapolated as being 150.2 °C. In practice, hydrogen peroxide will undergo potentially explosive thermal decomposition if heated to this temperature. Overdoses of hydrogen peroxide (more than 3%) can cause irritation, blistering,

vomiting and several deaths. The chemical structure of hydrogen peroxide is shown in Figure 2.13.

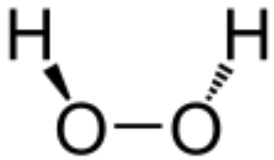

Figure 2.13 Chemical structure of hydrogen peroxide.

2.3.1.3 UV – visible spectrophotometer for film type analysis [30]

The UV-Vis-ISR-2600/2600plus is designed to be mounted in the sample compartment of the spectrophotometer to measure the reflection of solid samples and the transmittance of liquid and film samples. UV-Vis-ISR-2600/2600plus is a machine that combines with photomultiplier. The measureable wavelength range is 220 nm to 850 nm. The measurement can be performed on liquid samples and solid samples. The compartments of this instrument are shown in Figure 2.14.

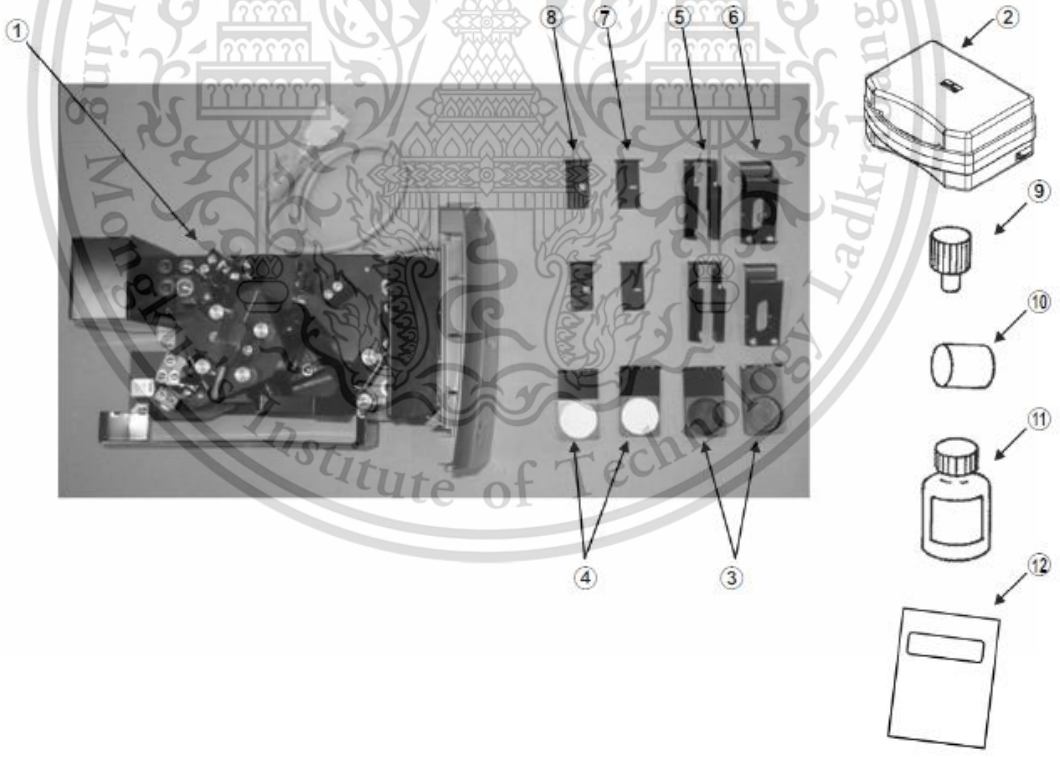

No.	Check	Part Name	No.	Q'ty
①		Integrating sphere main unit	206-28224-91 (ISR-2600) 206-28224-92 (ISR-2600Plus)	1
②		Housing case	206-28466-91	1
③		Powder sample holder	204-05189-01	2
④		Powder sample holder (Filled with barium sulfate powder)	206-21865-91	2
⑤		Square cell holder for transmission measurement	204-52472-01	2
⑥		Film holder	204-03878-03	2
⑦		Mask (2 x 5)	206-61585-03	2
⑧		Mask (5 x 5)	206-61585-02	2
⑨		Knurled screw	202-31975-01	4
⑩		Glass rod	201-99041	1
⑪		Barium sulfate powder, 500 g	017-41646-01	1
⑫		Instruction Manual (this manual)	206-97457	1

Figure 2.14 Compartments of UV-Vis-ISR -2600 / 2600 plus.

1. Optical system diagram

Sample light makes a 0-degree incidence (normal incidence) and reference light make an 8-degree incidence to the integrating sphere. By using the S/R exchange then can measure the reflectance of sample on the sample side. Optical system diagram and light pathway of spectrophotometer for film measurement are shown in Figure 2.15 and Figure 2.16.

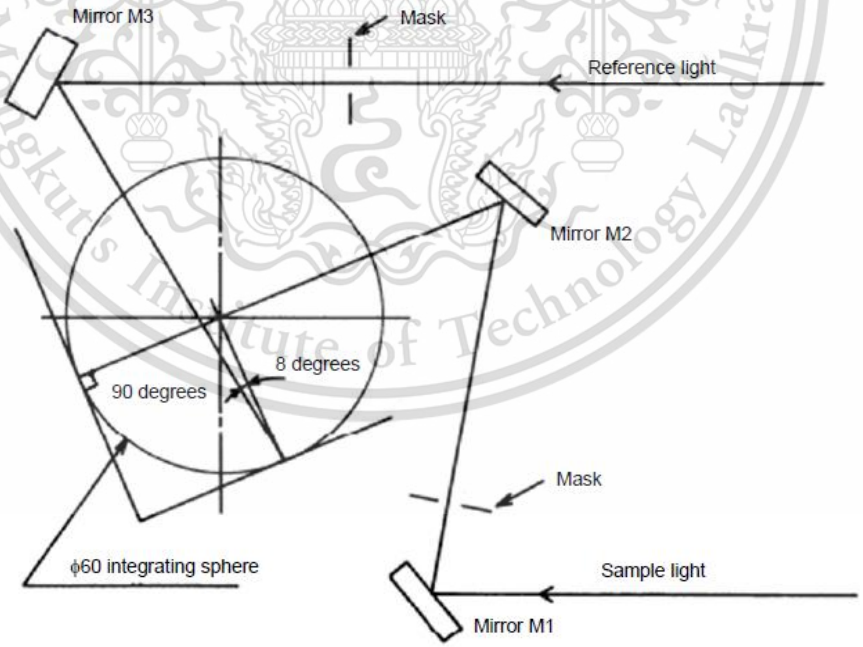

Figure 2.15 Optical system diagram.

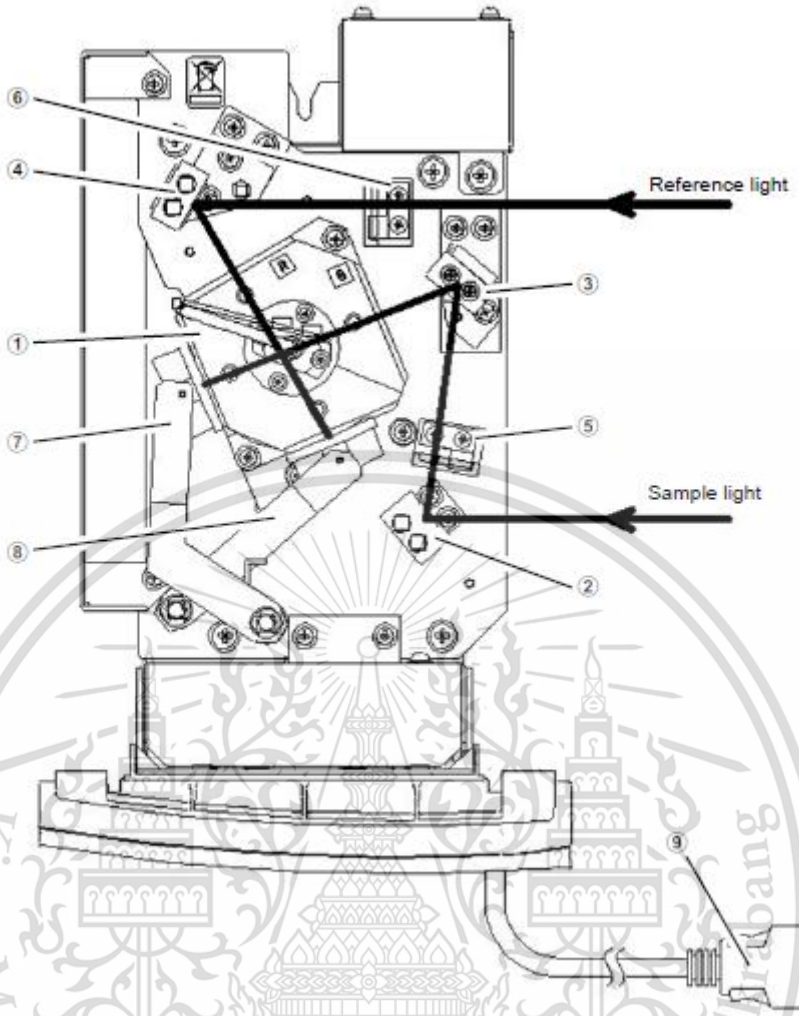

No.	Name	Description
①	Integrating sphere ASSY	The assembly consists of an integrating sphere coated with barium sulfate.
②	Mirror M1	This mirror leads the light on the sample side to the integrating sphere.
③	Mirror M2	This mirror leads the light on the sample side to the integrating sphere.
④	Mirror M3	This mirror leads the light on the reference side to the integrating sphere.
⑤	Mask holder (S side)	This holder is used to reduce the beam size in the reflectance measurement position on the sample side.
⑥	Mask holder (R side)	This holder is used to reduce the beam size in the reflectance measurement position on the reference side.
⑦	Sample holder (S side)	This bar keeps the sample on the sample side in close contact.
⑧	Sample holder (R side)	This bar keeps the sample on the reference side in close contact.
⑨	Signal cable	This cable connects to the spectrophotometer and helps send measurement signals.

Figure 2.16 Light pathway of spectrophotometer for film measurement.

2. Basic operation for measuring of diffuse reflection

This procedure used for measuring of diffuse reflection for an incident angle of 0 degree using a standard white plate. This procedure is used to measure samples with high diffusibility (resin plates, powders, etc.) Figure of measurement of diffuse reflectance is shown in Figure 2.17.

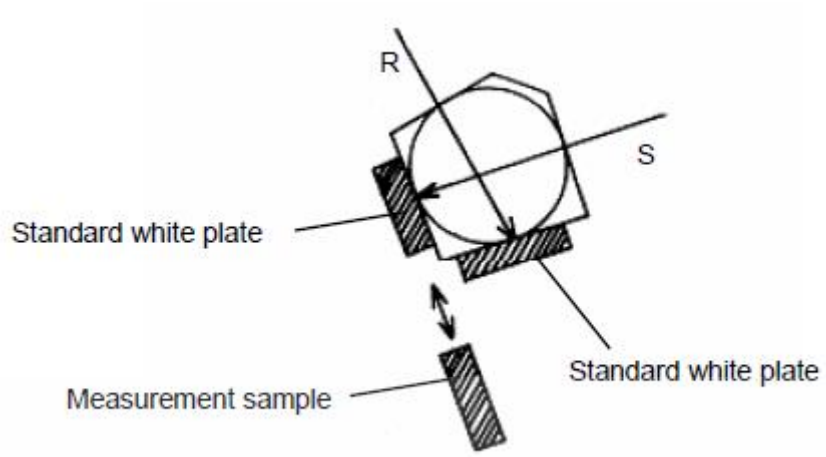

Figure 2.17 Measurement of diffuse reflectance.

1. Set a standard white plate at each exit window on both the sample and reference side of the integrating sphere to correct the baseline.

2. After correct the baseline, replace the standard white plate on the sample side with the measurement sample.

2.3.2 Detection principle

Detection principle is based on the reaction of embedded AuNPs with hydrogen peroxide due to redox reaction in the acidic medium. In the presence of H_2O_2, the wine-red color of the AuNPs solution is decreased as Au^0 is oxidized to become Au (III) [31].

$$2\,Au^0\,(s) + 3\,H_2O_2\,(l) + 6\,H^+\,(aq) \rightarrow 2\,Au^{3+}(aq) + 6\,H_2O\,(l)$$

wine-red — pale yellow

2.3.3 Literature Reviews

2.3.3.1 Literature reviews based on bacterial cellulose nanopaper

E. Zor [26] using in-situ silver nanoparticles embedded nanopaper for chiral recognition of cysteine. Nanopaper was punched into a circular piece and put on the wax-printed PET film to produce 2-dimensional cuvette. This research was found that AgNPs sensing was response toward D-cysteine and cause aggregation of AgNPs with LOD value of 4.88 μM.

S. Abbasi-Moayed *et al.* [32] developed a ratiometric fluorescence sensor (RF) with a variety of light-emitting colors on bacterial cellulose nanoparticles (BC) for biological differentiation of biothiols to detect N-Acetyl L-cysteine covered with the green quantum dots of CdTe-Rhodamin B (GQDs-RhB) and two red spots of CdTe QDse (0 and 5 mM) at the concentration of NaOH (0 and 5 mM), which are components for differentiating biothiols. Due to the high association of thiols (SH) with the surface of CdTe QDs and the combination of QDS, the light emission of fluorescence (FL) of QDs changes while CD and Rhodamine B emission were almost unchanged. The rainbow fingerprint was used to identify patterns for specifying the characteristics and differences of biothiols.

N. Pourreza *et al.* [33] synthesized the in-situ silver nanoparticles using nano-cellulose materials from bacteria that are flexible and transparent. In this method, the silver ions absorbed on the cellulose nanoparticles are reduced by the hydroxyl group of nano-cellulose bacteria. Embedded silver nanoparticles used as a new analyzer for the optical detection of cyanide ions (CN^-) and 2-mercapto benzothiazole (MBT) in water samples. Changes in absorption intensity with surface plasmon resonance is linearly proportional to the concentration in the range of 0.2 - 2.5 μg mL^{-1} and 2 - 110 μg mL^{-1} with the detection limits of 0.012 μg mL^{-1} and 1.37 μg mL^{-1} for CN^- and MBT, respectively.

E. Zor *et al.* [34] synthesized nanopaper from cellulose fibers at the nanoscale level which is produced from *A. Xylinum*. The diameter of the fibers is 40 ± 10 nm. In this research, nitrogen was droped on the carbon quantum dots, which is attached to the bacteria cellulose. Then nanopaper was cut to a circle or rectangular sheet and inserts it into a wax sheet to use as a microcuvette for spectrofluorometer. The nanopaper was used for iodine determination in seawater. The limit of detection and limit of quantitation is 48 and 144 μM, respectively.

2.3.3.2 Literature reviews based on determination of hydrogen peroxide

W.Z. Lin *et al.* [35] using DNA-modified gold nanoparticles for colorimetric detection of hydrogen peroxide. The reaction has 2 steps. First, using ferrous ion to react with H_2O_2 to produce hydroxyl radical based on Fenton reaction. Then the radical breaks the phosphodiester bond in DNA result in decreasing of DNA on the surface of AuNPs and the color change from red to purple due to aggregation. The detection was complete in 15 min with LOD 1 μM.

F. Wen *et al.* [36] synthesized horseradish peroxidase functionalized gold nanoclusters for hydrogen peroxide sensing. The blackish green HRP-AuNCs emits intense red fluorescence at 650 nm. In the presence of H_2O_2 at 25 °C for 10 min under pH 9.0, it was found that the fluorescence at 450 nm was significantly increased and decreased at 650 nm. Linearity range is 100 nM – 100 µM with LOD 30 nM.

Y. Wu *et al.* [37] integrating the peroxidase-like property of glutathione protected gold nanoclusters to accelerate the decomposition of H_2O_2 to hydroxyl radicals. The radicals then reacts with terephthalic acid to produce hydroxyterephthalate with has dual emission peaks at 430 and 600 nm. The emission peak at 430 nm is increased proportional to H_2O_2 while the emission peak at 600 nm still constant. The ratiometric fluorescence sensor has a detection limit of 10 nmol L^{-1} for H_2O_2 and 20 nmol L^{-1} for glucose.

M.M. Khan *et al.* [38] synthesized the positively charged gold nanoparticles using an electrochemical active biofilm for colorimetric detection of hydrogen peroxide. In the presence of H_2O_2, the positively charged AuNPs could catalyze the oxidation of 3,3,5,5-tetramethylbenzidine dihydrochloride and developed the blue product which provides absorption peak at 655 nm. This developed method can determine H_2O_2 in the range of 1.0 – 2.5 x 10^{-3} M.

J. Sophia *et al.* [39] used a non-enzymatic approach polyvinylpyrrolidone stabilized gold nanoparticles for hydrogen peroxide detection. The detection is performing on cyclic voltammetry, chronoamperometry and impedance spectroscopy. The linearity of this method is in the region 0.8 – 80 µM.

W. Wang *et al.* [40] used heme proteins immobilized gold nanoparticles-bacterial cellulose nanocomposite modified glassy carbon electrode for amperometric determination of hydrogen peroxide. The reaction is based on the reduction of H_2O_2 in the presence of the mediator hydroquinone. This biosensor exhibited a fast response to H_2O_2 within 1 min with good linearity range from 0.3 µM to 1.00 mM and LOD 0.1 µM.

2.4 Theory and literature reviews for quality control of iodized table salts

2.4.1 Concepts and theories

2.4.1.1 Iodine deficiency disorders (IDD) [41-42]

Iodine deficiency disorders are a symptom of the body caused by insufficient iodine intake. This symptom causes the thyroid gland unable to produce enough thyroid hormones. Thyroid hormones play an important role to control the growth of body, control of metabolic processes and control the growth processes of brain development.

Iodine is a nutrient that the body cannot produce itself and resulting in iodine deficiency which will affect the body. For example, in pregnant women, it will have severe effects on the fetus. The baby may die in the womb or miscarriage or become disabled due to mental retardation, intellectually impaired and slow in brain development. In adults with iodine deficiency, there is a low level of thyroid hormones resulting in laziness and weakness.

Iodine deficiency can be found in areas that far away from the sea or at high altitudes from the sea. Sources of iodine can found in seafood, seaweed or foods that added with iodized salt. Adding iodine to table salt usually added in the form of potassium iodate (KIO_3), which is a stable form.

1) **Cretinism [43]**

Cretinism is a term of thyroid deficiency occurring in infants and children. Untreated of this disease are results in impairment of both physical and mental development. Symptoms of cretinism may include goiter, deaf mutism, squint, spastic diplegia, and disorders of stance and gait, dwarfism, coarse and dry skin, and husky voice.

2) Goiter [44]

Goiter may be defined as an enlargement of the thyroid gland, which is not due to inflammation or malignancy. There are two general types of goiters: (1) nontoxic goiters, which produce either (a) normal amounts of hormone (simple goiter) or (b) below normal amounts of hormone (hypothyroid), and (2) the toxic goiters, which produce excessive amounts of hormone (hypertrophy). Furthermore, a defect or deficiency at any trophic step can also result in thyroid disease. Iodine deficiency (endemic goiter) is well known in iodine-deficient areas of the world. Most of goiter is caused by iodine deficiency, being around 200-800 million people.

2.4.1.2 The daily reference intakes (DRI) for iodine [42]

The amount of iodine that should be received is shown in Table 2.2.

Table 2.2 The daily reference intakes (DRI) for iodine

Life Stage	Iodine (µg)
Infants	
0-6 Months	110
7-12 Months	130
Children	
1-8 Years	90
Males	
9-13 Years	120
14-70 Years	150
> 70 Years	150
Females	
9-13 Years	120
14-18 Years	150
19-70 Years	150
> 70 Years	150
Pregnancy	
< 18 - 50 Years	220
Lactation	
< 18 Years	290
19-30 Years	290
31-50 Years	290

2.4.1.3 Sources of iodine [42]

Food sources of iodine are listed in the table below.

Table 2.3 Food sources of iodine

Food	Iodine (µg)
Salt, iodized, 1 teaspoonful	400
Haddock, 75g	104 - 145
Bread, regular process, 1 slice	35
Cheese, cottage, 2% fat, 1/2 cup	26 - 71
Shrimp, 75g	21 - 37
Egg, 1	18 - 26
Cheese, cheddar, 30g	5 - 23
Ground beef, 75g, cooked	8

2.4.1.4 Standard method for the iodine determination [45]

Iodometry is a method to determine the amount of iodine in sample. Redox titration is using sodium thiosulphate ($Na_2S_2O_3$) as a reducing agent with starch as an indicator. The equations of titration are given as follow:

$$I_3^- + 2\ e^- \rightleftharpoons 3\ I^- \ (E_o = +\ 0.5355\ V)$$

Together with reduction potential of thiosulfate

$$S_4O_6^{2-} + 2\ e^- \rightleftharpoons 2\ S_2O_3^{2-} \ (E_o = +\ 0.08\ V)$$

The overall reaction is thus:

$$I_3^- + 2\ S_2O_3^{2-} \longrightarrow S_4O_6^{2-} + 3\ I^- \ (E_{reaction} = +\ 0.4555\ V)$$

This method is highly accurate. But requires operation skills to observe the endpoint and this method consumed large amounts of reagents.

2.4.1.5 Paper-based analytical device [46-47]

Paper is a well-known material for writing, printing, drawing and packaging. Cellulose fiber is the main component of paper and this can be highly attractive for certain applications due to it allows liquid to pass through its hydrophilic fiber without any pump or external source. Paper-based analytical devices (PAD) are novel analytical tools that are fabricated with paper material capable of analyzing complex and small amounts of samples and reagent. The introduction of paper-based microfluidics to the scientific world was attributed to Whitesides' group at Harvard University, whose first device was a protein-glucose assay created by a lithography method in the paper. Since then, a large variety of fabrication techniques have been developed. There are several techniques of fabrication method include photolithography, analogue plotting, inkjet printing and etching, plasma treatment, paper cutting, wax printing, flexography printing, screen printing, and laser treatment. Techniques were chosen depending on the type of material used and the type of modification required. Example of the PAD is shown in Figure 2.18

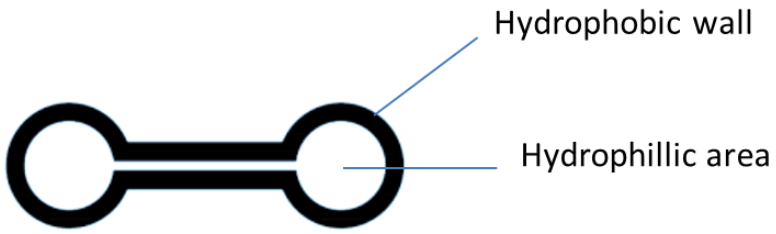

Figure 2.18 Example of the PAD [47]

2.4.1.6 Spectrofluorometer [48]

Spectrofluorometer is an instrument for analyzing the properties of substances which include excitation and emission wavelength and intensity. The analytical method is based on the absorption of UV and visible radiation which causes the molecules to be stimulated and vibrate, causing them to be stimulated from the ground state to a higher energy level (Excited state). Then the energy was emitted as fluorescence and appears the spectrum which specific to each substance. There are two basic types of fluorometers, the filter fluorometer and the spectrofluorometer. The difference between them is the way they select the wavelengths of incident light. A filter fluorometer use filters while a spectrofluorometer use grating monochromators. Filter fluorometers are often built at a lower cost but are less sensitive and have less resolution than spectrofluorometers.

2.4.1.6.1 Components of a fluorescence spectrometer

Components of the spectrophotometer are shown in Figure 2.19

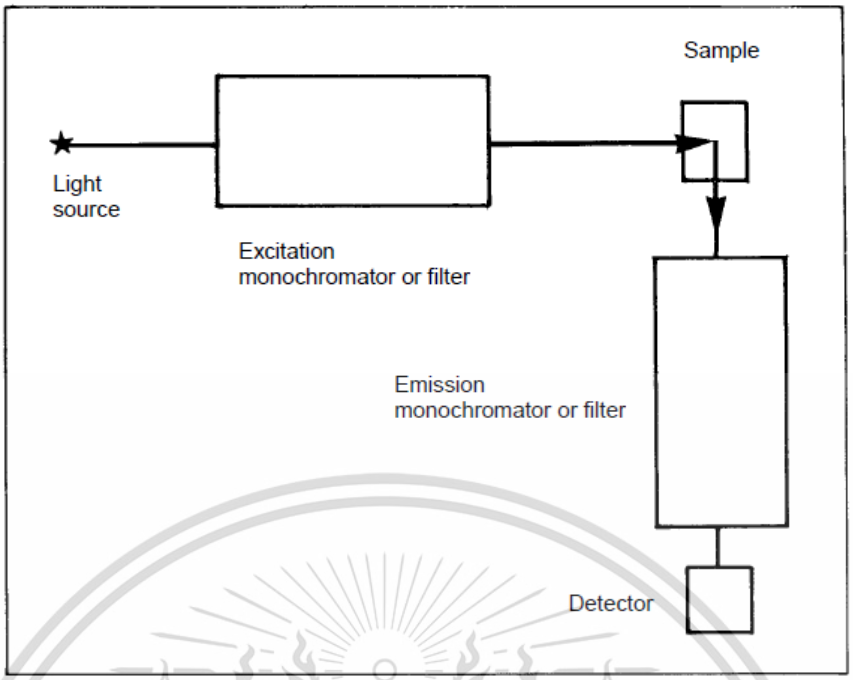

Figure 2.19 Essential components of a fluorescence spectrometer.

1) Light source

Light source is used for emit light at a wavelength to stimulate the substance. There are many types of light sources, such as xenon lamps, mercury vapor lamps, lasers and LED.

2) Wavelength selection

Spectroscopy fluorometers generally use grating as a monochromator which can select the desired wavelength. The characteristics of filters and gratings are the same as those used on UV-optical devices. The only difference is that there are two monochromators: excitation monochromator and emission monochromator which must be in the 90 degree position of each other.

3) Sample container

Sample container is a cuvette made of quartz and has four clear sides in order to allow the light to pass in and measure the fluorescent light that comes out perpendicularly (90 degrees).

4) Detector

There are 2 types of fluorometers: Photomultiplier Tube (PMT) and Photodiode (PD).

5) Signal Processor and Data Read Out

The signal from the detector goes through the electronic process and shows the result in form of numbers or digitally.

2.4.1.7 Stern – Volmer's Reletionship [49]

Processes such as fluorescence and phosphorescence are examples of intramolecular deactivation (quenching) processes. An intermolecular deactivation is where the presence of another chemical species can accelerate the decay rate of a chemical in its excited state. Stern-Volmer equatiom is the equation showing the relationship between the intensity of fluorescence and the concentration of ions that affect the reduction of fluorescence (Quencher). The equation is shown as follow:

$$\frac{I_f^0}{I_f} = 1 + k_q \tau_0 [Q]$$

When:

I_f° is Fluorescence intensity without Quencher [Q]

I_f is Fluorescence intensity with Quencher [Q]

k_q is The quencher rate coefficient

τ_0 is Fluorescence lifetime without Quencher

[Q] is Concentration of quencher

From the equation, the Stern-Volmer graph can be made into a linear graph as shown in Figure 2.20, where the y-intercept is always equal to 1. Linear equation can be applied to quantitative analysis to find the concentration of quencher.

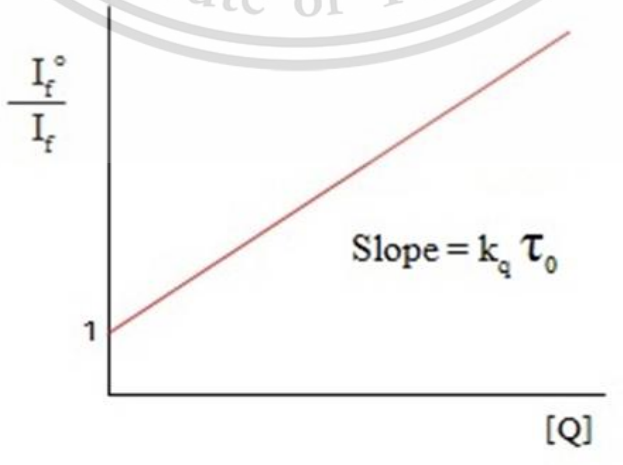

Figure 2.20 The relationship between the Stern-Volmer equations.

2.4.1.8 RGB color model [50]

The RGB color model is the model that assembles the primary light spectra of Red (R), Green (G), and Blue (B) together in various combinations to produce new spectrum of colors as shown in Figure 2.21. The RGB color model is used in various technologies producing color images, such as conventional photography and the display of images in electronic systems.

The RGB color space could be represented as a cube by normalized RGB color values in the range (x_R , y_G , z_B) with gray values on the main diagonal of the black values (0,0,0) and on the opposite corner the white values (255, 255, 255).

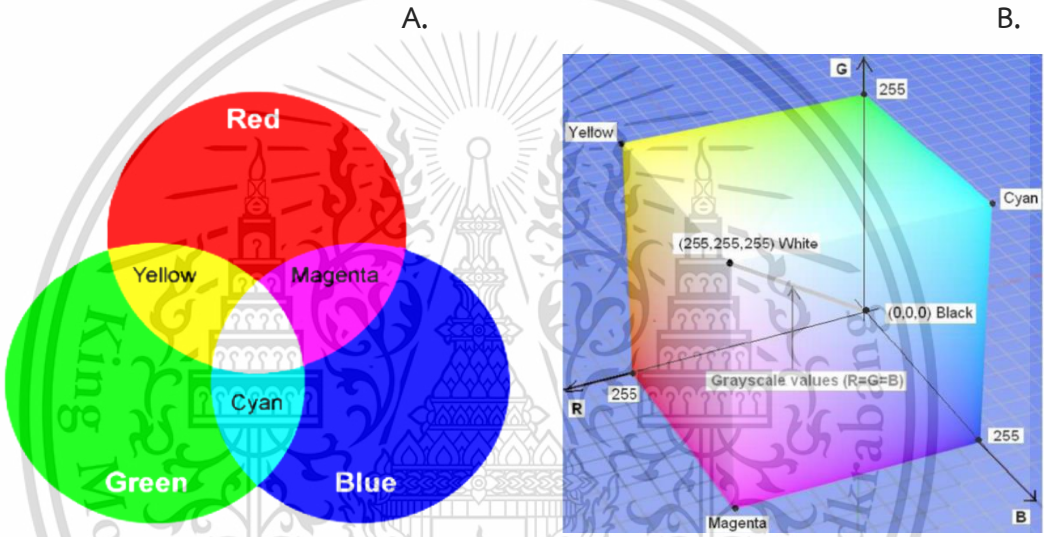

Figure 2.21 RGB color model: The primary color (A) and the primary color cube (B)

2.4.2 Detection principle [51]

The analytical method for paper-based determination of iodate is using the mixing of iodate with an excess of iodide and sulfuric acid to causing iodide (I^-) to oxidized iodate under acidic conditions to generate iodine (I_2). The excess amount of iodide is then reacted with iodine to form tri-iodide (I_3^-). Tri-iodide/iodide is then reacted with the solution of AuNCs resulting in the quenching of AuNCs which proportional to the amount of iodate.

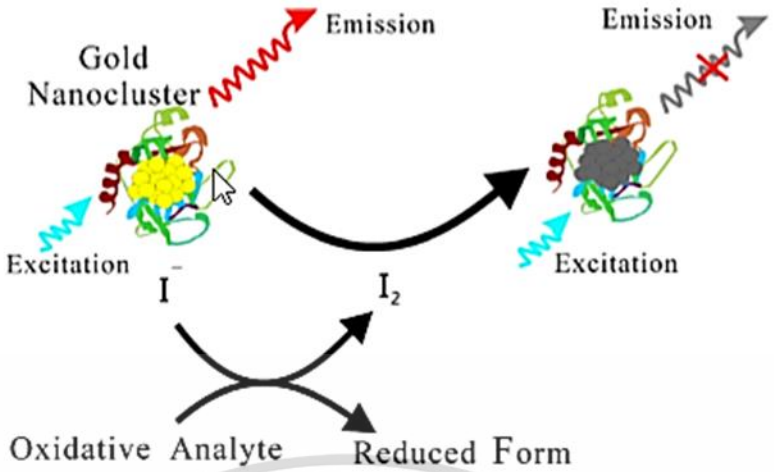

Figure 2.22 Mechanism of quenching reaction of AuNCs with oxdative agent.

2.4.3 Literature Reviews

2.4.3.1 Literature reviews based on using laboratory equipment for the iodate determination

S.D. Kumar *et al*. [52] used anion chromatography with conductivity detection of iodate and sulphate. This method is using onguard silver cartridges for chloride removal. Limit of detection for iodate and sulphate are 0.5 and 0.05 µg mL^{-1}, respectively with good recovery.

A. Salimi *et al*. [53] described the developed method for iodate, nitrite and periodate detection using the embedded catalase multiwall carbon nanotubes based on redox reaction in acidic solution. Under optimized condition of the amperometric method, the calibration range is 1 µM – 6 mM, 1 µM – 5 mM and 5 µM – 10 mM for periodate, iodate and nitrite, respectively. Detection limit for periodate, iodate and nitrite are 0.15 µM, 0.2 µM and 1.35 µM, consequently.

W. Hong-juan *et al*. [54] reported a new amperometric sensor based on 9,10- phenanthrenequinone derived graphene (PQ/DP) for sensitive and selective determination of iodate. The PQ/GP shows good catalytic activity towards the reduction of iodate. This sensor displays linear range from 5×10^{-8} – 6×10^{-3} mol L^{-1} with low detection limit (1×10^{-8} mol L^{-1}).

B. Narayana *et al*. [55] developed a method for iodate determination. The method is based on the reaction of iodate with potassium iodide in acid medium to liberate iodine. The liberated iodine bleaches the blue color of methylene blue and resulting in decreasing of absorbance at 665.6 nm. Linearity was found in the range of 0.5 -14 µg mL^{-1}. Limit of detection and limit of quantitation are 0.048 and 0.145 µg mL^{-1}, respectively.

A.H. Liang *et al*. [56] used rhodamine 6G combine into ion association particles reacted with I_3^- from IO_3^- and exceed I^-. Iodine concentration is proportional to the resonance scattering intensity at 400 nm in the range of 1.0 – 20 x 10^{-7} mol L^{-1}.

Although, these methods mentioned above have lower detection limit and high sensitivity, however, these still suffer from complicated analytical workflow. Therefore, some researchers then proposed the simple method for iodate determination using flow injection. The examples are described below:

N. Choengchan *et al*. [57] presented a flow injection for iodate determination. This system detected the blue complex of tri-iodide in the presence of starch at 590 nm. The calibration graph was obtained from 5.0 x 10^{-6} – 4.0 x 10^{-5} M with high sample throughput (65 injections per h) and the detection limit was 2 mg I/kg salt.

N. Choengchan *et al*. [58] determined iodine in ppb levels using the catalytic effect of iodide on the Ce (IV) – As (III) reaction. This method can determine total inorganic iodine in bottled drinking water that had iodate in the level of 100 µg L^{-1} with good recovery and sample throughput is 15 h^{-1}.

2.4.3.2 Literature reviews based on using the PAD as a sensing platform

N.M. Myers *et al.* [59] used a paper test card for iodometric titration. The dried reagents are reconstituted and combined through a surface tension enabled mixing mechanism. The test outcomes can be read both directly by eye and by using electronic image analysis over the range of 0.8 – 15 mg L^{-1}. This card can also use for other redox-active analytes via iodometric back titration.

M.O. Gorbunova *et al.* [60] developed a method for iodide determination using sensitive silver triangular nanoplates (AgTNPs) paper. Iodide is oxidized by Fe (II) to produce iodine which then reacted with AgTNPs and resulting in optical changed. Determination range of this method is 0.03 – 0.3 mg L^{-1} and the limit of detection is 0.01 mg L^{-1}.

2.4.3.3 Literature reviews based on synthesis of AuNCs and application

S. Govindaraju *et al.* [61] reported the stability, non-toxic and red fluorescence of serum albumin - gold nanoclustesr which specific to the measurements of dopamine in brain and spinal fluid. From the morphology of AuNCs, the average particle size is 4 - 6 nm. Dopamine determination is based on

the quenching reaction of gold nanoparticles. This method gave a linearity range of 0 to 10 nM and a detection limit was 0.622 nM.

Krishnendu C. *et al.* [62] conducted a determination of residual rifampicin for the treatment of meningitis and tuberculosis. This method is effective and economical for the determination of the rifampicin levels in urine samples using bovine serum albumin stabilized gold nanoclusters which is absorbed on paper. The concentration of rifampicin can detect by quenching reaction of gold nanoclusters. The color intensity was captured by a digital camera and further analyzed using ImageJ^{TM}. The decreased fluorescence intensity of BSA-AuNCs in the presence of rifampicin allows for the sensitive detection of rifampicin in a range from 0.5 - 823 μg mL^{-1}. The detection limit for rifampicin was measured as 70 ng/mL.

Pingping X. *et al.* [63] developed a method for measure the amount of uric acid by using the reaction of gold nanoclusters. First, uric acid is oxidized with enzyme uricase and allantoin and hydrogen peroxide were generated. Hydrogen peroxide was then destroyed the Au-S bond of gold nanoclusters causing the reduction of gold nanoclusters intensity. Under an optimized condition, the extent of quenching was found linearly related to uric acid concentration in the range of 0.7 – 80 μM, and uric acid as low as 120 nM could be detected.

Lei Yan *et al.* [64] developed a method for the synthesis of nanoclusters with microwaves by mixing tetrachloroauric acid, bovine serum albumin and sodium hydroxide. The mixture was then heated in a non-continuous microwave mode with a suitable condition to prevent the overheating generated during the synthesis. Finally, the color of the solution was changed from yellowish to brown color and appeared red emission under UV irradiation. The absorption and emission peak were located at 510 and 645 nm, respectively. This method was applied to determination of nitrogen oxide (NOx) based on quenching reaction.

T. Zhao *et al.* [65] synthesized gold nanoclusters using bovine serum albumin as stabilizer and used for nitric oxide detection. BSA-AuNCs were prepared by added tetrachloroauric acid into bovine serum albumin and stirred for 2 minutes. The solution was then added with NaOH and pH was adjusted to 12 with continuous stirring at 37 °C for 12 h. Finally, the solution was changed from yellowish to brown color and the size of as-prepared nanoclusters were 1.5 nm with red emission peak at 640 nm. The intensity of AuNCs was decreased when reacted with nitric oxide. Limit of detection of this method is 0.017 mM.

2.4.3.4 Literature reviews based on gold nanoclusters and the iodate determination

Ruiping L. *et al.* [66] described specific measurements and high sensitivity of iodate measurements using gold nanoclusters. In the excess of iodide solution, iodide is oxidized with iodate to form iodine (I_2). The iodine is combined with the remaining iodide to form tri-iodide and then react and erode gold nanoclusters resulting in decreasing of fluorescence intensity. Linear relationship between the concentration of iodate and fluorescence intensity is in the range of 10 nm - 1 μm. It was found that the limit of detection is 2.8 nanomolar and this method can applied to determination of iodate samples with good recovery.

Ruiping L. *et al.* [51] developed the method for determination of oxidative agents. Gold nanoclusters were synthesized using bovine serum albumin as stabilizer. The sensor was applied to iodine detection in which iodide was oxidized with an oxidative agent to form as iodine. Iodine acts as an oxidative agent and oxidizes gold nanoclusters to become a charged gold solution that is water-soluble and resulting in reducing of intensity of gold nanoclusters. The detection limits when applied to nitrite, bromate and periodate determination were 11.7, 1.7 and 1.5 μM, respectively.

Xue-Ling Cao *et al.* [67] described the application of gold nanoclusters as a sensitive and specific sensor for iodine detection. Study on fluorescence spectrum was found that gold nanoclusters had maximum intensity at 610 nm. When KI-I_2 was added, it was found that intensity of gold nanoclusters was decreasing with increasing of KI-I_2. Linearily was in the range of 1.8 – 30 nM.

Chapter 3
Research methodology

3.1 Chemicals and apparatus

3.1.1 Chemicals

Name	Chemical formula	% Purity	Suppliers
Tetrachloroauric (III) acid	$HAuCl_4 \cdot 3H_2O$	≥ 99.9	Sigma-Aldrich, USA
Trisodium citrate dihydrate	$C_6H_5Na_3O_7 \cdot 2H_2O$	≥ 99.0	Sigma-Aldrich, USA
Sodium chloride	NaCl	99.5	LOBA Chemie, India
Sodium hydroxide	NaOH	98.0	Rankem, India
Anti – PTH (ab 53040)	-	≥ 99.9	Abcam, UK
Phosphate buffer saline (PBS)	-	≥ 95	Sigma-Aldrich, Swizerland
Parathyroid hormone (PTH)	-	≥ 95	Sigma-Aldrich, USA
Hydrogen peroxide	H_2O_2	39.0 – 41.0	Carlo Erba, Italy
D-Glucose	$C_6H_{12}O_6$	≥ 99.5	Sigma-Aldrich, USA
Ammonium sulfate	$(NH_4)_2SO_4$	≥ 95	Carlo Erba, Italy
Potassium dihydrogen phosphate	KH_2PO_4	> 99.0	Merck, Germany
Magnesium sulfate	$MgSO_4 \cdot 7H_2O$	> 99.0	Carlo Erba, Italy
Peptone	-	-	SRL, India
Yeast	-	-	JT group, Japan
Bovine serum albumin	-	-	Across, USA
Potassium iodate	KIO_3	99.4 -100.4	Ajax Finechem, Australia
Potassium iodide	KI	99.5	Sigma-Aldrich, Switzerland
Sulfuric acid	H_2SO_4	95 -97	Fisher Chemical, UK
Citric acid	$C_6H_8O_7$	> 99.0	Ajax Finechem, Australia
Di-Sodium Hydrogen Phosphate Anhydrous	Na_2HPO_4	99.0	Carlo Erba Analytical Reagent, Spain

3.1.2 Apparatus

1) Volumetric flask
2) Erlenmeyer flask
3) Micropipette
4) Beaker
5) Microcentrifuge tube
6) Hotplate – IKA® C-MAG HS7, Malaysia
7) Vortex mixer - Gennie Z Vortex, USA
8) UV - visible spectrophotometer - Jasco V630, USA
9) pH meter – METTLER TOLEDO Five Easy Plus ™, Germany
10) Digital Balance - Shimadzu, Chaina
11) Minicentrifuge - TOMOS laboratory products MiniStar Centrifuge, Singapore
12) Water bath - LAUDA AQUAline AL25, Germany
13) UV-Visible spectrophotometer – ISR-2600 Plus, Japan
14) Microwave oven – Samsung ME81KS-1, Korea
15) Permanent pen - 1225 Faber-Castel™ multimark permanent, Germany
16) Transmission electron microscope, FEI-TECNAI T20 G^2, Netherlands
17) Spectrofluorometer – Jasco FP6300, USA
18) Field Emission Scanning Electron Microscopes (FE-SEM) - HITACHI SU-8010, Japan

3.2 Research methodology

3.2.1 Clinical diagnosis of hyperparathyroidism

All chemical solutions were prepared using autoclaved deionized-distilled (DI) water throughout the experiment.

3.2.1.1 Chemical preparation

(1) Preparation of the solutions for the synthesis of gold nanoparticles (AuNPs)

1.1) 0.01 % w/v tetrachloroauric (III) acid

Dissolve 0.01XX g of tetrachloroauric (III) acid and adjust to 100.00 mL with DI water.

1.2) 1.00 % w/v trisodium citrate

Dissolve 0.25XX g of trisodium citrate and adjust to 25.00 mL with DI water.

(2) Preparation of pH 7.0 phosphate buffer saline solution (PBS)

Dissolve 1 tablet of phosphate buffer saline in 200.00 mL of DI water to get 0.01 mol L^{-1} pH 7.00 phosphate buffer saline solution.

(3) Preparation of conjugation solution

3.1) 0.10 mg mL^{-1} anti - parathyroid hormone

Pipettes 10.00 µL from stock 1 mg mL^{-1} of anti - parathyroid hormone and adjust to 100 µL with phosphate buffer saline solution.

3.2) 10.00 % w/v sodium chloride

Dissolve 0.10XX g of sodium chloride and adjust to 1.00 mL with DI water.

3.3) 1.00 mol L^{-1} sodium hydroxide

Dissolve 0.40XX g of sodium hydroxide and adjust to 10.00 mL with DI water.

3.4) 0.05 mol L^{-1} sodium hydroxide

Pipettes 0.50 mL of solution in 3.3) and adjust to 10.00 mL with DI water.

(4) Preparation of standard parathyriod hormone solution

4.1) 5 x 10^{-7} pg mL^{-1} parathyroid hormone

Dissolve 50 µg of stock parathyroid hormone and adjust to 1.00 mL with DI water.

4.2) 1, 10, 100, 1,000 and 5 x 10^{3} pg mL^{-1} parathyroid hormone

Pipette from standard 5 x 10^{5} pg mL^{-1} parathyroid hormone solution as in the table below and adjust with DI water to 1.00 mL.

Concentration of standard parathyroid hormone solution (pg mL^{-1})	Pipetted volume (µL)	Final concentration of standard parathyroid hormone solution in 1.00 mL volumetric flask (pg mL^{-1})
5 x 10^{5}	10	5 x 10^{3}
5 x 10^{3}	200	1000
1000	100	100
100	100	10
10	100	1

(5) Preparation of blood samples

Rat blood samples were purchased from National Laboratory Animal Center, Thailand. Each sample was centrifuged at 13,000 rpm for 40 min and then filtered through a 0.22 μm nylon membrane filter.

3.2.1.2 Experiment

(1) Synthesis of gold nanoparticles [53]

100.00 mL of 0.01 % w/v tetrachloroauric (III) acid was heated to boiling point, followed by rapidly adding 2.00 mL of 1.00 % w/v sodium citrate and stirred for 15 min. The solution was kept cooled at room temperature and stored at 4 °C. The particles were characterized using a transmission electron microscope (TEM) and a UV- Vis spectrophotometer.

(2) Conjugation of antibody and colloidal gold nanoparticles

100.00 μL of the gold nanoparticles was adjusted to pH 7.00 using 0.05 mol L^{-1} sodium hydroxide and then placed into a micro centrifuge tube followed by 15.00 μL of 0.1 mg mL^{-1} antibody and leaved for 5 min. Then, 15.00 μL of 10.00 % w/v sodium chloride was added and incubated at 25 °C for 1 hr. Finally, the solution was used without any purification.

(3) Procedure for parathyroid hormone determination

10.00 μL of each concentration of standard PTH was added to the conjugated gold nanoparticles and adjusted with PBS buffer to 150.00 μL and incubated for 1 hr at 25 °C. The surface plasmon bands of the particles were measured from 400 – 800 nm using UV – Vis spectrophotometer.

3.2.1.3 Study on optimization conditions

3.2.1.3.1 Study on effect of pH of gold nanoparticles on conjugation of antibody

pH of gold nanoparticles solution was adjusted to finally pH 5 - 9 using 0.05 mol L^{-1} sodium hydroxide before conjugated with antibody. Conjugation procedure was the same as described above.

3.2.1.3.2 Study on effect of antibody volume

Effect of antibody volume on conjugation with gold nanoparticles was studied from 0 - 20 μL. Conjugation procedure was the same as described above.

3.2.1.3.3 Study on effect of reaction time

Effect of reaction time was studied from 30 min - 2 hr. Detection procedure was the same as described in section 3.2.1.2 (3).

3.2.1.4 Study on analytical performances

3.2.1.4.1 Accuracy (recovery)

Accuracy was studied by evaluation on analytical recovery. Spiked samples were prepared by adding 10.00 µl of 50.00 and 100.00 pg mL^{-1} standard PTH solutions into microcentrifuge tube. Each tube was contained with 100.00 µL of AuNPs, 15.00 µL of antibody, 15.00 µL of NaCl and 10 µL of the blood sample. The measurement procedure is described in section 3.2.1.2 (3).

3.2.1.4.2 Precision (% RSD)

% RSD was considered for precision of the method. The reproducibility was studied by a series of ten repetitive measurements of 10 and 100 pg mL^{-1} PTH.

3.2.1.4.3 LOD and LOQ

The limit of detection (LOD) and the limit of quantitation (LOQ) were calculated by the calibration curve method using the following equations:

$$LOD = y_B + 3S_B$$

$$LOQ = y_B + 10S_B$$

Where y_B is intercepts of regression line and S_B is standard deviation of intercepts of regression line.

3.2.2 Determination of hydrogen peroxide

All chemicals are analytical reagent grade and deionized-distilled (DI) water from Zeneer up 900 (Human corporation, USA) was used throughout.

3.2.2.1 Chemical preparation

(1) Preparation of the solutions for preparation of bacterial cellulose

1.1) Hestrin-Schramm's medium [68]

Dissloved 10.xxxx g glucose, 2.5xxx peptone, 2.5xxx g of yeast extract, 1.35xx g Na_2HPO_4 and 0.6xxx g citric acid in 500.00 mL DI water and adjusted pH to 5.25 using 1 $molL^{-1}$ NaOH. The medium was separated into 5

Erlenmeyer flasks each flask was covered with cotton balls and then autoclaved at 121°C for 15 min. 5 mL of starter BC from coconut juice was added to each flask and kept for growing.

1.2) Erhan Zor's medium [26]

Dissloved 25.xxxx g glucose, 2.5xxx g of yeast extract, 2.5xxx g $(NH_4)_2SO_4$, 2.xxxx g KH_2PO_4 and 0.05xx g $MgSO_4 \cdot 7H_2O$ in 500.00 mL DI water and adjusted pH to 5.2 – 5.3 using 1 $molL^{-1}$ NaOH. The medium was separated into 5 Erlenmeyer flasks each flask was covered with cotton balls and then autoclaved at 121°C for 15 min. 5 mL of starter BC from coconut juice was added to each flask and kept for growing.

(2) **Preparation of the solutions for embedding of AuNPs on nanopaper**

2.1) Stock solution of 50 mmol L^{-1} $HAuCl_4$

Dissolving 1.97 g of $HAuCl_4 \cdot 3H_2O$ and adjust with DI water to 100.00 mL.

2.2) 0.75 mmol L^{-1} $HAuCl_4$

Pipetting an aliquot of 375 µL of the stock $HAuCl_4$ solution and making to 25.0 mL with water (freshly prepare).

(3) **Preparation of solutions for hydrogen peroxide determination**

1 – 20 % v/v H_2O_2 solutions were pipette from standard 35 % v/v H_2O_2 solution as in the table below and adjust with DI water to 100.00 mL.

Concentration of H_2O_2solution (% v/v)	Pipetted volume (mL)	Final concentration of standard H_2O_2 solution in 100.00 mL volumetric flask (mmol L^{-1})
35	2.86	1
	14.28	5
	28.57	10
	57.14	20

(4) **Preparation of wound cleaner samples**

All wound cleaner samples can use without any further purification.

3.2.2.2 Experiment

3.2.2.2.1 Preparation of bacterial cellulose nanopaper (BC)

(1) Study on effect of culture medium

There are 2 difference culture media were competed, Hestrin-Schramm's medium [68] and Erhan Zor's medium [26] respectively. BC in each medium was kept for growing for 6 days. The BC was then purified by soaking in 5 % w/w NaOH at ambient temperature for 24 h. and bleached in the mixture of 1 % w/w NaOH and 0.2 % w/v H_2O_2 at 80 °C for 1 h. Finally, the BC was washed with DI water several times until pH of washing water is nearly 6.0. Physical properties of the BC were then characterized using scanning electron microscope (SEM, FEI: QUANTA 250, USA). The criteria for choosing a suitable medium are growth rate and transparency of nanopaper.

3.2.2.2.2 Preparation of the AuNPs-BC nanopaper

Briefly, 25.0 mL of 0.75 mmol L^{-1} $HAuCl_4$ was boiled until 90 °C. Then, a piece of the purified wet BC nanopaper (30 mm ∅ and 3 mm thickness) was put into the boiled $HAuCl_4$ solution. This solution was continuously heated for 60 min under vigorous stirring. The AuNPs-BC nanopaper was washed with 20 mL water to removed excess $HAuCl_4$ before use. The wet as-prepared nanopaper was dried overnight (~12 h) at ambient temperature. The dried AuNPs-BC nanopaper was characterized using a UV-visible spectrophotometer and a Field Emission-Scanning Electron Microscope (FE-SEM) with an Energy Dispersive X-Ray Spectrometer (EDS), for evaluation of its absorption spectrum, morphology and Au^0 content, respectively.

3.2.2.2.3 Optimization study for the detection of H_2O_2

(1) Effect of pH of citrate buffer

The effect of pH of the citrate buffer solution was studied from pH 3.0 to 6.0 when the concentration of the buffer was kept at 20 mmol L^{-1}. A concentration of 30 % (v/v) H_2O_2 was studied. The ΔAbs at 525 nm ($Abs_{\textit{before dropping hydrogen peroxide}} - Abs_{\textit{after dropping hydrogen peroxide}}$) was calculated and was plotted against the investigated pH value.

(2) Effect of citrate buffer concentration

The effect of the concentration of citrate buffer was studied from 1 to 40 mmol L^{-1} when pH of the buffer was fixed at 6.0. A concentration of 30 % (v/v) H_2O_2 was investigated.

(3) Effect of incubation temperature

The effect of the incubation temperature was investigated from the ambient temperature (~ 25 °C) to 50 °C by using 20 mmol L^{-1} citrate buffer (pH 6.0).

(4) Effect of incubation time

The effect of incubation time was evaluated from 5 to 50 min when 20 mmol L^{-1} citrate buffer (pH 6.0) was exploited.

3.2.2.2.4 Study on analytical performances

(1) Determination of hydrogen peroxide in wound cleaner samples

The dried AuNPs-BC nanopaper was cut into a piece with dimension of 10 mm width x 25 mm length x 1 mm thickness. Aliquots of 400 µL of 20 mmol L^{-1} citrate buffer (pH 6.0) and 100 µL of standard H_2O_2 (or samples) were transferred onto the AuNPs-BC nanopaper. The nanopaper was then put in a plastic zip-lock bag and placed into the thermostat bath (40 °C) for 10 min. Later, the nanopaper was directly attached in front of the sample holder inside a UV-visible spectrophotometer. The absorbance readings at 525 nm of each nanopaper before and after dropping of H_2O_2 solution were recorded. Difference in the absorbances (ΔAbs_{525nm}) was evaluated. Calibration was constructed by plotting the ΔAbs_{525nm} against the concentrations of the standard solutions of H_2O_2

(2) Accuracy (recovery)

Accuracy was studied by evaluation on analytical recovery. Recovery study was carried out by spiking of the standard H_2O_2 solutions of 3 % (v/v) into wound cleaner samples, respectively.

(3) Precision (% RSD)

Precision of the developed method was studied by pipetting an aliquot of 100 µL of standard H_2O_2 (10 % v/v) onto 10 different sheets of the AuNPs-BC nanopapers. The RSD was calculated based on using the absorbance reading obtained by each nanopaper.

(4) LOD & LOQ

The limit of detection (LOD) and the limit of quantitation (LOQ) were calculated by the calibration curve method using the following equations:

$$LOD = y_B + 3S_B$$

$$LOQ = y_B + 10S_B$$

Where y_B is intercepts of regression line and S_B is standard deviation of intercepts of regression line.

3.2.3 Quality control of iodized table salts

All chemical solutions were prepared using deionized-distilled (DI) water throughout the experiment.

3.2.3.1 Chemical preparation

(1) Preparation of the solutions for the synthesis of gold nanocluster

1.1) 10 mmol L^{-1} tetrachloroauric (III) acid

Dissolve 0.0985 g of tetrachloroauric (III) acid and adjust to 25.00 mL with DI water.

1.2) 50 mg mL^{-1} bovine serum albumin

Dissolve 1.25xx g of bovine serum albumin and adjust to 25.00 mL with DI water.

1.3) 1 M sodium hydroxide

Dissolve 0.40xx g of sodium hydroxide and adjust to 10.00 mL with DI water.

(2) Preparation of solutions for the iodate determination

2.1) 200 mmol L^{-1} citrate – phosphate buffer pH 7.00

200 mmol L^{-1} citrate – phosphate buffer (pH 7.00) was-prepared by adding 0.1 mol L^{-1} citric acid in 0.2 mol L^{-1} disodium hydrogen phosphate. This solution was adjusted to a final pH of 7.00 by using either citric acid or disodium hydrogen phosphate and volume of the solution was adjusted to 100.00 mL by DI water.

2.2) 0.1 mol L^{-1} potassium iodide

Dissolve 0.1660 g of potassium iodide and adjust to 10.00 mL with DI water.

2.3) 1 mol L^{-1} sulfuric acid

Pipette 0.56 mL from stock 95 % sulfuric acid and adjust to 10.00 mL with DI water.

2.4) 10 mmol L^{-1} potassium iodate

Dissolve 0.0535 g of potassium iodide and adjust to 10.00 mL with DI water.

2.5) 0.005 – 0.10 mmol L^{-1} potassium iodate

Pipette from standard 10 mmol L^{-1} potassium iodate solution as in the table below and adjust with DI water to 10.00 mL.

Concentration of standard potassium iodate solution (mmol L^{-1})	Pipetted volume (µL)	Final concentration of standard potassium iodate solution in 10.00 mL volumetric flask (mmol L^{-1})
10	5	0.005
	10	0.010
	20	0.020
	30	0.030
	40	0.040
	50	0.050
	80	0.080
	100	0.100

(3) Preparation of salt and fish sauce samples

3.1) The solution salt samples were prepared by dissolved 10.xxxx g of each sample with DI water and adjusted to 100.00 mL.

3.2) Fish sauce samples were used without any sample pretreatment step.

3.2.3.2 Experiment

(1) Fabrication of the foldable PAD

Fig. 3.1 shows an image of the foldable PAD for membraneless gas-separation. The rectangular PAD (35 x 90 mm^2) was made of a laboratory filter paper No. 2 (Advantec, Taiwan). Two circular reservoirs with the same dimension (∅ = 9 mm i.d.) are assigned as the acceptor and the donor. The hydrophobic barrier (2 mm thick) of each reservoir was created by painting with a 1225 Faber-Castel permanent pen (Nanmee, Thailand) and a commercially available plastic template. The ink was dried at room temperature (1 min) for complete

evaporation of the ink solvent. A 3M™ two-sided mounting tape (2 mm thickness) was attached on top of the paper around the donor reservoir. This offers proximity mounting the acceptor and the donor after folding. It is also useful for preventing leakage of volatile analyte out of the PAD headspace.

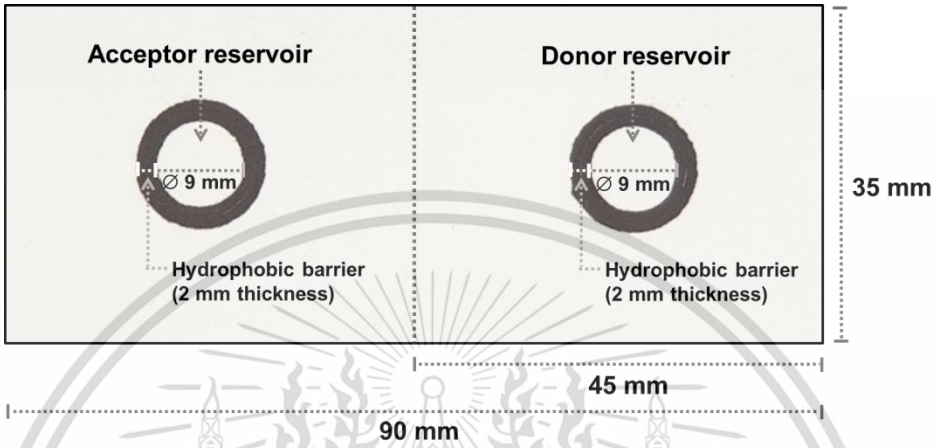

Figure 3.1 An optical image of the foldable PAD (with its dimensions) for membraneless gas-separation.

(2) Synthesis of gold nanoclusters

AuNCs were synthesized with some modification from Lei Y. *et al*. [49] At first, 2.0 mL of 10 mM $HAuCl_4$ was introduced into a dark bottle, followed by adding 2.0 mL of 50 mg mL^{-1} BSA and 0.2 mL of 1.0 mol L^{-1} NaOH. The solution was heated using a microwave oven at 100 watt for 9 min. The as-prepared AuNCs was kept in dark under 4 °C and were optical characterized by a spectrophotometer and a fluorometer.

(3) Analytical procedure for determination of iodate

An aliquot of 60 µL buffer pH 7.00 and 60 µL of 15.63 x 10^{-3} mmol L^{-1} AuNCs was dropped onto the acceptor side of the PAD. Later, 60 µL of tri-iodide from salt sample containing IO_3^-, 0.10 mol L^{-1} I^- and 1.00 mol L^{-1} H_2SO_4 were transferred onto the donor side. The PAD was then folded from left to right and mounted together by two pieces of 2 mm thickness adhesive tapes. After folding, head-space between both sides was generated. Iodine vapour is diffused from the donor side to react with AuNCs on the acceptor side. Then, fluorescence intensity and color intensity under UV irradiation of reacted AuNCs was measured within 15 min using fluorometer and captured by a smartphone, respectively.

3.2.3.3 Study on optimization conditions

3.2.3.3.1 Study on optimization conditions for synthesis of AuNCs

1) Study on effect of heating power

Heating power for synthesis of AuNCs was studied from 90 - 300 watt. Procedure for synthesis of AuNCs was the same as described above.

2) Study on effect of heating time

Heating time for synthesis of AuNCs was varied from 6 - 12 min. Procedure for synthesis of AuNCs was the same as described above.

3) Study on effect of albumin concentration

Effect of albumin concentration was studied from 30 - 80 mg mL^{-1}. Procedure for synthesis of AuNCs was the same as described above.

4) Study on effect of sodium hydroxide concentration

Effect of albumin concentration was studied from 0.25 - 3.00 mol L^{-1}. Procedure for synthesis of AuNCs was the same as described above.

3.2.2.3.2 Study on optimization conditions for determination of iodate

1) Study on effect of potassium iodide concentration

Potassium iodide concentration was studied form 0.01 – 1 mol L^{-1}. Detection procedure was the same as described above.

2) Study on effect of sulfuric acid concentration

Effect of H_2SO_4 concentration was studied from 0.10 - 1.50 mol L^{-1}. Procedure for iodate determination was the same as described above.

3) Study on effect of pH of buffer

pH of buffer was varied from pH 4 – pH 8. Detection procedure was the same as described above.

4) Study on effect of AuNCs volume

Effect of AuNCs volume was studied from 20 – 80 µL. Procedure for iodate determination was the same that described above.

5) Study on effect of buffer volume

Effect of buffer volume was studied from 20 – 80 µL. Procedure for iodate determination was the same as described above.

6) Study on effect of tri - iodide volume

Effect of tri - iodide volume was studied from 20 – 80 µL. Procedure for iodate determination was the same as described above.

7) Study on effect reaction time

Reaction time for iodate determination was studied from 5 – 20 min. Detection procedure was the same as described above.

3.2.3.4 Study on analytical performances

3.2.3.4.1 Accuracy (recovery)

Accuracy was studied by evaluation on analytical recovery. Recovery was measured by adding standard iodate solution to salt sample solution and fish sauce to obtain the final added concentration of 40 µmol L^{-1}. The experiment was carried out using spectrofluorometer as the detector.

3.2.3.4.2 Precision (% RSD)

% RSD was considered for precision of the method. Reproducibility was verified by applying 0.1 mmol L^{-1} iodate to 10 different PADs.

3.2.3.4.3 Selectivity

Selectivity was studied in the test tubes by adding 10 µL of 1 mM of each interference into the mixture solution of 10 µL of 0.10 M KI and 10 µL of 1 M H_2SO4 and the solution was incubated for 9 min. After that 10 µL of AuNCs was then added and adjusted with buffer solution pH 7.0 to 1.00 mL. The solution was kept in dark for reaction for 20 min and the fluorescence intensity of the solution was measured using spectrofluorometer.

3.2.3.5 Validation

The developed method was validated against iodometric titration method. Samples for validation were the same solution prepared in section 3.2.2.1 (3). The results were compared using ANOVA test.

Chapter 4
Results and Discussion

4.1 Clinical diagnosis of hyperparathyroidism

4.1.1 Characteristics of the as-prepared gold nanoparticles and their conjugation with antibody

Gold nanoparticles (AuNPs) were synthesized by the reduction of tetrachlorouric acid solution using sodium citrate as a reducing agent. The as-prepared AuNPs were then conjugated with antibody. Surface plasmon bands and TEM images of the non-conjugated AuNPs and the conjugated AuNPs are shown in Figure 4.1 and 4.2, respectively.

Results in Figure 4.1 show that the color of the non-conjugated AuNPs is red-wine and the maximum peak of the surface plasmon band is located at 521 nm. The result from TEM image also shows that shape of the non-conjugated AuNPs is spherical with an average size of 10.71 ± 4.64 nm.

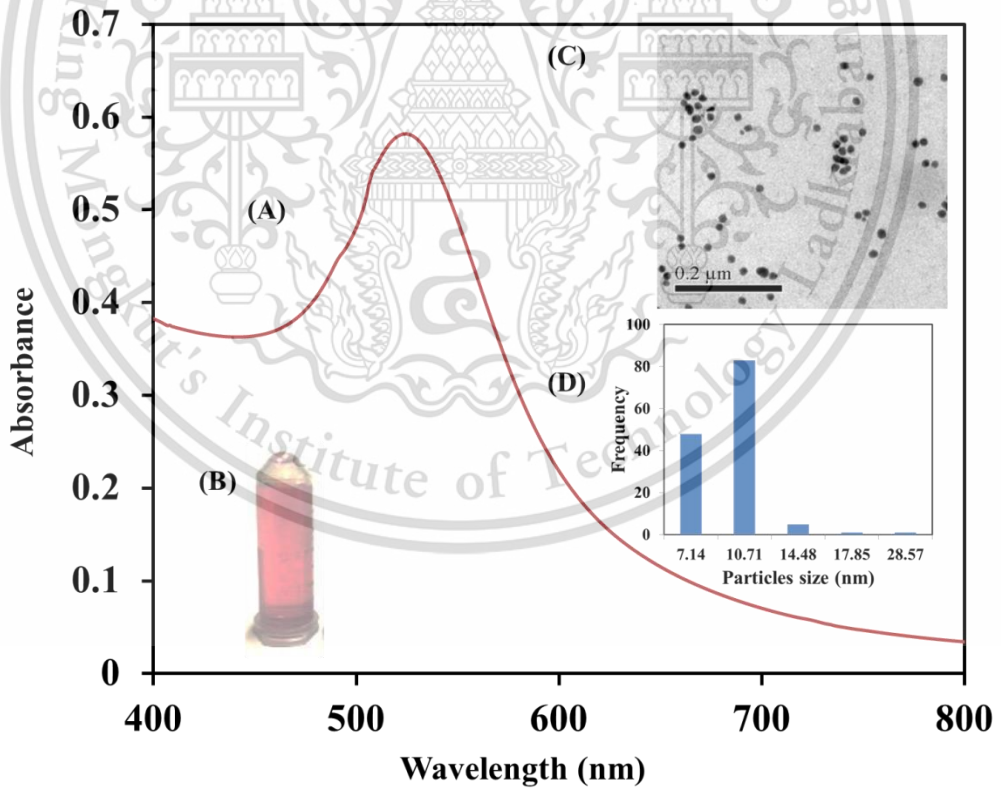

Figure 4.1 (A) surface plasmon band (B) color (C) TEM images of the as-prepared AuNPs and (D) size distribution of the as-prepared AuNPs.

After conjugation, the surface plasmon band is slightly shifted from 521 to 531 nm. TEM images before and after conjugation (Figure 4.2 (B) and (C)) also show that the size of particles are slightly bigger due to the interaction of the antibody and colloidal AuNPs. The antibody can be adsorbed on the surface of AuNPs by 3 phenomena: 1) hydrophobic attraction between antibody and NPs surface 2) interaction between negatively charged NPs and the positively charged site of antibody and 3) dative bonding between the metal and nitrogen and sulfur atom of antibody [69]. Interaction between AuNPs and antibody were shown in Figure 4.3.

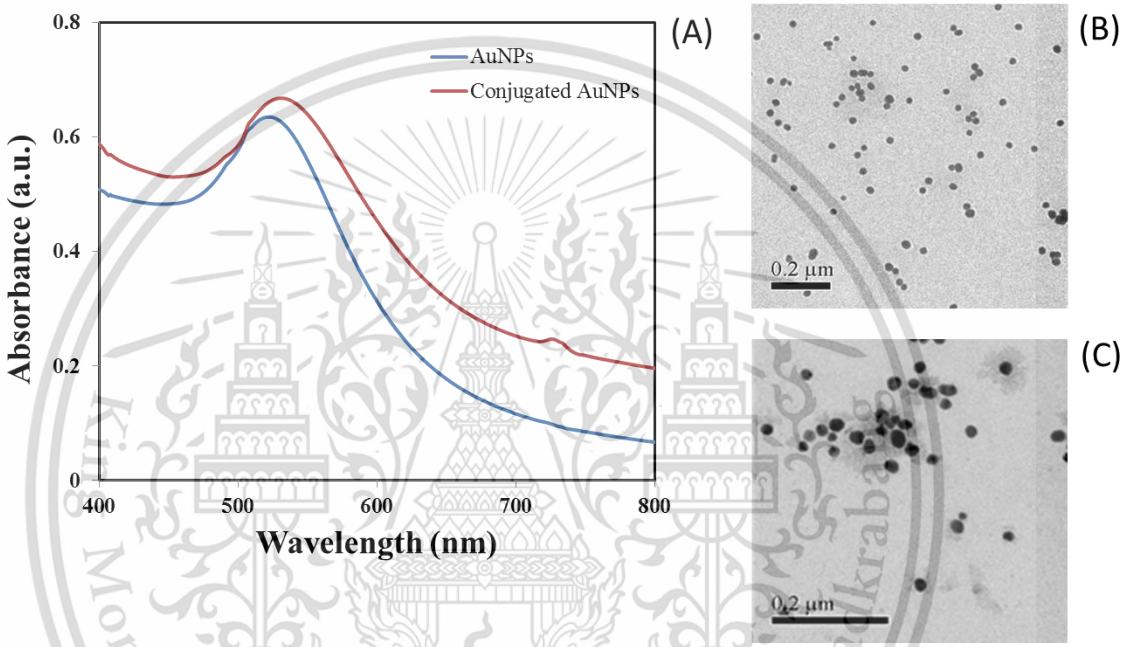

Figure 4.2 (A) surface plasmon bands of the conjugated AuNPs (B) and (C) TEM images of non-congugated AuNPs and conjugated AuNPs, respectively.

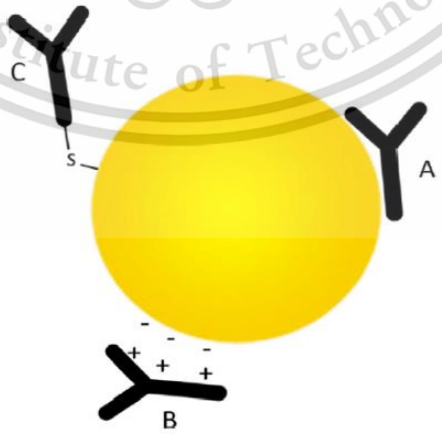

Figure 4.3 Hydrophobic and ionic interactions between antibody and gold nanoparticle surface. A) hydrophobic interaction B) ionic interaction C) a covalent bond is formed due to dative binding [70].

4.1.2 Preliminary results on the parathyroid hormone determination

The conjugated AuNPs solution was used for the parathyroid hormone (PTH) determination by adding individual concentration of standard PTH and the reaction was incubated for 1 hr. Results are shown in Figure 4.4.

Results show that absorbances of the AuNPs are decreased proportionaly to the concentration of PTH in the range of 10 – 1,000 pg mL^{-1} and the surface plasmon band is shifted to 541 nm because of interaction between carboxyl and amino group of PTH with the conjugated AuNPs. This results in aggregation of AuNPs.

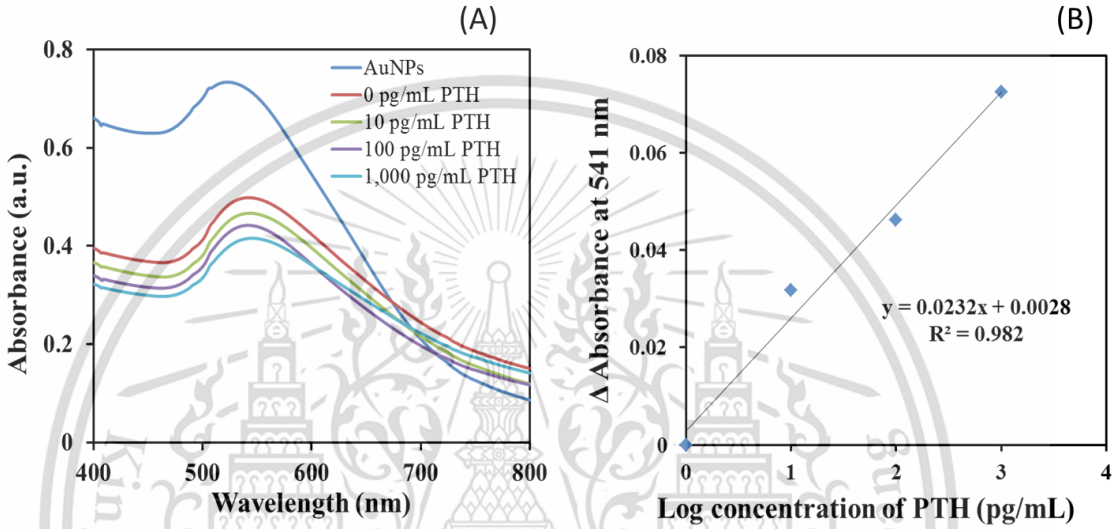

Figure 4.4 (A) spectra of AuNPS after interaction with PTH and (B) linear calibration for the PTH determination (from 10 – 1,000 pg mL^{-1} PTH).

4.1.3 Study on optimization conditions

4.1.3.1 Effect of pH of AuNPs on conjugation of antibody

The pH of gold nanoparticles solution was adjusted to finally pH 5 - 9 using 0.05 mol L^{-1} sodium hydroxide. The adjustment was carried out before conjugation with antibody. Critiria for selection of the suitable pH are based on the wavelength shift and the absorbance reading change. The pH that can maintain the red-wine color of the AuNPs solotion, without the changes of wavelength and the absorbance, is regarded as the optimal pH. Results are shown in Table 4.1 and Figure 4.5.

Results in Table 4.1, after the pH adjustment, maximum wavelength was not shift. The red-wine colored AuNPs solution was observed (Figure not shown). This confirms that self-aggregation of the nanoparticles were not occurred. After pH adjustment, the AuNPs were then conjugated with antibody. Results in Figure 4.5 show that the absorbance reading at pH 7.0 are not different. This also confirms that self-aggregation was not allowed. However, at lower or higher

pH values, the absorbance readings are strongly decreased. This is due to denature of antibody which can bring about precipitation of the nanoparticles.

Table 4.1 Maximum wavelength and absorbance of AuNPs before and after conjugation at difference pH.

pH	Maximum wavelength (nm)			Absorbance at 521 nm	
	Before pH adjusted	After pH adjusted	After conjugation	Before conjugation	After conjugation
5	521	521	534	0.60	0.31
6	521	524	533	0.62	0.48
7	521	522	531	0.63	0.66
8	521	522	539	0.82	0.36
9	521	521	533	0.84	0.66

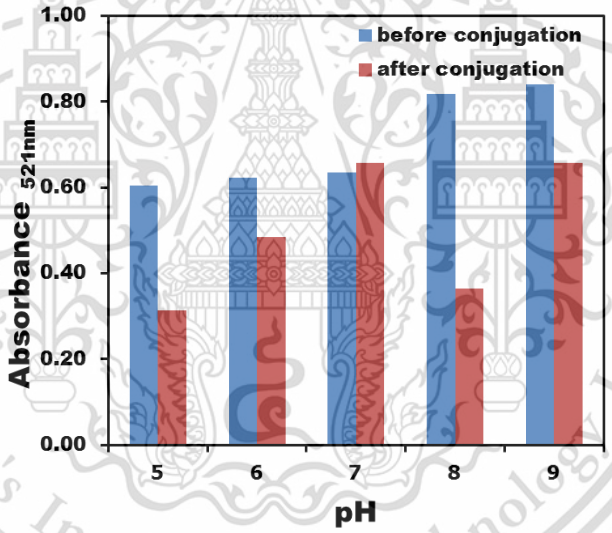

Figure 4.5 Absorbance of AuNPs at difference pH values between before and after conjugation.

4.1.3.2 Effect of antibody volume on conjugation of antibody

The effect of antibody volume on conjugation with AuNPs was studied from 0 - 20 µL. The minimum volume of antibody that can stabilize colloidal AuNPs form aggregation is considered as the optimum volume. Results are shown in Table 4.2 and Figure 4.6.

It is found from Figure 4.6 (A) that at 15 and 20 µL of antibody, $\Delta\lambda_{max}$ values are minimum. This refers to slightly shift of the maximum wavelength before and after addition of the antibody. This implies that self-aggregation was not

found. A volume of 15 µL was suitable as regarding in term of low reagent consumption.

Table 4.2 Maximum wavelength and absorbance of AuNPs before and after conjugation at difference antibody volume.

Antibody volume (µL)	Maximum wavelength (nm)		Absorbance at 521 nm	
	Before conjugation	After conjugation	Before conjugation	After conjugation
0	521	521	0.96	0.96
3	521	548	0.96	0.37
5	521	550	0.96	0.41
10	521	540	0.96	0.73
15	521	535	0.96	0.80
20	521	535	0.96	0.78

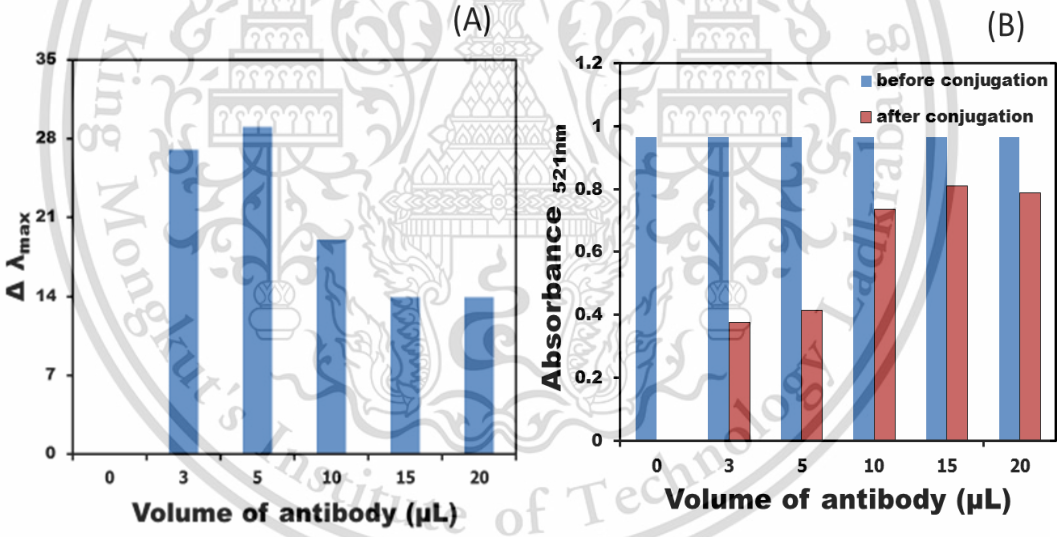

Figure 4.6 (A) Δ maximum wavelength and (B) absorbance of AuNPs after conjugation at difference antibody volumes.

4.1.3.3 Effect of reaction time

The effect of reaction time was studied from 30 min - 2 hr. Results are presented in Table 4.3 and Figure 4.7. Results from Table 4.3 and Figure 4.7 show that poor linearity (r^2 = 0.554) is observed at 30 min due to incomplete reaction. In contrast, good linearities are providing at 1 and 2 h (r^2 > 0.98). It is because the reactions reached the equilibrium. So, 1 h reaction time was selected.

Table 4.3 Maximum wavelength and absorbance of AuNPs at difference reaction time.

Concentration of PTH (pg mL^{-1})	Log concentration of PTH (pg mL^{-1})	Maximum wavelength (nm)			Absorbance		
		30 min	1 h	2 h	30 min	1 h	2 h
0	0	542	541	542	0.47	0.48	0.50
10	1	539	538	542	0.35	0.46	0.47
100	2	540	541	542	0.33	0.44	0.44
1,00	3	549	538	545	0.35	0.41	0.42

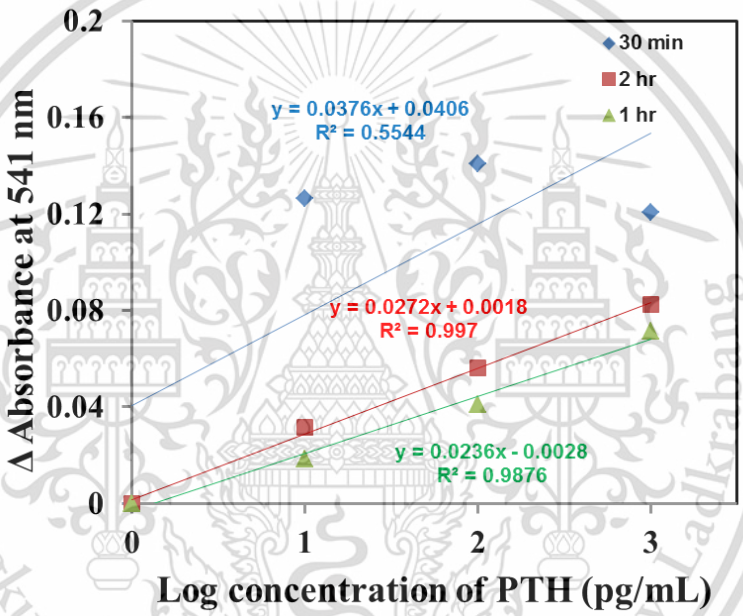

Figure 4.7 Linear calibrations at difference reaction times.

Optimum condition are summarized and shown in Table 4.4.

Table 4.4 Optimum condition for determination of PTH.

Condition	Studied range	Selected value
pH of AuNPs	pH 5 – pH 9	pH 7
Antibody volume	0 -20 µL	15 µL
Reaction time	30 min – 2 h	1 h

4.1.4 Analytical performances

4.1.4.1 Linear calibration

Under optimum conditions, the linear calibration between log of the concentration and Δ absorbance was plotted. It is found that, surface plasmon bands of AuNPs is decreased proportionally to PTH concentration and the color of the solution is changed from red to bluish-purple. This developed method can determine PTH concentration in the range of 10 – 1,000 pg mL^{-1} with good linearity. The results from TEM image is confirmed that after reaction, the AuNPs became aggregation.

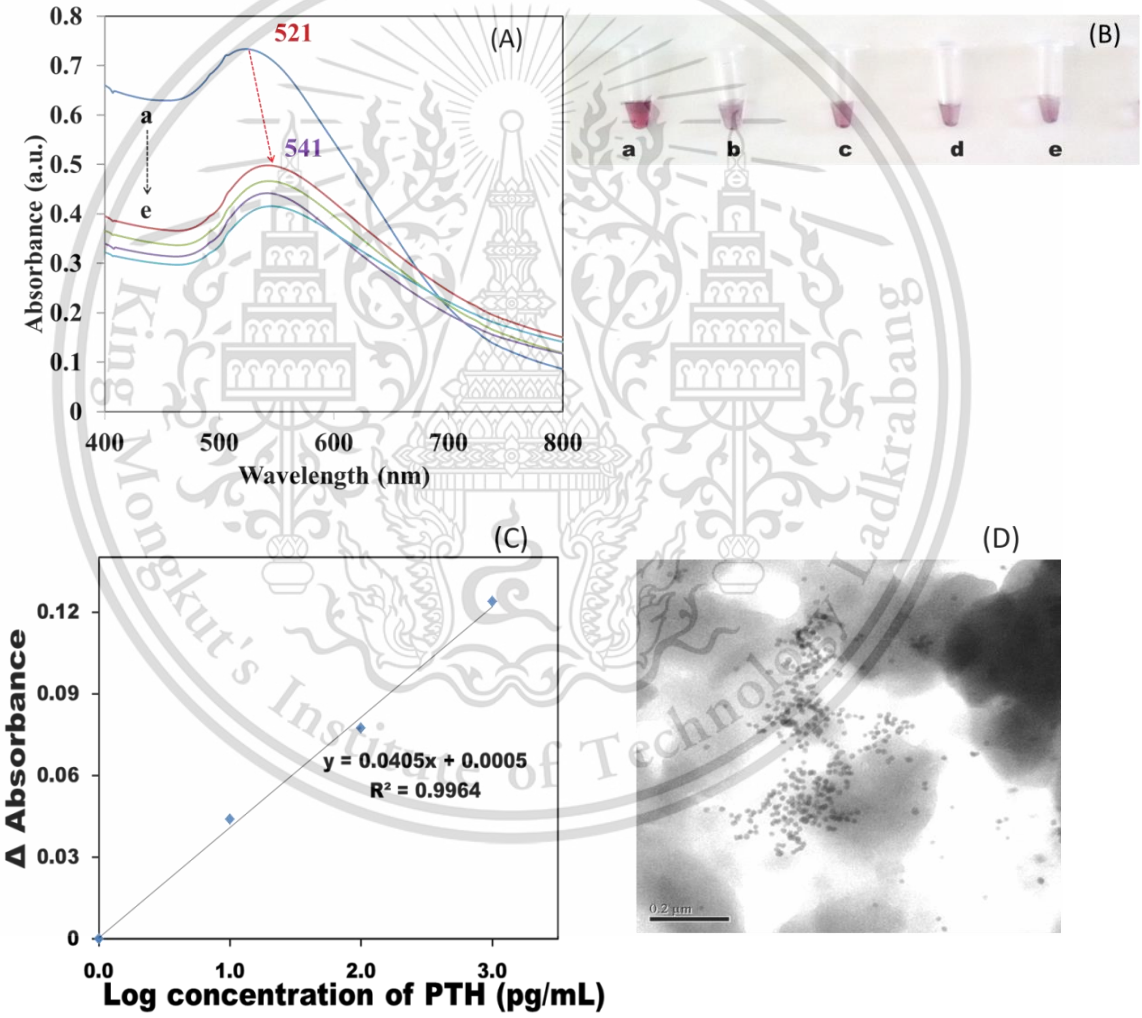

Figure 4.8 (A) spectra of AuNPs in the presence of various concentration of PTH ((a) pure AuNPs, (b) – (e) are the AuNPs in the presence of 0, 10, 100 and 1,000 pg mL^{-1}, respectively) (B) red wine to purple-colored solution of AuNPs and (C) linear calibration for PTH detection and (D) TEM image of AuNPs in the presence of PTH 100 pg mg^{-1}.

4.1.4.2 Accuracy (Recovery)

Accuracy was studied by evaluation on analytical recovery when mice blood samples were used. Results in Table 4.5. present that analytical recoveries are 98.36 and 104.94 %. This means matrix effect is not occurred.

Table 4.5 The recovery study of PTH determination.

Sample No.	Concentration of PTH (pg mL^{-1})			% Recovery
	Original	Added	Found	
S1	34.40	90.13	123.05	98.36
S2	19.05	57.54	79.43	104.94

4.1.4.3 Precision (% RSD)

% RSD was considered for precision of the method. The reproducibility was studied by a series of ten repetitive measurements of 10 and 100 pg mL^{-1} PTH. There are found that % RSD for 10 and 100 pg mL^{-1} PTH were 2.1 and 2.5 %, respectively. This implies that the method gave high precision.

4.1.4.4 LOD and LOQ

The limit of detection (LOD) and the limit of quantitation (LOQ) were calculated by the calibration curve method. This method provides LOD ($y_B + 3S_B$) of 1.7 and LOQ ($y_B + 10S_B$) of 5.7pg mL^{-1}.

Analytical performances are summarized and shown in Table 4.6.

Table 4.6 Summary on analytical performances of the developed method for the determination of PTH.

Performances	Value
Linearity range (pg mL^{-1})	10 – 1,000
Coefficient of determination (r^2)	0.9964
RSD (n = 10) at 10 and 100 pg mL^{-1} PTH (%)	2.1 and 2.5
Recovery (%)	98.4 – 104.9
LOD ($y_B + 3S_B$) (pg mL^{-1})	1.7
LOQ ($y_B + 10S_B$) (pg mL^{-1})	5.7

4.2 Determination of hydrogen peroxide

4.2.1 Preparation of bacterial cellulose nanopaper (BC)

4.2.1.1 Study on effect of culture medium

Effect of culture medium was studied by using 2 difference culture media, i.e. Hestrin-Schramm's medium and Erhan Zor's medium. The criterian for choosing suitable medium is its transparency. It is observed from Figure 4.9 that BC from Hestrin-Schramm's medium is pale milky-white and more transparence while the color of BC from Erhan Zor's medium was gray and turbid. Therefore, Hestrin-Schramm's medium is considered as suitable medium.

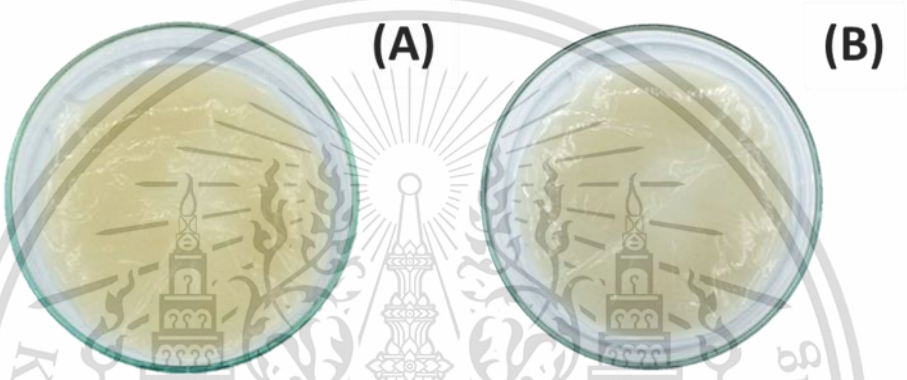

Figure 4.9 Optical image of BC obtained by difference culture medium: (A) Hestrin-Schramm's medium and (B) Erhan Zor's medium.

4.2.1.2 Physical characteristic of bacterial cellulose nanopaper (BC)

Physical characteristic of BC was studied using scanning electron microscope. Results are presented in Figure 4.10. The result reveals that structure of nanopaper is densely of fibers in submicro scale. Compared with Whatman filter paper no. 1, the size of filter paper was bigger. Therefore, the cellulose nanopaper was growth in nano - scale as expected.

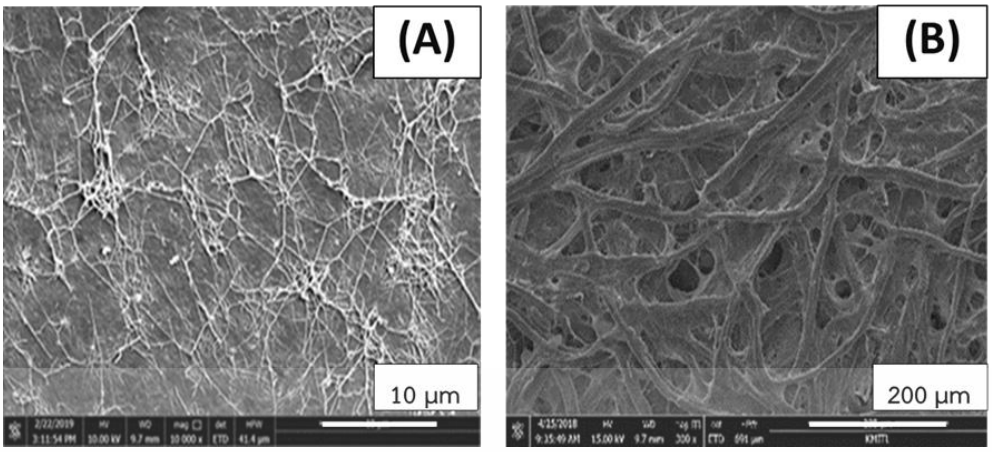

Figure 4.10 Scanning electron micrographs of (A) Bacterial cellulose nanopaper and (B) Whatman no. 1 filter paper.

4.2.2 Characterization of the AuNPs-BC nanopaper

The bare BC nanopaper exploited throughout this work was obtained using a bottom-up approach where the nanofibers were created by *Acetobactor xylinuim*, which synthesized cellulose and subsequently assembled bundles of cellulose nanofibrils. The bare BC nanopaper was used as both a reducing agent and a template for the preparation of the AuNPs-BC nanopaper. By this preparation, the penetrated Au (III) ions into the BC network were gradually reduced to the Au^0 nanoparticles due to the presence of hydroxyl groups on the surface of the bare BC nanopaper [71].

Figure 4.11A and 4.11B illustrate the photographic images of the wet bare BC nanopaper (after bleaching) and the dried AuNPs-BC nanopaper, prepared by this work, respectively. The color of the nanopaper is changed from milky-white to wine-red after the embedding process. The absorption spectra of these nanopapers were recorded by UV-visible spectrophotometer and were compared to the absorption spectrum of the colloidal AuNPs solution. Results in Figure 4.11C show that a shoulder peak at 525 nm is obtained by the AuNPs-BC while this shoulder is not appeared by the bare BC. This wavelength is the maximum absorption wavelength of the colloidal gold solution.

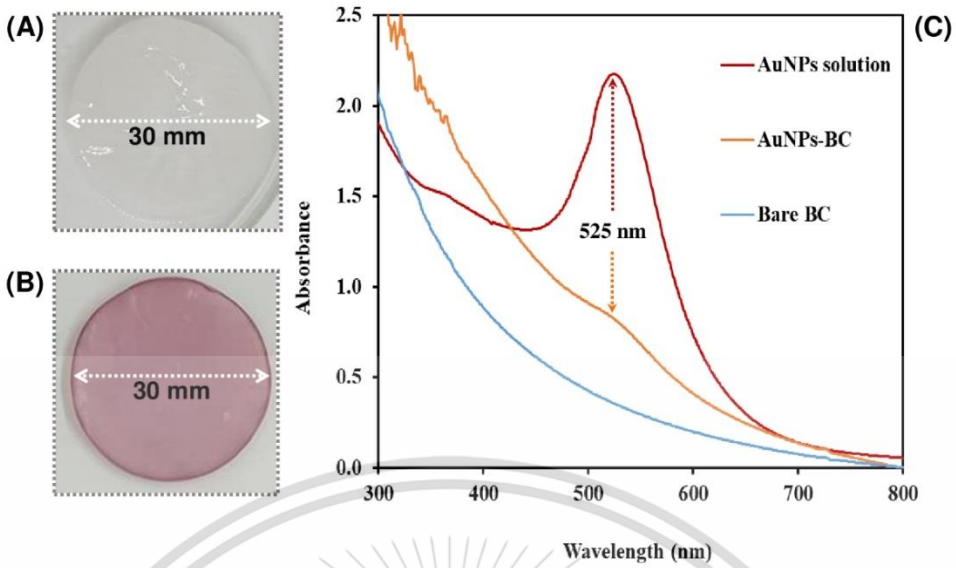

Figure 4.11 The photographic images of: (A) the wet bare BC nanopaper and (B) the dried AuNPs-BC nanopaper, synthesized using 0.75 mmol L^{-1} $HAuCl_4$ as the precursor solution. (C) The overlaid absorption spectra of 1.03 nmol L^{-1} of AuNPs solution, the dried AuNPs-BC nanopaper and the dried bare BC nanopaper.

. The nanopapers were further characterized by FE-SEM and EDS. The SEM images of the bare BC and the as-prepared AuNPs-BC nanopapers are presented in Figure 4.12A and 4.12B, respectively. Figure 4.12A shows that bundles of cellulose nanofibrils are observed. It is also clearly demonstrated in Figure 4.12B that Au° is occurred and is deposited onto the fibril of the nanopaper. Results by EDS in Figure 4.13 also reveal that the EDS line of Au^0 is existed and the Au^0 content of 97.3 weight % is found. These results confirm that the AuNPs-BC nanopaper was successfully prepared. However, the observed content of Au(0) is moderately high and is not represented for the Au(0) content of the whole nanopaper sheet. It is because the image of the as-prepared nanopaper was captured and then was focused especially on the area that there were a larger numbers of Au(0) nanoparticles, deposited in the BC nanopaper.

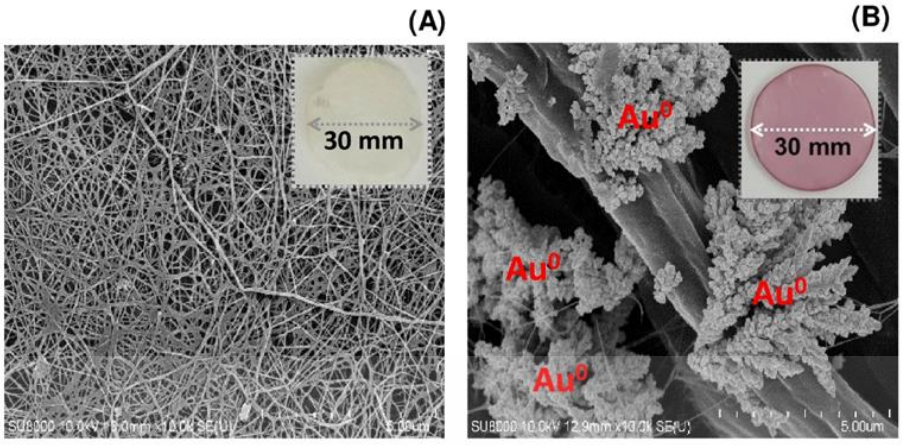

Figure 4.12 The SEM images of (A) the dried bare BC nanopaper and (B) the dried AuNPs-BC nanopaper, prepared when 0.75 mmol L^{-1} $HAuCl_4$ was used as the precursor.

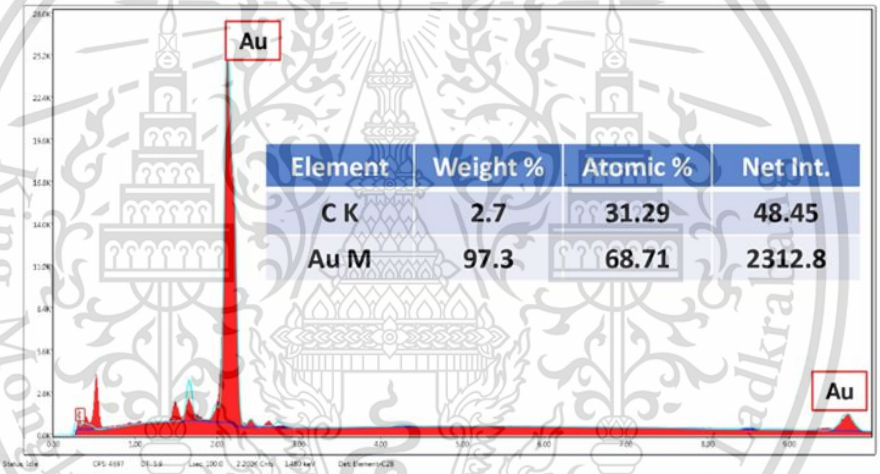

Figure 4.13 The EDS spectrum of the dried AuNPs-BC nanopaper and its corresponded Au^0 content obtained by the elemental analysis.

4.2.3 Optimization study for the detection of H_2O_2

4.2.3.1 Effect of pH of citrate buffer

The effect of pH of the citrate buffer solution was studied from the values of 3.0 to 6.0 when the concentration of the buffer was kept at 20 mmol L^{-1}. A concentration of 30 % (v/v) H_2O_2 was studied. The $\triangle$Abs of the nanopaper at 525 nm (Abs $_{before\ dropping\ hydrogen\ peroxide}$ – Abs $_{after\ dropping\ hydrogen\ peroxide}$) was calculated and was plotted against the investigated pH value. Results are shown in Figure 4.14 The $\triangle Abs_{525nm}$ is faintly increased when the pH value is increased. The low pH value can induce aggregation of gold nanoparticles which results in red shift of plasmonic absorption peak and decreasing in the absorbance reading at 525 nm [72,73]. As the pH value of 6.0 provides the highest signal, this value is selected

as the optimal pH value. Note that we also investigated the effect of the pH values from 7.0 to 9.0 using ammonium buffer (20 mmol L^{-1}). It was found that after dropping the buffer solution, the color of the AuNPs-BC nanopaper turned to dark purple. It might be because of the precipitation of colloidal gold nanoparticles at higher pH values [74].

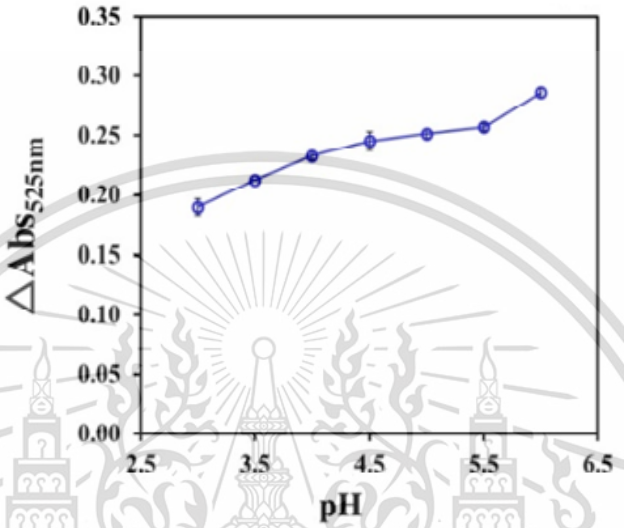

Figure 4.14 Effect of the pH solution of 20 mmol L^{-1} citrate buffer.

4.2.3.2 Effect of citrate buffer concentration

The effect of the concentration of citrate buffer was studied from 1 to 40 mmol L^{-1} when pH of the buffer was fixed at 6.0. A concentration of 30 % (v/v) H_2O_2 was investigated. Results in Figure 4.15 indicate that when the concentration of the buffer is increased from 1 to 20 mmol L^{-1}, the $\triangle Abs_{525nm}$ is also increased. At higher concentration, the $\triangle Abs_{525nm}$ is decreased. It was due to the self-aggregation effect of the AuNPs, induced by salt ions, existed in the buffer solution [75]. The concentration of 20 mmol L^{-1} is chosen as the highest signal is achieved.

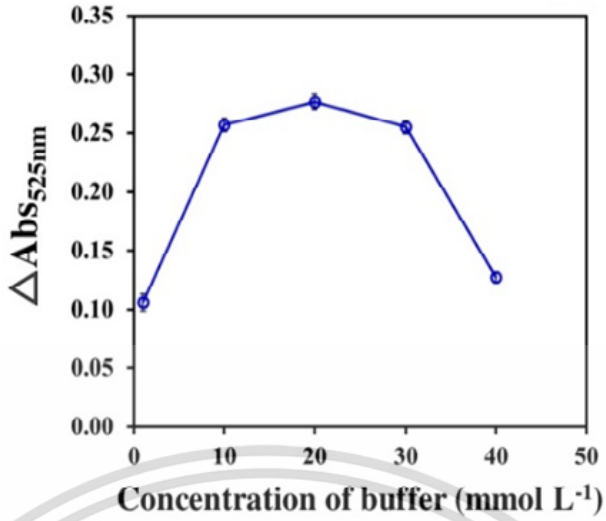

Figure 4.15 Effect of the concentration of the citrate buffer at pH 6.0.

4.2.3.3 Effect of incubation temperature

The effect of the incubation temperature was investigated from the ambient temperature (~ 25 ℃) to 50 ℃ by using 20 mmol L^{-1} citrate buffer (pH 6.0). Results in Figure 4.16 show that when the temperature is risen, the $\triangle Abs_{525nm}$ is increased up to 40 ℃. At higher temperature, the signal is decreased accordingly to the decomposition of H_2O_2 under too high temperature. Therefore, 40 ℃ is selected.

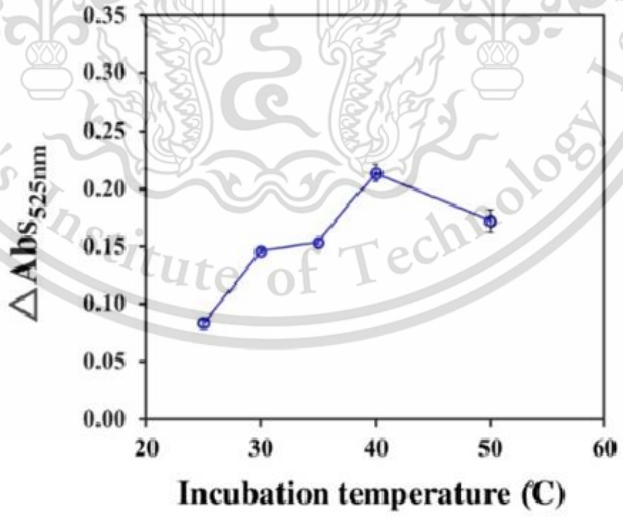

Figure 4.16 Effect of incubation temperature.

4.2.3.4 Effect of incubation time

The effect of incubation time was evaluated from 5 to 50 min when 20 mmol L^{-1} citrate buffer (pH 6.0) was exploited. Results in Figure 4.17 show that when the incubation time is increased to 10 min, the △Abs is dramatically increased. This implies that longer incubation time can result in higher sensitivity. However, the △Abs becomes stable and reaches its plateau after 10 min. As compromising between the sensitivity and the analysis time, the incubation time of 10 min is chosen as the optimal condition.

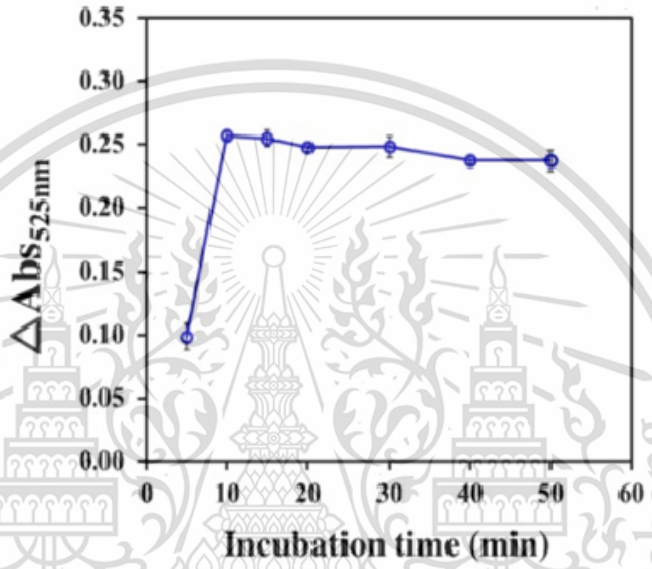

Figure 4.17 Effect of incubation time.

Summary of the studied ranges and the selected values for the detection of H_2O_2 were presented in Table 4.7.

Table 4.7 Summary on the optimization study for the spectrophotometric detection of H_2O_2 by the AuNPs-BC.

Parameters	Studied range	Selected value
pH of citrate buffer	3-6	6
Citrate buffer concentration (mmol L^{-1})	1-40	20
Incubation temperature (°C)	Ambient temperature - 50	40
Incubation time (min)	5-50	10

4.2.4 Analytical performances

4.2.4.1 Calibration curve and application to sample

When the concentration of H_2O_2 was increased, the wine-red color of the nanopaper was decreased as presented in Figure 4.18A. This result was clearly observed by naked eye. The calibration plot between the ΔAbs_{525nm} and the concentrations of the standard H_2O_2 solutions was presented in Figure 4.18B. The ΔAbs_{525nm} was increased when the concentration of the standard H_2O_2 was increased. The working range was observed from 1 - 20 % (v/v) with good linearity (r^2 = 0.984).

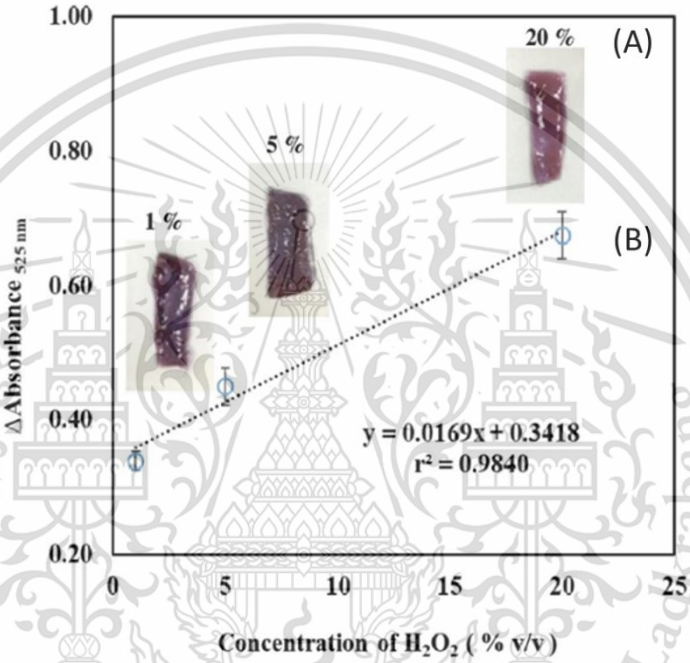

Figure 4.18 (A) The photographic images of the AuNPs-BC nanopaper in the presence of various concentrations of the standard H_2O_2. (B) An example of the linear calibration plot between the ΔAbs_{525nm} of the AuNPs-BC nanopaper and the concentrations of standard H_2O_2.

4.2.4.2 Accuracy (recovery)

Accuracy was studied by evaluation on analytical recovery. Results were shown in Table 4.8. It was found that the recovery was ranging from 90.2 - 97.2 %. This suggests that the developed method was free from the sample matrix effect.

4.2.4.3 Precision (% RSD)

Precision of the developed method was studied by pipetting an aliquot of 100 µL of standard H_2O_2 (10 % v/v) onto 10 different sheets of the AuNPs-BC nanopapers. The RSD was calculated based on using the absorbance reading obtained by each nanopaper. RSD of 3.3 % was obtained and this implies that the method provided high precision.

4.2.4.4 **Application to wound cleaner samples**

This developed method was applied for the spectrophotometric determination of H_2O_2 in wound cleaner samples. Results are summarized in Table 4.8. It was found that the calculated H_2O_2 concentrations in all samples are agreed well with the label concentrations with the relative error below than 8 %. This result indicates that the AuNPs-BC nanopaper provides high possibility to be applied as the 2D-microcuvette for the spectrophotometric determination of H_2O_2.

Table 4.8 Comparison of the H_2O_2 concentrations (% v/v) in samples.

Sample	H_2O_2 concentration (% v/v)		Relative error [a] (%)	Recovery (%)
	Label	This work (Mean ± SD)		
1	3	3.14 ± 0.03	4.6	97.0
2	3	2.84 ± 0.04	-5.4	95.1
3	3	2.78 ± 0.09	-7.2	90.2
4	3	2.79 ± 0.07	-6.9	97.2

Note: [a] Relative error was calculated as the following equation;

Relative error (%) = ((Calculated value – Label value) / Label value) x 100

4.2.4.5 LOD and LOQ

The limit of detection (LOD) and the limit of quantitation (LOQ) were calculated by the calibration curve method. This method provides LOD ($y_B + 3S_B$) of 0.79 and LOQ ($y_B + 10S_B$) of 2.19 % v/v.

Analytical performances are summarized and shown in Table 4.9.

Table 4.9 Summary on analytical performances.

Performances	Value
Linearity range (%v/v)	1 – 20
Coefficient of determination (r^2)	0.984
Recovery (%)	90.2 - 97.2
% RSD	3.3
LOD ($y_B + 3S_B$) (%v/v)	0.79
LOQ ($y_B + 10S_B$) (%v/v)	2.19

4.3 Quality control of iodized table salts

4.3.1 Fabrication of the foldable paper-based analytical device (PAD)

Fig. 4.19 shows an image of the foldable PAD for membraneless gas-separation. The rectangular PAD (35 x 90 mm^2) was made of a laboratory filter paper No. 2 (Advantec, Taiwan). Two circular reserviors with the same dimension (∅ = 9 mm i.d.) are assigned as the acceptor and the donor. The hydrophobic barrier (2 mm thick) of each reservoir was created by painting with a 1225 Faber-Castel permanent pen (Nanmee, Thailand) and a commercially available plastic template. The ink was dried at room temperature (1 min) for complete evaporation of the ink solvent. A 3M™ two-sided mounting tape (2 mm thickness) was attached on top of the paper around the donor reservoir. This offers proximity mounting the acceptor and the donor after folding. It is also useful for preventing leakage of volatile analyte out of the PAD headspace.

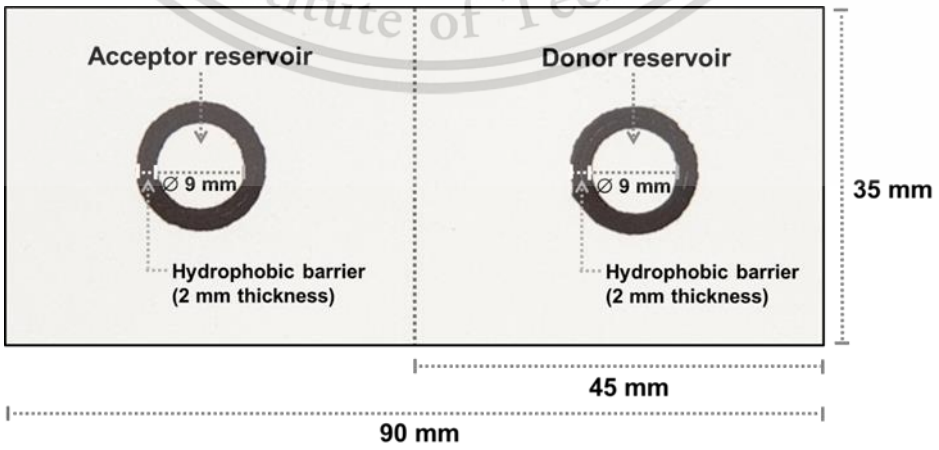

Figure 4.19 An optical image of the foldable PAD (with its dimensions) membraneless gas-separation.

4.3.2 Characteristic of gold nanoclusters

Gold nanoclusters (AuNcs) were synthesized by the reduction of tetrachlorouric acid solution using bovine serum albumin (BSA) as a reducing agent and stabilizing agent in basic medium. Then the properties of the as-prepared AuNCs were characterized using a spectrophotometer and TEM. Results are shown in Figure 4.20. Results reveal that the excitation and the emission wavelength are located at 490 and 630 nm, respectively. Color of the AuNCs solution is yellowish-brown and it appears pink emission under UV irradiation. Result from TEM image shown that the clusters consist of many gold atoms held together which average size is 3.7 ± 0.5 nm.

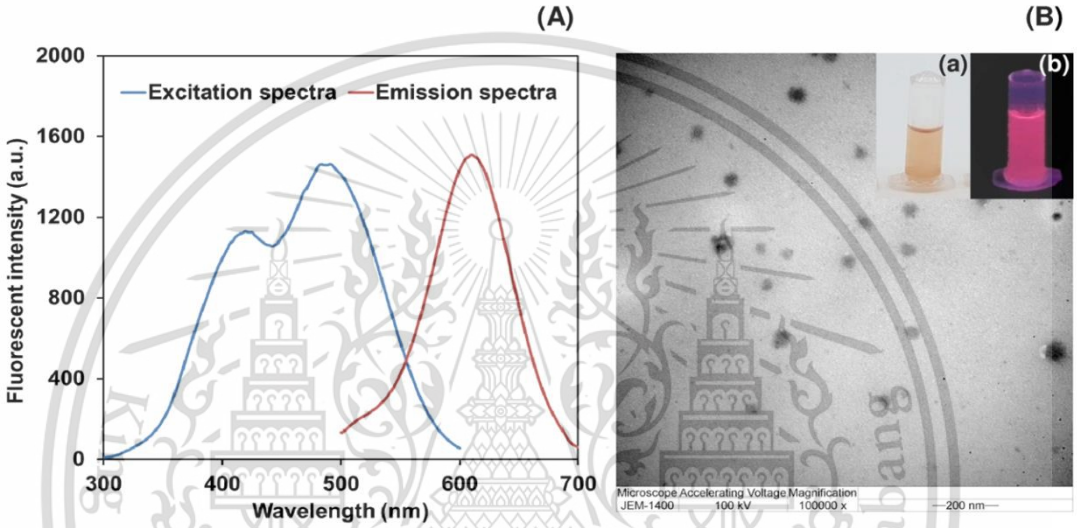

Figure 4.20 (A) Excitation and emission spectra and (B) TEM image of the BSA-AuNCs. Inset of Figure B is the photographic images of the BSA-AuNCs solutions: (a) without and (b) with UV irradiation, respectively.

4.3.3 Preliminary results for iodate determination

The PAD was then used for iodate determination based on quenching reaction of AuNCs in the present of iodate. The results are shown in Figure 4.21. Results show that fluorescence intensity of AuNCs is decreased proportional to the concentration of iodate in the range of 0.005 – 0.10 mM and the color of AuNCs under UV irradiation is changed from pink to blue. The reaction is based on quenching reaction between AuNCs and generated tri-iodide. Au (0) is converting to Au (I) and Au (III) by tri-iodide and resulted in decreasing of fluorescence intensity and fluorescence color under irradiation [66].

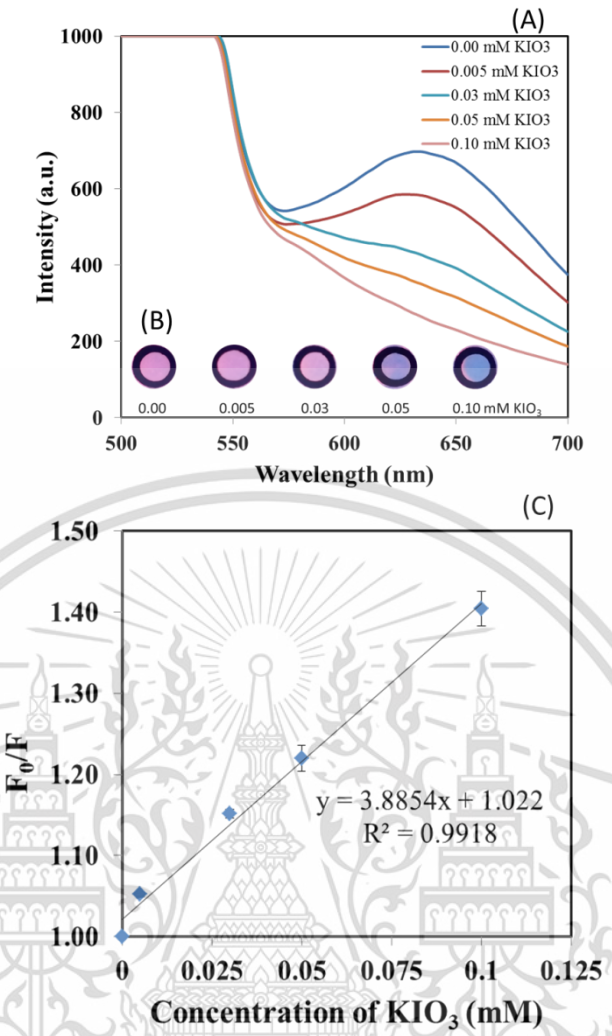

Figure 4.21 (A) spectra of AuNCs in the presence of various concentration of iodate (B) color of AuNCs in the presence of various concentration of iodate under UV irradiation and (C) Stern-Volmer's plot for iodate determination.

4.3.4 Study on optimization conditions

4.3.4.1 Study on optimization conditions for synthesis of AuNCs

1) Study on effect of heating power

Heating power for synthesis of AuNCs was studied from 90 - 300 watt. Results are shown in Figure 4.22. The fluorescence intensity of AuNCs solution is increased when heating power is increased and reached the maximum at 100 Watt. At heating power more than 100 Watt, fluorescent intensity was decreased because of too high heating power can cause overheating. Therefore, 100 Watt heating power is chosen.

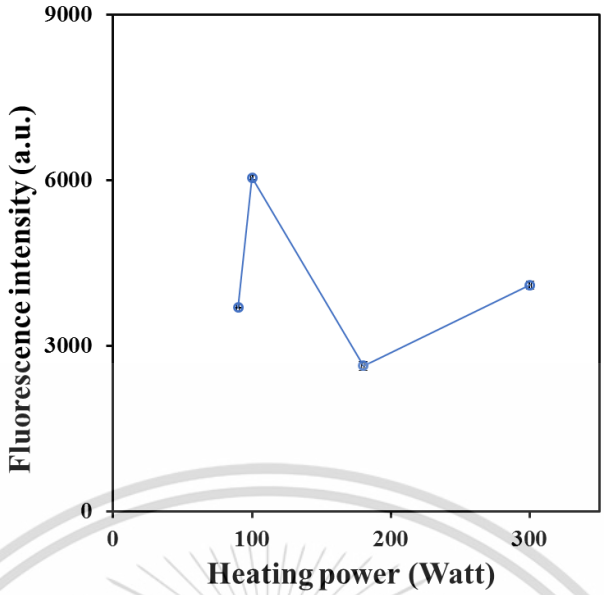

Figure 4.22 The fluorescence intensity of AuNCs at various heating power.

2) Study on effect of heating time

The effect of heating time was studied from 6 – 12 min. Results were shown in Figure 4.23. Results reveal that fluorescence intensity of AuNCs solution is increased and reached the maximum when heating time was increased to 6 min. At longer heating time, it was found that fluorescent intensity is decreased because of overheating. Moreover, BSA became flocculation and reduced its ability to use as reducing agent. Therefore, 6 min heating time is selected.

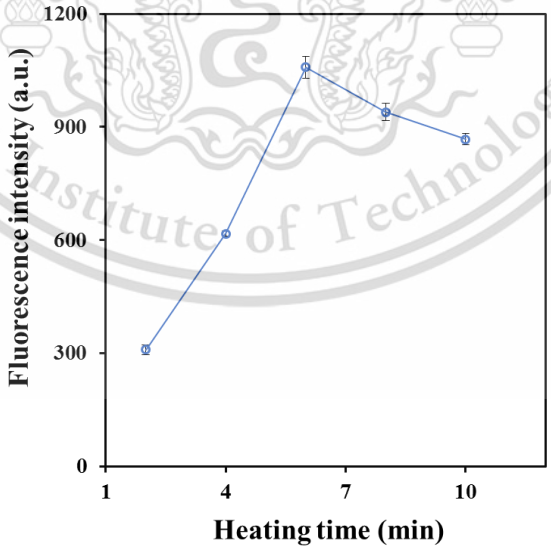

Figure 4.23 The fluorescence intensity of AuNCs at various heating time.

3) Study on effect of albumin concentration

Effect of albumin concentration was studied from 30 - 80 mg mL^{-1}. Results in Figure 4.24 show that the fluorescence intensity of AuNCs solution is slightly increased when albumin concentration is increased and reached the maximum at 50 - 65 mg mL^{-1}. Albumin acted as both stabilizing and reducing agent. Low concentration of albumin is not enough for synthesis of AuNCs and resulted in low fluorescence intensity. At too high concentration of albumin, it is found that fluorescent intensity is decreased because of flocculation of albumin. This can bring the solution unstable and precipitated. Therefore, albumin concentration of 50 mg mL^{-1} is selected.

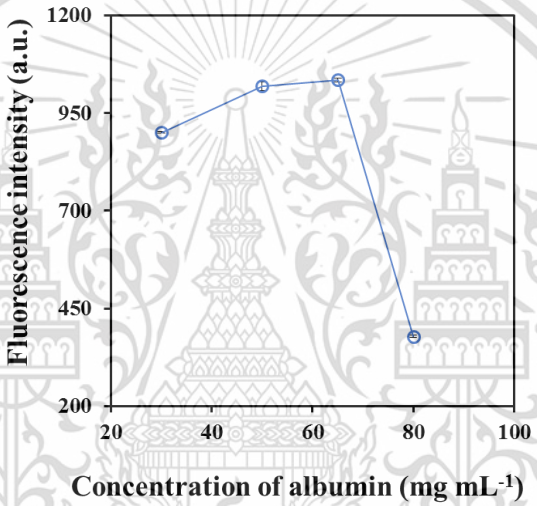

Figure 4.24 The fluorescence intensity of AuNCs at various albumin concentrations.

4) Study on effect of sodium hydroxide concentration

Effect of albumin concentration was studied from 0.25 - 3.00 mol L^{-1}. Results are illustrated in Figure 4.25. The fluorescence intensity of AuNCs solution is increased and reached the maximum when sodium hydroxide concentration is increased to 1 mol L^{-1}. It is because of phenolic group of tyrosine in albumin structure can reduce gold solution to become Au (0) in basic condition (pH > 10). Therefore, at low concentration of NaOH (pH < 10) is not enough to reduced gold solution. This resulted in low fluorescence intensity. At too high concentration of sodium hydroxide (> 1 mol L^{-1}), fluorescence intensity is decreased due to excess concentration of sodium hydroxide can quench the fluorescence intensity of AuNCs [64]. Therefore, in this work, 1 mol L^{-1} sodium hydroxide is chosen.

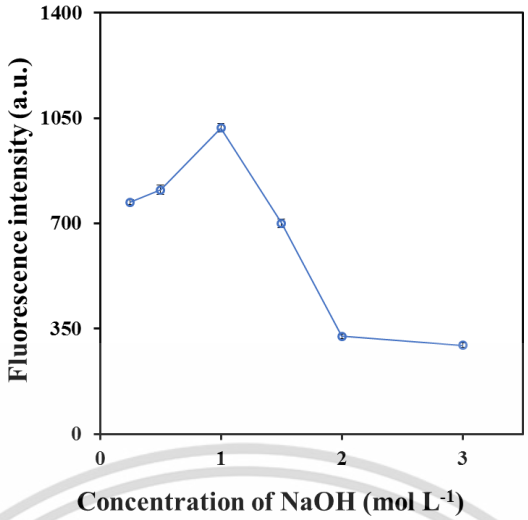

Figure 4.25 The fluorescence intensity of AuNCs at various sodium hydroxide concentrations.

Optimum condition for synthesis of AuNCs are summarized and shown in Table 4.10

Table 4.10 Optimum conditions for synthesis of AuNCs.

Parameter	Studied range	Selected value
Heating power	90 – 300 Watt	100 Watt
Heating time	6 – 12 min	9 min
Albumin concentration	30 – 80 mg mL^{-1}	50 mg mL^{-1}
Sodium hydroxide concentration	0.25 – 3.00 mol L^{-1}	1.00 mol L^{-1}

4.3.4.2 Study on optimization conditions for iodate determination

1) Study on effect of potassium iodide concentration

Potassium iodide concentration was studied form 0.01 – 1 mol L^{-1}. Results in Figure 4.26 indicate that sensitivity for iodate determination is increased when potassium iodide concentration is increased to 0.1 mol L^{-1}. The sensitivity become stable when the concentration of potassium iodide is higher than 0.1 mol L^{-1}. Therefore, 0.1 mol L^{-1} potassium iodide is chosen.

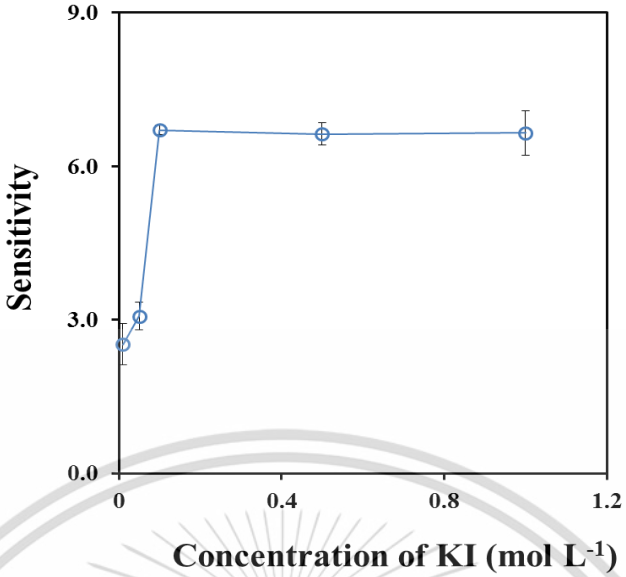

Figure 4.26 Sensitivity for the iodate determination at various potassium iodide concentrations.

2) Study on effect of sulfuric acid concentration

Effect of H_2SO_4 concentration was studied from 0.10 - 1.50 mol L^{-1}. Results are shown in Figure 4.27. The sensitivity for the iodate determination is increased when sulfuric acid concentration is increased to 1.0 mol L^{-1} because sulfuric acid can accelerate for generated of iodine. The concentration of 1.0 mol L^{-1} was chosen as a compromise between sensitivity and the amount of the acid used.

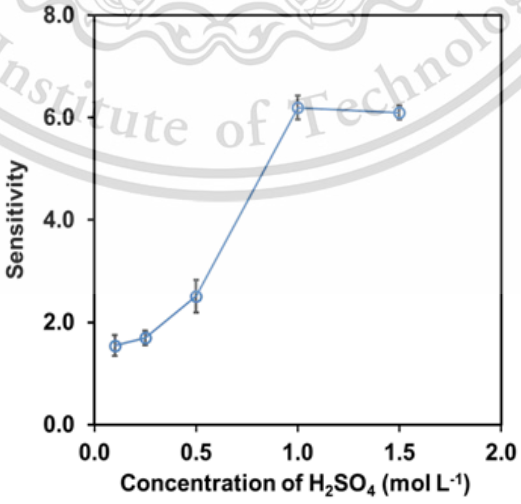

Figure 4.27 Sensitivity for the iodate determination at various sulfuric acid concentrations.

3) Study on effect of pH of buffer

pH of buffer was varied from pH 4 – pH 8. Results are shown in Figure 4.28. It was found that low sensitivity is observed at low pH values. This was due to BSA precipitation, causing aggregation of the nanoclusters. The highest sensitivity was found at pH 7.0, so this pH value was selected.

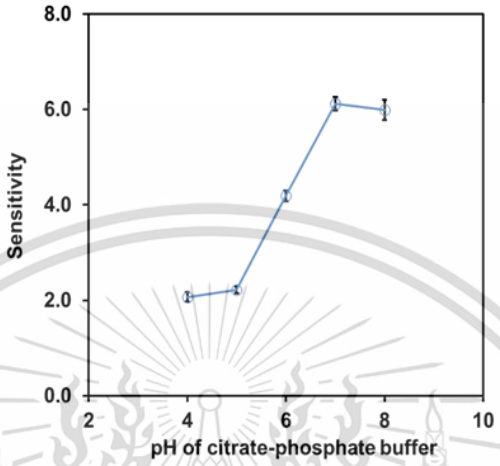

Figure 4.28 Sensitivity for the iodate determination at various pH of buffer.

4) Study on effect of AuNCs volume

Effect of AuNCs volume was studied from 20 – 80 µL. Results in Figure 4.29 show that sensitivity for the iodate determination is increased when AuNCs volume is increased. The sensitivity is decreased when AuNCs volume is greater than 60 µL due to the solution was over-flow from the reservoir. Thus, in this work, 60 µL of AuNCs volume was considered for suitable.

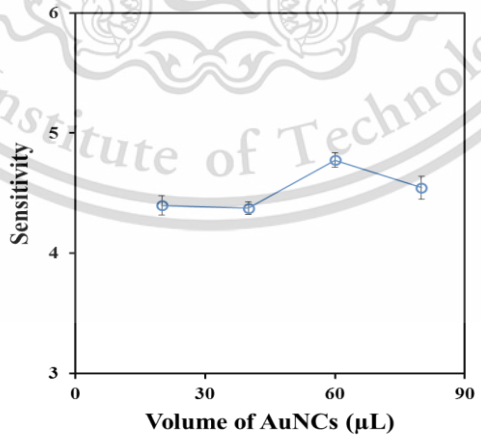

Figure 4.29 Sensitivity for iodate determination at various AuNCs volumes.

5) Study on effect of buffer volume

Effect of buffer volume was studied from 20 – 80 µl. Results are shown in Figure 4.30. The sensitivity for the iodate determination was increased when buffer volume was increased. The sensitivity was decreased when buffer volume was increased more than 60 µL due to the solution was over-flow from the reservoir. Iin this work, 60 µL of buffer volume was selected.

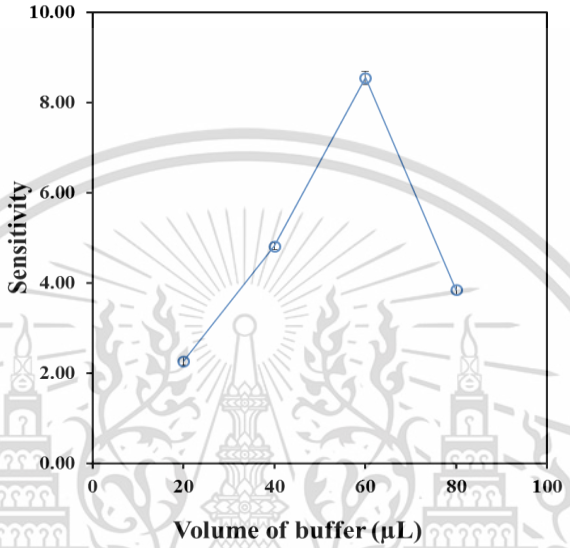

Figure 4.30 Sensitivity for the iodate determination at various buffer volumes.

6) Study on effect of tri - iodide volume

Effect of tri - iodide volume was studied from 20 – 80 µL. Results in Figure 4.31 reveal that sensitivity for the iodate determination was increased when tri - iodide volume was increased and then sensitivity was decreased when tri – iodide volume was increased at greater than 60 µL due to the solution was over-flow. Therefore, in this work, 60 µL of tri - iodide volume was chosen.

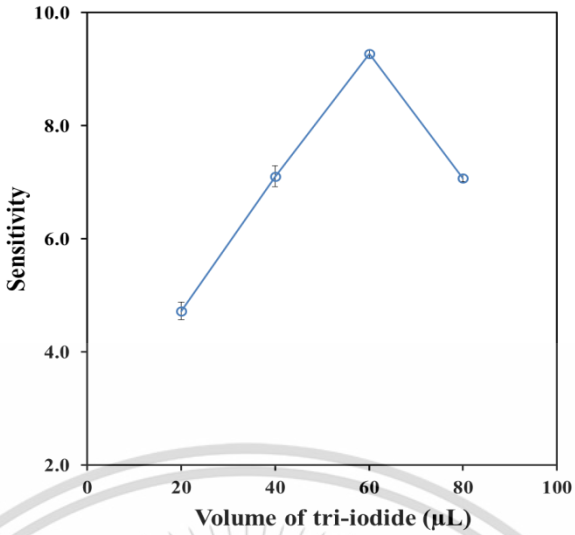

Figure 4.31 Sensitivity for the iodate determination at various tri - iodide volumes.

7) Study on effect of reaction time

Reaction time for the iodate determination was studied from 5 – 20 min. Results are shown in Figure 4.32. The sensitivity for the iodate determination was increased when reaction time was increased. Reaction time of 15 min is chosen as regarding in term of sensitivity and analysis time.

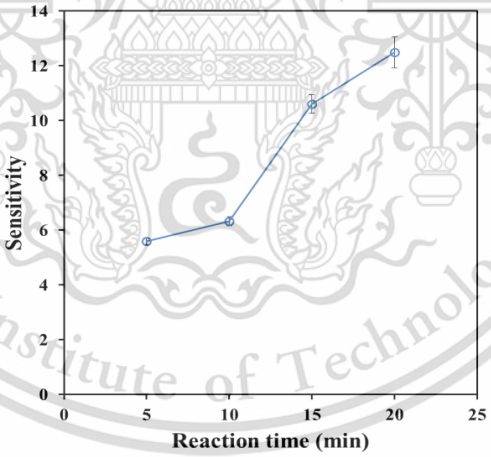

Figure 4.32 Sensitivity for the iodate determination at various reaction times.

Optimum condition for iodate determination are summarized in Table 4.11.

Table 4.11 Optimum conditions for the iodate determination.

Parameter	Studied range	Selected value
Concentration of KI (mol L^{-1})	0.01 – 1	0.1
Concentration of H_2SO_4 (mol L^{-1})	0.10 -1.50	1.0
pH of buffer	pH 4 - 8	pH 7
AuNCs volume (µL)	20 – 80	60
Buffer volume (µL)	20 – 80	60
Tri – iodide volume (µL)	20 – 80	60
Reaction time (min)	5 – 20	15

4.3.5 Calibration methods and their analytical characteristics

4.3.5.1 Linear calibration

Using the selected parameters in Table 4.11, two calibration plots were constructed for the different detection methods: (i) fluorometric detection using the PAD holder and (ii) image capture of the acceptor reservoir under UV light. The fluorescent spectra in Figure 4.33A show that the intensity decreased as the concentration of iodate increased. Results in Fig. 4.33B indicate that the F_0/F ratio values dramatically increased with increasing in the concentration of iodate from 0.005 to 0.1 mmol L^{-1}. However, the ratios slightly increased at the concentrations greater than 0.1 mmol L^{-1}. The calibration plot based on Stern-Volmer relationship (inset in Figure 4.33B) found linear dynamic range from 0.005 to 0.1 mmol L^{-1} iodate (r^2 > 0.99). For image capture, the color of the acceptor on the PAD, changed from red to blue, under UV irradiation, when the concentration of iodate increased (Figure 4.34A). Their corresponded RGB color intensities were evaluated through ImageJ™. The mean values of R and B intensities were found to decrease and increase, respectively, with increasing concentration of iodate whereas the mean G value remained almost constant. It was also observed that the ratio of the R/B intensity values decreased proportionally with iodate concentration and this ratio led to better linearity than both the R value alone and the R/G intensity ratios (Data not shown). Thus, the R/B intensity ratios were employed in constructing the calibration. Figure 4.34B shows that the ratios decreased as the concentrations increased and linearity range were found up to 0.1 mmol L^{-1} iodate (r^2 > 0.98, see inset in Figure. 4.34B). The other characteristics are summarized in Table 4.13. Reproducibility was verified by applying 0.1 mmol L^{-1} iodate to ten different PADs: the relative standard deviation (RSD) values were lower than 3.0 %, these implying high precision. The lower limits of detection of 0.005

mmol L^{-1} and 0.01 mmol L^{-1} were observed by fluorometric detection and image capture, respectively.

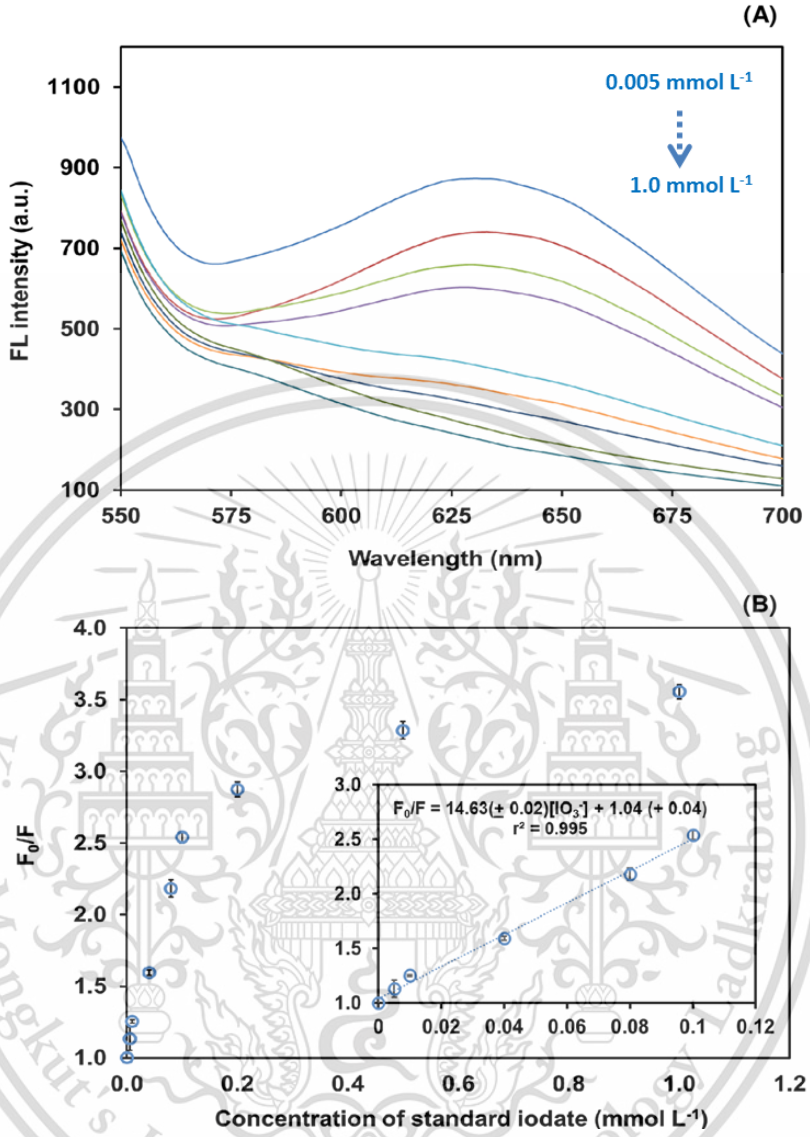

Figure 4.33 (A) Emission spectra of the BSA-AuNCs solution (λ_{ex}: 490 nm, λ_{em}: 630 nm) in the acceptor reservoir when applying different concentrations of standard iodate into the donor reservoir (from top to bottom: 0, 0.005, 0.01, 0.04, 0.08, 0.1, 0.2, 0.50 and 1.0 mmol L^{-1} iodate). (B) Corresponding Stern-Volmer plots.

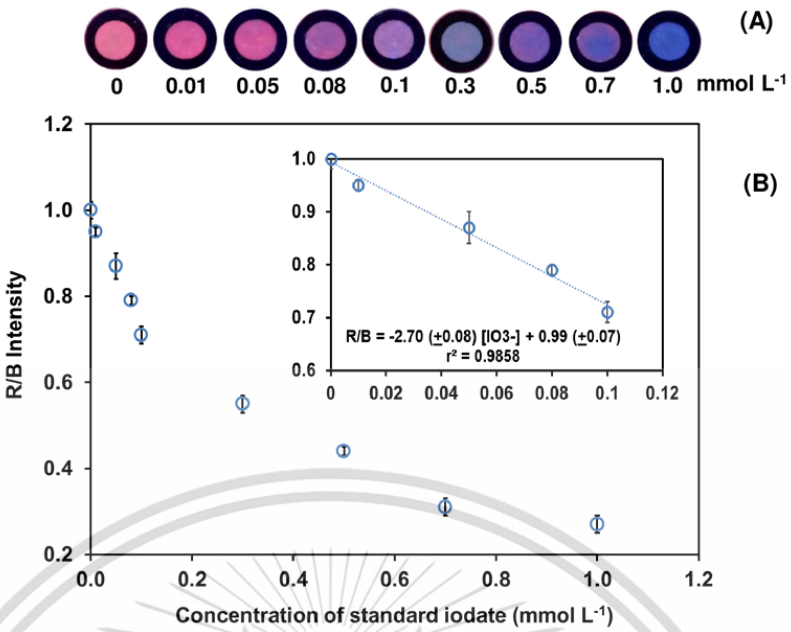

Figure 4.34 (A) The optical images of the BSA-AuNCs in the acceptor reservoir of the PAD under UV light after applying various concentrations of standard iodate solutions (0 – 1.0 mmol L^{-1}) into the donor reservoir. (B) The plots of the R/B color intensity ratios against standard iodate concentrations.

4.3.5.2 **Accuracy (Recovery)**

Accuracy was studied by evaluation on analytical recovery. Results were shown in Table 4.12. The recoveries were in the range of 90.5 to 102 %. Thus, the method was free from the sample matrix effect. These results confirm that, based on the merit of membraneless gas-separation, selective determination by the PAD is accomplished.

Table 4.12 Recovery of the developed PAD method for the determination of iodate in iodized salts and fish sauces.

Sample	Iodate content (μmol L^{-1}, mean ± SD, n = 3)			Recovery (%)
	Original	Added	Found	
S1	52.5 ± 1.08	40	91.2 ± 1.23	96.8
S2	59.4 ± 0.99	40	95.9 ± 1.92	91.3
S3	57.2 ± 1.10	40	93.9 ± 0.95	91.8
S4	61.2 ± 1.23	40	97.4 ± 1.09	90.5
F1	37.8 ± 1.34	40	78.4 ± 1.89	102
F2	41.2 ± 0.89	40	80.7 ± 0.98	98.8

Note: S1-S4 and F1-F2 are iodized salts and fish sauces, respectively.

4.3.5.3 Precision (% RSD)

Reproducibility was verified by applying 0.1 mmol L^{-1} iodate to ten different PADs: the relative standard deviation (RSD) values were 2.12 % and 2.87 % for using fluorometer and ImageJ™, respectively. These can imply that this method gave high precision.

Analytical performances are summarized and shown in Table 4.13.

Table 4.13 Summary on analytical performances

Performances	Value	
	Fluoroometer	ImageJ™
Linearity range (mmol L^{-1})	0.005 – 0.10	0.005 – 0.10
Coefficient of determination (r^2)	0.9975	0.9909
Recovery (%)	95 - 102	-
RSD (n = 10) (%)	2.12	2.87
LOD (mmol L^{-1})	0.005	0.01

4.3.6 Selectivity

The foreign ions which can be co-existed in salt sample were investigated. Results in Figure 4.35 (A) obviously show that only KIO_3 causes the solution color under UV irradiation changed from red to colorless and from Figure 4.35 (B) was found that the ratio of F/F_0 was decreased only when reacted with KIO_3. This implies that the AuNCs-paper-based device is more selective to the iodate measurement than the other investigated foreign ions.

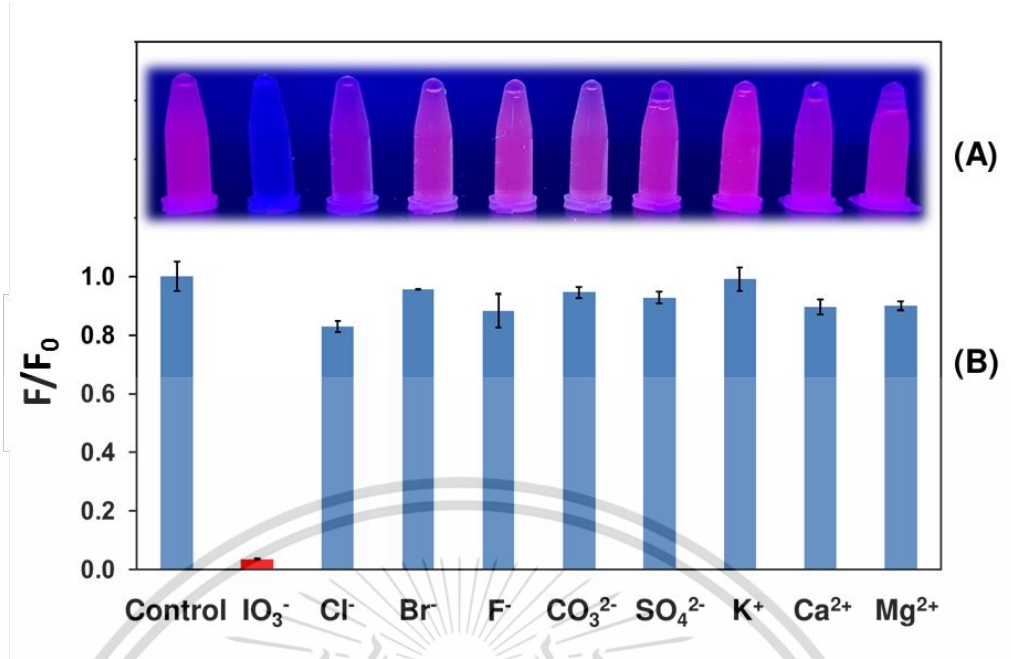

Figure 4.35 (A) The color of AuNCs solution under UV irradiation and (B) Comparison of the F/F_0 ratio, derived from adding of either 1 mM iodate or 1 mM foreign ions into the tube of AuNCs solution.

4.3.7 Application to real samples: validation

The developed method was applied to determination of IO_3^- in iodized-table salt samples and fish sauce samples. The results were validated against the contents determined by iodometric titration method. Their comparison are shown in Table 4.14 and Table 4.15.

Table 4.14 Comparison of the concentrations of iodate in iodized salts (as mg I $\cdot$ kg salt^{-1}), determined by this work and by iodometric titration.

Sample	Label	This work (Mean ± SD, n = 3)						Iodometric titration (Mean ± SD, n=3)		
		Fluorometric detection			Image capture					
S1	20	23.5	±	0.35	23.2	±	0.21	22.7	±	0.42
S2	20	21.3	±	0.44	23.6	±	0.18	22.3	±	0.10
S3	20	24.7	±	0.59	24.5	±	0.67	23.8	±	0.27
S4	30	32.1	±	0.26	31.4	±	0.35	31.9	±	0.27
S5	30	29.8	±	0.54	30.7	±	0.29	31.2	±	0.25
S6	30	32.4	±	0.41	33.1	±	0.73	32.2	±	0.24

Table 4.15 Summary on the iodate concentrations (as mg I L^{-1}) in fish sauces.

Sample	Label	Concentration of iodate (Mean ± SD, n = 3)		% Relative error	
		Fluorometric detection	Image capture	Fluorometric detection	Image capture
F1	3.0	2.88 ± 0.05	3.13 ± 0.04	- 4.0	4.3
F2	3.0	3.11 ± 0.07	3.06 ± 0.06	3.7	2.0

Note: Relative error was calculated as: Relative error (%) = ((Calculated value – Label value)/Label value) x 100

The iodate contents in salt samples in Table 4.14 are not significant difference amongst the compared methods by an ANOVA test (F_{stat}: 0.02, F_{cri}: 3.68, at 95 % confidence level). The developed PAD was then applied to fish sauces. As shown in Table 4.15, results agreed with claims on the manufacturers' labels, with relative error < 5 %. These results mean that our method offers high accuracy, when used with samples containing complicated matrices and without any sophisticated pre-treatment.

Chapter 5
Conclusions and Suggestions

5.1 Conclusions

5.1.1 Clinical diagnosis of hyperparathyroidism

The method for the determination of parathyroid hormone was successfully developed. Based on the aggregation of AuNPs in the presence of parathyroid hormone, the color of AuNPs was changed from red wine to bluish-purple. The developed method can measure parathyroid hormone levels in the range of 10 - 1,000 pg mL^{-1} and the developed method was successfully applied for the determination of parathyroid hormone in blood with satisfied accuracy (Recovery: 98.4 - 104.9 % and high precision (RSD: 2.1 – 2.5 %).

5.1.2 Quality control of hydrogen peroxide in wound cleaner samples

The AuNPs-BC nanopaper was successfully prepared. The bare BC nanopaper was exploited as both the reducing agent for conversion of Au (III) to become the gold nanoparticles (Au^0) and as the scaffold for Au^0. The AuNPs-BC nanopaper showed the characteristic absorption peak at 525 nm, similar to the characteristic peak obtained by the colloidal AuNPs solution. By the FE-SEM and EDS results, the Au^0 content was observed at 97.3 weight % in the as-prepared nanopaper. The AuNPs-BC nanopaper was effectively applied as the sensing platform and the 2D-microcuvette for the spectrophotometric measurement of H_2O_2 based on the simple redox reaction between the analyte and the embedded AuNPs in the nanopaper. The linear calibration plot between the $\triangle Abs_{525nm}$ ($Abs_{\textit{before dropping hydrogen peroxide}} - Abs_{\textit{after dropping hydrogen peroxide}}$) and the concentration of the standard H_2O_2 solutions was achieved up to 20 % (v/v). The developed method was successfully applied to determine the H_2O_2 contents in wound cleaner samples with high accurate and precise results.

5.1.3 Quality control of iodized table salts

This is the first time that a foldable PAD was reported for the effective analysis of analyte using the membraneless gas-separation idea. The donor and the acceptor reservoirs were located on the same paper device for ease-of-use. The hydrophobic barriers of the donor and acceptor reservoirs were simply and cost-effectively patterned by painting the paper using a permanent pen and a plastic template. After folding and mounting the donor and the acceptor, the air space in

between the reservoirs allowed effective separation of volatiles from the sample matrix without using an expensive gas-permeable membrane.

The PAD was efficiently demonstrated for the selective determination of the iodate contents in iodized salts and fish sauces. The samples were directly analyzed without any pre-treatment, excepting simple dissolution of the salts in water. As exploiting the PAD as the analytical platform, two detection methods, namely fluorometric detection and image capture were viable for the quantitative analysis of iodate. Using the BSA-AuNCs as the sensing probe, detection of iodate at 5.0 μmol L^{-1} was feasible. Calibration curves with good linearity ($r^2 > 0.98$) were observed up to 0.1 mmol L^{-1} IO_3^-. Our method was also successfully validated against the conventional iodometric titration.

5.2 Suggestions

5.2.1 Clinical diagnosis of hyperparathyroidism

1. All glassware, microcentrifuge tubes and DI water should be autoclaved to get rid of contamination.

2. For further study, the solution should be centrifuge and re-suspension to remove excess citric acid and unbound antibody before the determination of parathyroid hormone.

3. In the next study, the attempt to shorten the reaction time should be carried out.

5.2.2 Quality control of hydrogen peroxide in wound cleaner samples

1. Culture medium need to be autoclaved in order to removal of contamination.

2. In process of growing of BC, the flask should be kept in clean area and beware of impurity and fungus.

5.2.3 Quality control of iodized table salts

1. For AuNCs synthesis, BSA must be added to the solution slowly to prevent flocculation that decreases the property of BSA for act as a reducing agent.

2. After loading the tri-iodide solution, the PAD should fold and mount together immediately to prevent the loss of iodine vapor.

References

[1] Amra, B. 2019. "Different applications of nanomaterials and their impact on the environment." **SSRG International Journal of Material Science and Engineering (IJMSE).** 5(1) : 1-7.

[2] Lucas, F. de F., Gustavo H.C.V., Jorge G. dos S.B. and Ademar B.L. 2018. "An overview of the synthesis of gold nanoparticles using radiation technologies." **Nanomaterials.** 8(11) : 939-961.

[3] Lu, S., Ping, C. and Lie, L. 2016. "Enhanced molecular spectroscopy via localized surface plasmon resonance." Chapter 18. 383-404 in **Applications of Molecular Spectroscopy to Current Research in the Chemical and Biological Sciences.** InTech.

[4] Halawa, M.I., Lai, J. and Xu, G. 2018. "Gold nanoclusters: synthetic strategies and recent advances in fluorescent sensing." **Materials Today Nano.** 3: 9-27.

[5] Daniel, M.C., Amares, C., and Peng, Z. 2012. "Properties and applications of protein-stabilized fluorescent gold nanoclusters: short review." **Journal of Nanophotonics**. 6 : 064504-1- 064504-16.

[6] Online available: https://en.wikipedia.org/wiki/Parathyroid_hormone. Search: 19 June 2019.

[7] Online available: https://en.wikipedia.org/wiki/Parathyroid_gland. Search: 19 June 2019.

[8] Online available: https://www.assignmentpoint.com/science/biology/about-parathyroid-hormone.html. 19 June 2019.

[9] Online available: http://www.kamery-termowizyjne.co/ZXcvasMS/p/parathyroid-hormone-feedback-loop.html. Search: 19 June 2019.

[10] Ejigayehu, G.A. and Bart, L.C. 2017. "Review of Hypoparathyroidism." **Frontiers in Endocrinology**. 7 (172) : 1-7.

[11] Henry, G.B., William, H.S. and Charles,Y. C. P. 1977. "Diagnosis of hyperparathyroidism." **Annual Reviews of Medicine.** 28 : 111-117.

[12] Online available: https://en.wikipedia.org/wiki/Immunoassay. Search: 21 June 2019.

[13] Online available: https://microbiologyinfo.com/antigen-properties-types-and-determinants-of-antigenicity/ Search: 21 June 2019.

[14] Su, D.K., Ki-Roo, S. and Byoung-Tak, Z. 2004. "Molecular immunocomputing with application to alphabetical pattern recognition mimics the characterization of AB0 blood type." **IEEE Xplore.** 2549-2556.

[15] Online available: https://microbionotes.com/bonds-in-antigen-antibody-reaction/ Search: 21 June 2019.

[16] Nikita, H.P. 2015. "Basic principle, working and iInstrumentation of experimental Techniques." Chapter 2. 57-101 in Ph. D. Thesis / Sardar Patel University.

[17] Marĺa, T.J., Jose, M.B., Marĺa, L.G., Pau, M., Antonio, A., Manel ,P.D. and Anna. L. 2013. "Intact parathyroid hormone measurement at 24 hours after thyroid surgery as predictor of parathyroid function at long term." **The American Journal of Surgery**. 206 : 783-789.

[18] Esther, P.G.S, Jesús, M.F., Aurora, G.R., Bruno, M.T., Fernando, M. de P., M. Carmen, M.C., Virginia, M.A. and Susana, S.G. 2014. "Rapid intraoperative determination of intact parathyroidhormone during surgery for primary hyperparathyroidism. Experience at our center." **Endocrinogia Y Nutricion.** 61(1) : 3-8.

[19] Valerie, C., Noah, S., Michael, P. H., Martin, J.B., Michael, T., Elizabeth, M., Xun, Z., and Richard. J.P. 2008. "Cost savings associated with post-thyroidectomy parathyroid hormone levels." **Otolaryngology–Head and Neck Surgery**. 138 : 204-208.

[20] Dittmer, W.U., Kievit, P., Prins, M.W., Vissers, J.L.M., Mersch, M.E.C. and Martens, M.F.W.C. 2008. "Sensitive and rapid immunoassay for parathyroid hormone using magnetic particle labels and magnetic actuation." **Journal of Immunological Methods.** 338 : 40–46.

[21] Çiğdem, S.Ş, Münteha, N.S.K. and Mustafa, K.S. 2015. "A new immobilization procedure for development of an electrochemical immune sensor for parathyroid hormone detection based on gold electrodes modified with 6-mercaptohexanol and silane." **Talanta**. 144 : 210-218.

[22] Veronique, J., Jeroen, H.N., Jacco, P.H.F. van Son, Mike, F.W.C.M. and Joost, L. M. Vissers. 2011. "A fast intraoperative PTH point-of-care assay on the Philips handheld magnotech system." **Langenbeck's Archives of Surgery.** 396 : 337–343.

[23] Marika, K., Paul, C., Richard, D.V., Lily, L., Zengji, L., Xiaoyan, M. (Sharon), Steven, F. and Christopher, M.R. 2004. "Analysis of non-covalent aggregation of synthetic hPTH (1–34) by size- exclusion chromatography and the importance of suppression of non-specific interactions for a precise quantitation." **Journal of Chromatography B.** 810 : 151-155.

[24] Shaligram, S.R., Alkesh, A., Rustom, M. and Padmaja, P. 2012. "Development and validation of RP-HPLC and RP-UPLC methods for quantification of parathyroid hormones (1-34) in medicinal product formulated with meta-cresol." **Journal of Pharmaceutical Analysis**. 2(2) : 136–142.

[25] Erin, E.C., Mary, E.L., Jon, B., Sally, H., Cristina, L.Q., Norman, S., Kenneth, Eileen, F, and Elizabeth, T. 2013. "High sensitivity LC–MS/MS method for direct quantification of human parathyroid 1–34 (teriparatide) in human plasma." **Journal of Chromatography B**. 938 : 96-104.

[26] Erhan, Z. 2018. "Silver nanoparticles-embedded nanopaper as a colorimetric chiral sensing platform." **Talanta**. 184 : 149-155.

[27] Puji, L., Nitariani, E., Ani, S. and Yadi, S. 2014. "Study on the production of bacterial cellulose from *Acetobacter xylinum* using ago-waste." **Jordan Journal of Biological Science.** 7 : 75-80.

[28] Online available: https://en.wikipedia.org/wiki/Hydrogen_peroxide. Search: 10 January 2020.

[29] Hydrogen Peroxide, 3% w/w Safety Data Sheet according to Federal Register / Vol. 77, No. 58 / Monday, March 26, 2012 / Rules and Regulations.

[30] ISR-2600 for UV-2600/2700 ISR-2600Plus for UV-2600 "Integrating Sphere Attatachment" instruction manual, Shimadzu Corporation.

[31] Shuji, H. 1998. "Fundamental reaction mechanisms of hydrogen peroxide bleaching." **Japan Tappi Journal.** 52 : 595-607.

[32] Samira, A., Hamed, G.i, Arafeh, B. and M. Reza, H. 2018. "A rainbow ratiometric fluorescence sensor array on bacterial nanocellulose for visual discrimination of biothiols." **Analyst** 143 : 3415-3424.

[33] Nahid, P., Hamed, G., Tina, N. and Hossein, Y. 2015. "Green in-situ synthesized silver nanoparticles embedded in bacterial cellulose nanopaper as a bio nano composite plasmonic sensor." **Biosensors and Bioelectronic.** 74 : 353-359.

[34] Erhan, Z., Sabri, A., Aylin, A., Muhammed, E. S. and Haluk, Bingol. 2018. "Photoluminescent nanopaper-based microcuvette for iodide detection in Seawater." **Sensors and Actuators B: Chemical.** 254 : 1216-1224.

[35] Wen-Zhi, L., Chun-Yan, Y., Chih-Kai, L.,Yi-Huei, H., Cheng-Che, L. and Shao-Yi, H. 2018. "A colorimetric sensor for the detection of hydrogen peroxide using DNA-modified gold nanoparticles." **Journal of the Taiwan Institute of Chemical Engineers.** 89 : 49-55.

[36] Fang, W., Yanhua, D., Lu, F., Song, W., Sichun, Z., and Xinrong Z. 2011. "Horseradish peroxidase functionalized fluorescent gold nanoclusters for hydrogen peroxide sensing." **Analytical Chemistry.** 83 : 1193-1196.

[37] Yifan, W., Yanfang, G. and Jianxiu, D. 2019. "Bifunctional gold nanoclusters enable ratiometric fluorescence nanosensing of hydrogen peroxide and glucose." **Talanta.** 197 : 599-604.

[38] Mohammad, M. K. and Moo, H. C. 2018. "Positively charged gold nanoparticles for hydrogen peroxide detection." **Bio Nano Science.** 8: 537-543.

[39] Sophia, J. and Muralidharan, G. 2015. "Gold nanoparticles for sensitive detection of hydrogen peroxide: a simple non-enzymatic approach." **Journal of Applied ElectroChemistry**. 45 : 963-971.

[40] Wei, W., Tai-Ji, Z., De-Wen, Z., Hong-Yi, L., Yu-Rong, M., Li-Min, Q., Ying-Lin, Z. and Xin-Xiang, Z. 2011. "Amperometric Hydrogen Peroxide Biosensor Based on the Immobilization of Heme Proteins on Gold Nanoparticles-Bacteria Cellulose Nanofibers Nanocomposite." **Talanta**. 84(1) : 71-77.

[41] Zihao, L., Ruiyi, L., Guofeng, X., Tong, W. and Siyu, L. 2017. "A novel fluorometric and colorimetric sensor for iodide determination using DNA-templated gold/silver nanoclusters." **Biosensors and Bioelectronics**. 96 : 44-48.

[42] Umesh, K. 2007. "Health consequences of iodine deficiency." **Sultan Qaboos University Medical Journal.** 7(3) : 267-272.

[43] Online available: https://en.wikipedia.org/wiki/Congenital_iodine_deficiency_ syndrome. Search: 18 August 2019.

[44] J. Jerry, K. 2008. "Thyroid function." Chapter 20. 623-634 in **Clinical Biochemistry of Domestic Animals, 6th Edition.** Elsevier Inc.

[45] Online available: https://en.wikipedia.org/wiki/Iodometry

[46] Devi, D.L., Burkhard, R., J. Justin, G. and Edith, C. 2012. "Recent advances in paper-based sensors." **Sensors.** 12 : 11505-11526.

[47] Tugce, A., Basabe-Desmonts, L., Fernando B.L. 2018. "Review on microfluidic paper-based analytical devices towards commercialization." **Analytica Chimica Acta.** 101 : 1-17.

[48] "An Introduction to Fluorescence Spectroscopy." 2000. 1-36 PerkinElmer, Inc.

[49] Online available: https://en.wikipedia.org/wiki/Stern%E2%80%93Volmer_relation ship. Search: 23August 2019.

[50] Ibraheem, N.A., Hasan, M.M., Khan, R.Z. and Mishra, P.K. 2012. "Understanding color models : A Review." **ARPN Journal of Science and Technology**. 2(3) : 265-275.

[51] Ruiping, L., Pingping, X., Yifeng, T. and Jilin Y. 2016. "Albumin-stabilized gold nanoclusters as viable fluorescent probes in non-titrimetric iodometry for detection of oxidizing analytes." **Microchimica Acta.** 183 : 497-502.

[52] Kumar, S.D., Maiti, B. and Mathur, P.K. 2001. "Determination of iodate and sulphate in iodized common salt by ion chromatography with conductivity detection." **Talanta.** 53 : 701-705.

[53] Abdollah, S., Abdollah, N. and Mohammad, G. 2007. "Amperometric detection of nitrite, iodate and periodate at glassy carbon electrode modified with catalase and multi-wall carbon nanotubes." **Sensors and Actuators B.** 123 : 530–537.

[54] Wang, H.J., Cheng, N.N., Yang, X.Y., Li, X.M. and Zhu, L.D. 2013. "Highly sensitive and selective amperometric sensor for iodate based on 9,10-phenanthrenequinone derived graphene." **Chemical Research in Chinese Universities.** 29(1) : 132-138.

[55] Narayana, B., Chand, P., Tom, C. and Mendalin, M. 2006. "Spectrophotometric method for the determination of iodate using methylene blue as a chromogenic reagent." **Bulletin of the Chemical Society of Ethiopia.** 20(1) : 143-147.

[56] Ai-Hui, L., Zhi-Liang, J., Biao-Ming, Z., Qing-Ye, L., Jie, L. and Xi, L. 2005. "A new resonance scattering spectral method for the determination of trace amounts of iodate with rhodamine 6G." **Analytica Chimica Acta**. 530 : 131–134.

[57] Choengchan, N., Uraisin, K., Choden, K., Veerasai, W., Grudpan, K. and Nacapricha, D. 2002**.** "Simple flow injection system for colorimetric determination of iodate in iodized salt." **Talanta**., 58 : 1195-1201.

[58] Choengchan, N., Lukkanakul, K., Ratanawimarnwong, N., Waiyawat, W., Wilairat, P. and Nacapricha, D. 2003. "Use of pseudo-first order kinetics in flow injection for determination of trace inorganic iodine." **Analytica Chimica Acta**. 499 : 115-122.

[59] Nicholas, M.M., Emalee, N.K. and Marya, L. 2015. "Lab on paper: Iodometric titration on a printed card." **Analytical Chemistry**. 87 : 3764-3770.

[60] Marina, O.G., Anastasiya, A.B., Margarita, S.K., Vladimir, V.A., Aleksei, A.F., Alexey, V.G. and Stanislava, G.D. 2019. "Determination of iodide based on dynamic gas extraction and colorimetric detection by paper modified with silver triangular nanoplates." **Microchemical Journal**. 145 : 729-736.

[61] Saravanan, G., Seshadri, R.A., Buddolla, V., Jongsung, K. and Kyusik, Y. 2017. "Fluorescent Gold Nanoclusters for Selective Detection of Dopamine in Cerebrospinal fluid." **Scientific Reports.** 7 : 1-12.

[62] Krishnendu, C., Chiung, W.K., Ann, C. and Peilin, C. 2015. "Detection of residual rifampicin in urine via fluorescence quenching of gold nanoclusters on paper." **Journal of Nanobiotechnology**. 13(46) : 1-9.

[63] Pingping, X., Ruiping, L., Yifeng, T. and Jilin, Yan. 2015. "A gold nanoclusters-based sensor for sensitive uric acid detection." **Talanta**. 144 : 704-709.

[64] Lei, Y., Yuqing, C., Baozhan, Z., Hongyan, Y., Yong, G., Dan, X. and Martin M.F.C. 2011. "Microwave-assisted synthesis of BSA-stabilized and HSA-protected gold nanoclusters with red emission." **Journal of Materials Chemistry**. 22 : 1000-1005.

[65] Zhao, T., Xuan, Z.Q., Wan, A. and Gui, R. 2016. "Bovine serum albumin template synthesis of fluorescent gold nanoclusters for nitric oxide detection in vitro." **Material Technology**. 31 : 341-347.

[66] Ruiping, L., Pingping, X., Jun, F., Junwei, D., Yifeng, T. and Jilin, Y. 2014. "Sensitive iodate sensor based on fluorescence quenching of gold nanocluster." **Analytica Chimica Acta**. 827 : 80-85.

[67] Xue-Ling, C., Ya-Nan, L., Li-Li, L., Yu-Qing, W. and Da-Wei L. 2015. "Selective detection of iodine/iodide using BSA-stabilized gold nanoclusters-based fluorescence probe." **Chemistry Letters**. 44 : 1392-1394.

[68] Hestrin, S. and Schramm, M., 1945. "Synthesis of Cellulose by Acetobacter xylinum." **Biochemical Journal**. 58(2): 345-352.

[69] Ying, W., Lifang, W., Jianwei, Z., Guangxi, W., Wenbi, C., Lin, C. and Xilin, Z. 2014. "Preparation of colloidal gold immunochromatographic strip for detection of paragonimiasis skrjabini." **Plos One**. 9 : 1-6.

[70] Mir, H.J., Hamed, A., Ali, A.P., Hamidreza, P.T., Bijan, S. 2016. "Various methods of gold nanoparticles (GNPs) conjugation to antibodies." **Sensing and Bio-Sensing Research.** 9 :17-22.

[71] Eden, M.N., Hamed, G., Tina, N., Hossein, Y., Uliana, K., Daniel, H., Nahid, P. and Arben, M., 2015. "Nanopaper as an Optical Sensing Platform." **ACS Nano**., 9: 7296 - 7305.

[72] Park, S.H., Lee, W.J., Park, S.M, Choi, D.W., Kim, S.J. and Park, N.Y., 2019. "Reversibly pH-responsive gold nanoparticles and their applications for photothermal cancer therapy" **Sciencetific Reports**. 9: 1-9.

[73] Zhu, J., Li, W.B., Zhu, M., Zhang, W., Niu, W.C. and Liu, G.H., 2014. "nfluence of the pH value of a colloidal gold solution on the absorption spectra of an LSPR-assisted sensor." **AIP Advances**. 4: 1-5.

[74] Polyakov, A.Y., Lebedev, V.A., Shirshin, E.A., Rumyantsev, A.M., Volikov, A.B., Zherebker, A., Garshev, A.V., Goodilin, E.A. and Perminova, I.V., 2017. "Non-classical growth of water-redispersible spheroidal gold nanoparticles assisted by leonardite humate." **Cryst. Eng. Comm**., 19: 876-886.

[75] Kumar S., Gandhi K.S. and Kumar R, 2017. "Modeling of Formation of Gold Nanoparticles by Citrate Method." **Industrial & Engineering Chemistry Research.** 46: 3128-3136.

Appendix

Appendix A

Preliminary study on preparation of AuNPs-BC nanopaper

1 Embedding of AuNPs on nanopaper

1.1 Study on effect of pH of the BC for embedding of AuNPs on nanopaper

pH of BC was compared between non-washed (pH 11) and washed BC (pH 6) results were shown in Figure A.1.

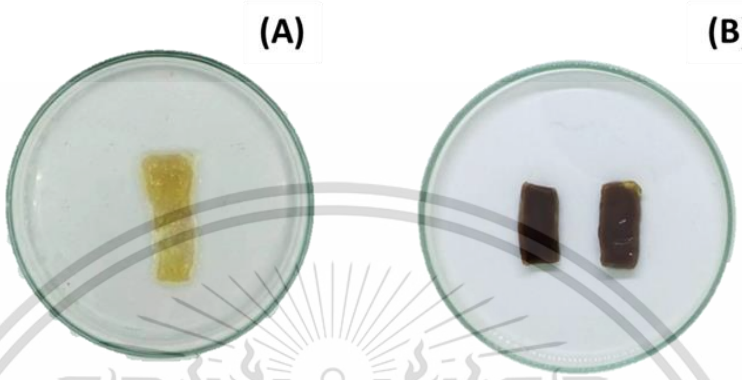

Figure A.1 Embedded AuNPs on nanopaper (A) From BC pH 11 and (B) From BC pH 6.

It was observed that color of embedded AuNPs from non-washed BC was yellow due to hydroxyl group in BC structure cannot able to reduce $HAuCl_4$ to AuNPs result in the color on BC still yellow as same as color of $HAuCl_4$ solution while color of embedded AuNPs from BC pH 6 was red because of AuNPs was occurred and embedded on BC. Consequently, it is necessary to wash BC with DI water to pH 6 before embedding of AuNPs.

1.2 Study on effect of embedding method

Soaking method and *'in situ'* method with different thickness of BC from 2 – 5 mm were studied in this research. Results are shown in Figure A.2 – A.4 and Table A.1.

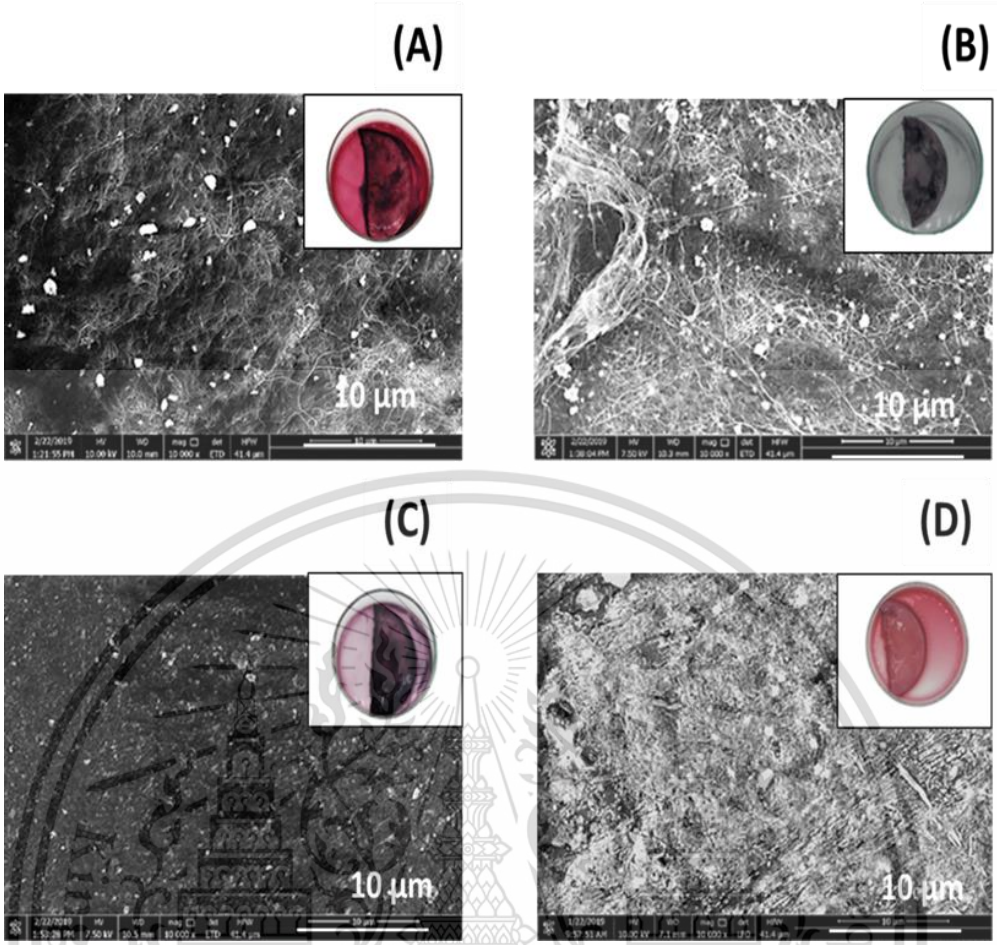

Figure A.2 Scanning electron micrographs of AuNPs embedded nanopaper using soaking method at different thickness of BC (A) 2 mm. (B) 3 mm. (C) 4 mm. (D) 5 mm.. Inset is photographs of observed color.

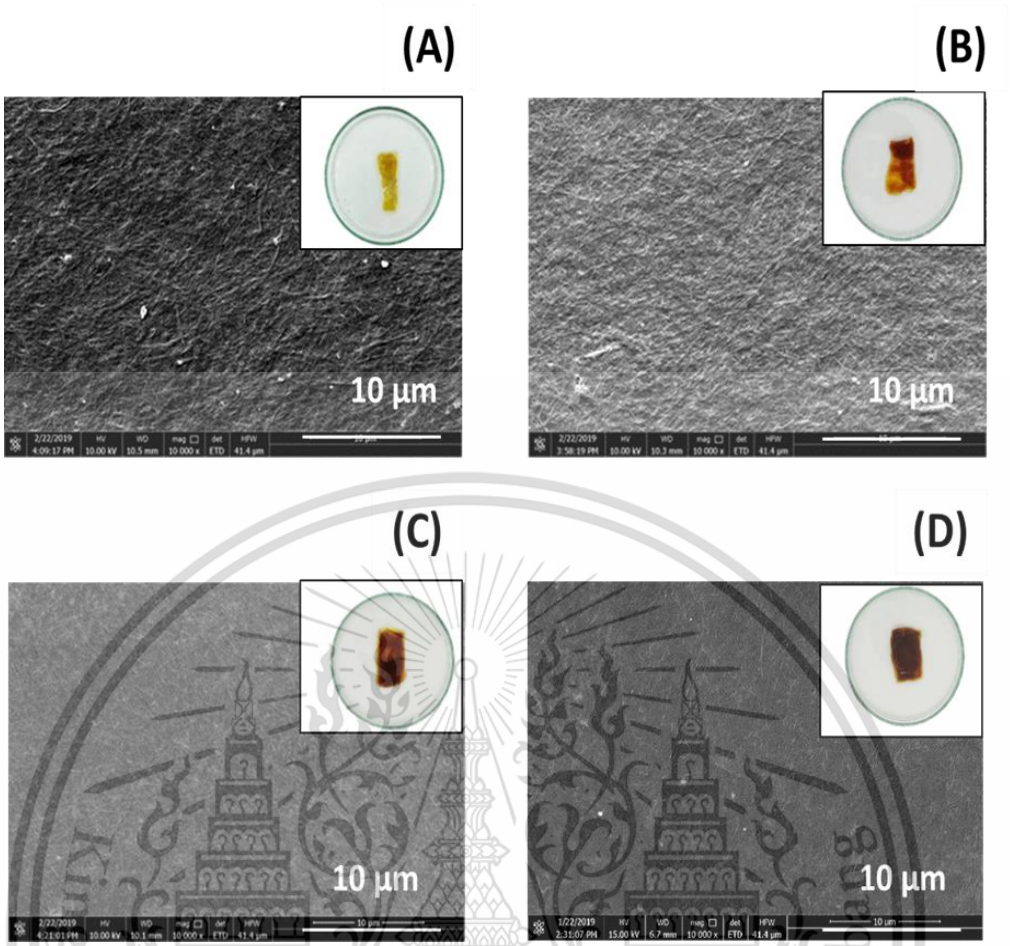

Figure A.3 Scanning electron micrographs of AuNPs embedded nanopaper using *'in situ'* method at different thickness of BC (A) 2 mm. (B) 3 mm. (C) 4 mm. (D) 5 mm.. Inset is photographs of observed color.

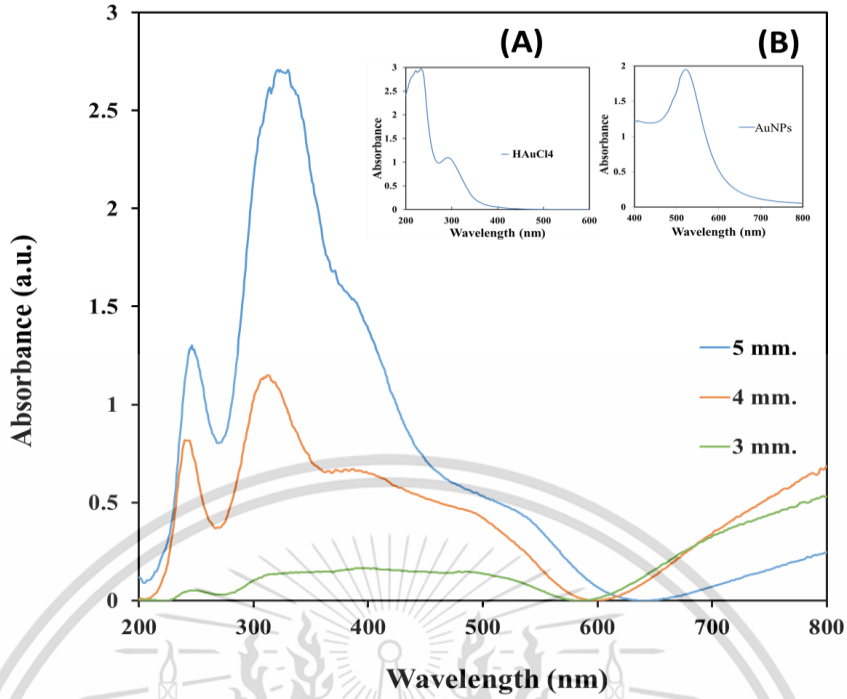

Figure A.4 Absorbance spectra of AuNPs embedded BC at different thickness of BC. Inset is (A) Absorbance spectra of HAuCl4 solution and (B) Absorbance spectra of AuNPs solution.

Table A.1 Wt % of Au at different thickness of bacterial cellulose (From EDS).

Thickness of bacterial cellulose (mm.)	Wt % of Au	
	Soaking method	*'in situ'* method
2	0.20	9.87
3	0.26	7.09
4	0.47	23.49
5	0.67	34.82

Results from SEM in Figure A.2 and A.3 and EDS in Table A.1 evinced that 5 mm thickness with *'in situ'* method gave highest % of Au (34.8 %). The experimental results were consistent with results from UV-Vis spectrophotometer (ISR-2600 Plus, Japan) in Figure 4.14 that the absorbance spectrum of AuNPs is also highest at 5 mm thickness due to at higher thickness of BC, there are more as both reducing agent and substrate for produced AuNPs. Therefore, *'in situ'* method with 5 mm thickness of BC has considered as appropriate method for embedding of AuNPs on nanopaper. Results in Figure A.4 also shown that there were absorption peak around 300 and 530 nm which were similar to

absorption peak of $HAuCl_4$ and AuNPs solution respectively (Inset A and B). These results can guarantee that the AuNPs embedded BC nanopaper was successfully prepared and excess $HAuCl_4$ still remained in the nanopaper.

1.3 Study on effect of $HAuCl_4$ concentration

Concentration of HAuCl4 was studied from 30 – 50 mM. Results are shown in Figure A.5 and A.6.

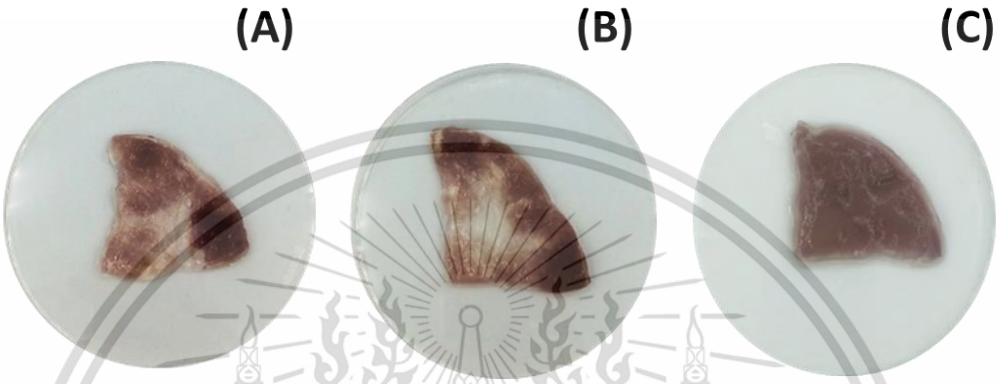

Figure A.5 Color of AuNPs embedded BC at different concentration of $HAuCl_4$ (A) 30 mM (B) 40 mM and (C) 50 mM.

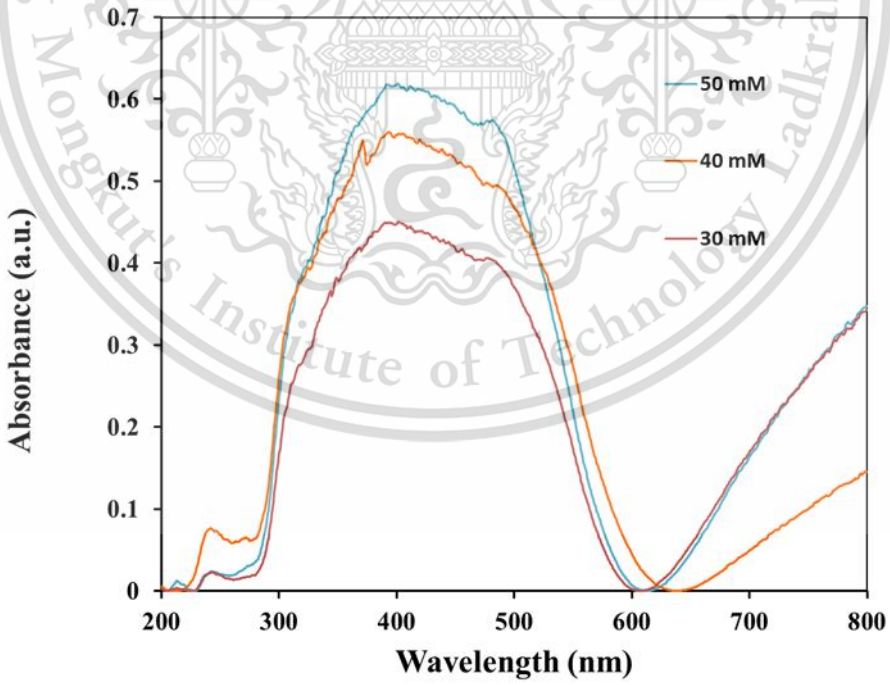

Figure A.6 Absorbance spectra of AuNPs embedded BC at different concentration of $HAuCl_4$.

Results in Figure A.5 were found that the color intensity of AuNPs embedded BC is proportional to the concentration of the solution. This result was consistent with the absorption spectra in Figure A.6 that the absorbance increased when the concentration of $HAuCl_4$ solution is increased. From these results, 50 mM $HAuCl_4$ was selected for used as precursor of AuNPs synthesize.

4.2.2.4 Study on effect of embedded time

Embedded time was studied in the range of 15 – 120 min using '*in situ*' method. The results were then characterized using UV-Vis spectrophotometer.

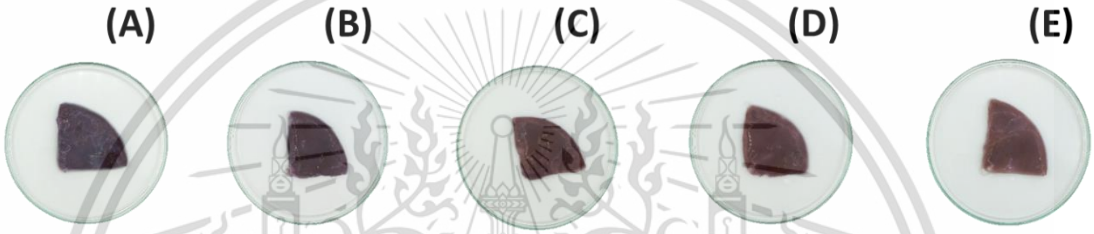

Figure A.7 Color of AuNPs embedded BC at different embedded time (A) 15 min (B) 30 min (C) 60 min (D) 90 min and (E) 120 min.

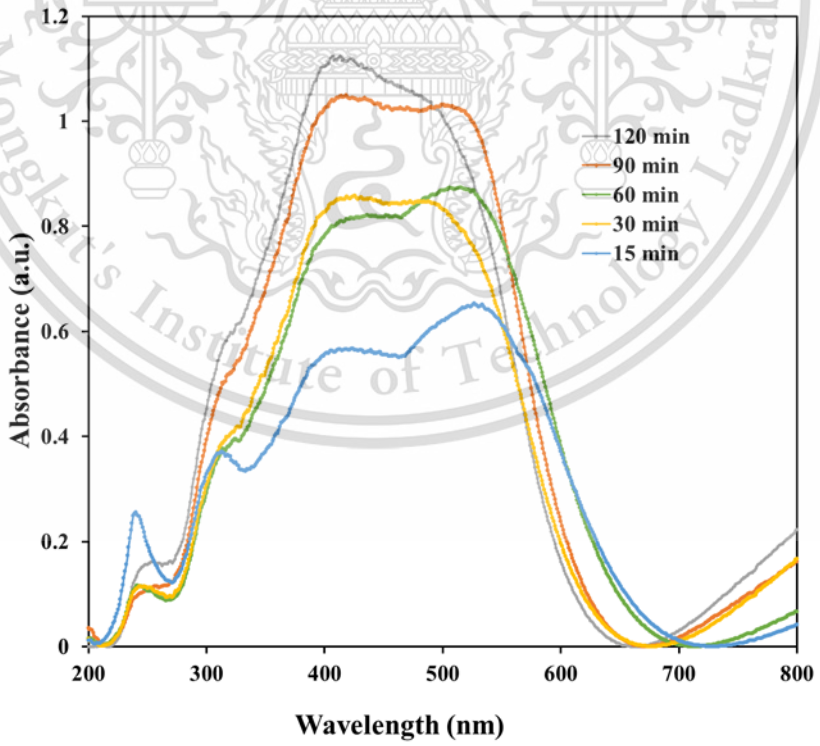

Figure A.8 Absorbance spectra of AuNPs embedded BC at different embedded time.

From Figure A.7, it was found that color of BC had changed from pale yellow to red – purple and absorbance spectra at 525 nm (in Figure A.8) were increased when embedded time was increased and reached the maximum at 90 min. Therefore, 90 min was appropriated for embedded time.

Optimum conditions for embedding of AuNPs on nanopaper are summarized and shown in Table A.2

Table A.2 Optimum conditions for embedding of AuNPs on nanopaper

Condition	Studied range	Selected value
pH of BC	pH 6 and pH 11	pH 6
Embedded method	soaking and *'in situ'*	*'in situ'*
$HAuCl_4$ concentration	30 – 50 mM.	50 mM
Embedded time	15 – 120 min	90 min

Appendix B

International publications and conference proceedings

Gmail

Nathawut Choengchan <nchoengchan@gmail.com>

Acceptance of CMJS.30.03.20-10876(C810)

1 message

CMJS journal <cmjs.chem@gmail.com> Tue, Jun 30, 2020 at 7:46 AM
To: Nathawut Choengchan <nchoengchan@gmail.com>

MS No.: CMJS.30.03.20-10876(C810) "In-situ" Preparation of Gold Nanoparticles-Bacterial Cellulose Nanopaper and Its Application as 2D-Microcuvette for Colorimertic Determination of Hydrogen Peroxide

Dear Dr. Nathawut Choengchan

I am pleased to inform you that your above manuscript has now passed through our refereeing procedure and has been accepted for publication in Chiang Mai Journal of Science.

The manuscript will be further prepared for the proofreading which will be sent to you for correction before publishing. Please contact cmjs@cmu.ac.th if you do not receive the proofread within 2 months.

On behalf of our Editorial Board, may I thank you very much indeed for publishing your work in our Chiang Mai Journal of Science and I sincerely hope that you will consider submitting further articles in the future.

Yours respectfully,

Jaroon Jakmunee
Associate Editor
Chiang Mai Journal of Science

Chiang Mai Journal of Science
Faculty of Science
Chiang Mai University
Chiang Mai
THAILAND 50200
https://epg.science.cmu.ac.th/ejournal/

Tel + 66 53 941909
Fax + 66 53 941909
E-mail cmjs.chem@gmail.com

Chiang Mai Journal of Science
Journal of the Science Faculty of Chiang Mai University

PAPER IN PRESS (24)

Content Vol.47 No.4 Special Issue II : July 2020

Author: Editorial Board Member
E-mail: cmjs@cmu.ac.th
(Vol.47 No.4 (Special Issue II : July 2020))
(Page -)

Abstract

Capacitance Optimization of Planar Carbon-based Supercapacitor

Author: Ukrit Jitropas, Chumphol Yunphuttha, Sumeth Siriroj and Worawat Meevasana*
E-mail: worawat@g.sut.ac.th
(Vol.47 No.4 (Special Issue II : July 2020))
(Page -)

Abstract

Patterned Borosilicate Glass by a Simplified Flash Foam Stamping Technique as a Back Passivation Layer for Photovoltaic Structure

Author: Kamonchanok Mekmork, Thipwan Fangsuwannarak*, Supanut Laohawiroj, Peerawoot Rattanawichai and Warakorn Limsiri
E-mail: thipwan@g.sut.ac.th
(Vol.47 No.4 (Special Issue II : July 2020))
(Page -)

Abstract

FOREWORD Chaing Mai J. Sci. 2020; 47(4)

Author: Dr. Robert Molloy
E-mail: cmjs@cmu.ac.th
(Vol.47 No.4 (Special Issue II : July 2020))
(Page -)

Abstract

The Study of Silica Fume Incorporated Calcium Silicate Nanocomposite for Mechanical Energy Harvesting Application

Author: Jirapan Sintusiri, Wittawat Thongthapthai, Viyada Harnchana*, Vittaya Amornkitbamrung and Prinya Chindaprasirt
E-mail: viyada@kku.ac.th
(Vol.47 No.4 (Special Issue II : July 2020))
(Page -)

Abstract

Effects of Mg and La Co-doping on Dielectric, Ferroelectric, and Piezoelectric Properties of Barium Calcium Zirconate Titanate Ceramics

Author: Panupong Jaiban*, Pimpilai Wannasut, Puripat Kantha, Methee Promsawat and Anucha Watcharapasorn
E-mail: p.jaiban@gmail.com
(Vol.47 No.4 (Special Issue II : July 2020))
(Page -)

Abstract

Effect of Sr Substitution on Structural, Ferroelectric and Magnetic Properties of La1-xSrxFeO3 Perovskite Oxides

Preparation of Gold Nanoparticles-Bacterial Cellulose Nanopaper and Its Application as 2D-Microcuvette for Spectrophotometric Determination of Hydrogen Peroxide

Aurachat Lert-itthiporn [1,2], Saranya Phunpruch[3], Munlika Prommajun[1,2], Pongpichet Srikritsadawong[1,2], Nathawut Choengchan[1,2*]

[1] Flow Innovation and Research for Sciences and Technology Laboratories (FIRST Labs), Bangkok, Thailand

[2] Department of Chemistry and Applied Analytical Chemistry Research Unit, Faculty of Science, King Mongkut's Institute of Technology Ladkrabang, Chalongkrung Road, Ladkrabang, Bangkok, 10520 Thailand

[3] Department of Biology, Faculty of Science, King Mongkut's Institute of Technology Ladkrabang, Bangkok, 10520 Thailand

Abstract

This work presents a new method development using the gold nanoparticles (AuNPs)-bacterial cellulose (BC) nanopaper for the spectrophotometric determination of hydrogen peroxide (H_2O_2). The AuNPs were embedded in the BC nanopaper, where the nanopaper played two roles as both the reducing agent and the template for the as-prepared AuNPs. The preparation process was started by putting the wet bare BC nanopaper (∅ 30 mm and 3 mm thickness) into 0.75 mmol L^{-1} $HAuCl_4$ (25.0 mL). This solution was vigorously and

continuously stirred for 60 min at 90˚C. After the embedding process, color of the nanopaper was changed from milky-white to wine-red. The AuNPs-BC nanopaper was characterized by UV-visible spectrophotometer, FE-SEM and EDS. Absorption spectrum of the nanopaper showed the characteristic peak of Au^0 at 525 nm. The amount of 97.3 weight % of Au^0 was found. The spectrophotometric assay was carried out by dropping the aliquots of 100 µL of sample and 400 µL of 20 mmol L^{-1} citrate buffer (pH 6.0) onto the AuNPs-BC nanopaper. The nanopaper was then kept in a plastic bag for 10 min. In the presence of H_2O_2, the wine-red color of the AuNPs-BC nanopaper was turned to pale red accordingly to reduction of Au^o to Au(III) by H_2O_2. Decreasing in the absorbance of the nanopaper at 525 nm was monitored using UV-visible spectrophotometer. Detection limit ($y_B + 3S_B$) of 0.79 % (v/v) was observed and this value was enough sensitive for the determination of H_2O_2 in wound cleaner samples. The H_2O_2 contents in all samples were agreed well with the label values. Good analytical recovery (90.2 to 97.2 %) with high precision (RSD: 3.3 %) were obtained. These results confirmed that the as-prepared nanopaper was successfully synthesized and was effectively applied as the two dimensional (2D)-microcuvette for the spectrophotometric determination of H_2O_2 in real samples.

Keywords: Nanopaper, Gold nanoparticles, 2D-microcuvette, Spectrophotometry, Hydrogen Peroxide.

*Corresponding author's e-mail: nchoengchan@gmail.com (N. Choengchan).

Tel: +66-2-326-8400-11 Ext. 290, 650; Fax: +66-2-329-8428

1. INTRODUCTION

Hydrogen peroxide (H_2O_2) plays dual role in physiological and pathological conditions of living organisms [1]. It is either extremely useful or harmful depending on its concentration level in the cells. For industrial applications, H_2O_2 has been widely employed as an essential mediator in food, medicine, wound cleaner and some cosmetic products such as hair dye [2, 3]. Therefore, the quantitative analysis of H_2O_2 has become a necessity. A number of analytical methods have been reported for the measurement of the concentration of H_2O_2 in aqueous solution based on various detection principles, such as colorimetry [4-7], fluorometry [8, 9], chemiluminescence [10], electrochemistry [11] and titration [12]. The widely used method for practical determination of H_2O_2 is titrimetric method. However, it requires back-titration steps, which are tedious and time-consuming. Despite the good sensitivity of fluorometric, chemiluminescent and electrochemical methods, they are rather complicated and expensive. Due to the benefits of simplicity and economical, spectrophotometric methods are regarded as one kind of the most promising methods for quantitative analysis of H_2O_2.

Recently, bacterial cellulose (BC) nanopaper has offered new opportunities for the development of precise, accurate and cost-effective analytical devices. The BC nanopaper as a sheet/film composed of continuous network of nanosized cellulosed fibers are usually produced by specific non-pathogenic bacteria such as *Acetobacter xylinum* [13]. The optical transparency, high chemical, mechanical and thermal stability lead the BC nanopaper to be an excellent substrate for the development of optical analytical platform. With the aforementioned benefits, the nanopaper has attracted great attention for exploiting as a two-dimensional (2D) microcuvette for quantitative analyses of various analytes, including albumin [14], methimazole [13], thiourea [13], cysteine [15], cyanide [13] and iodide [16]. However, to the best of our literature reviews, the BC nanopaper has not been reported for the spectrophotometric determination of H_2O_2 so far.

This work was therefore aimed to develop the new analytical method based on using the BC nanopaper as both the analytical platform and the 2D-microcuvette for the spectrophotometric measurement of H_2O_2. We interested in exploiting the gold nanoparticles (AuNPs) as the detection probes. With the recent advances in nanotechnology, AuNPs have attracted considerable attentions due to their sensitivity, stability and controllable size and shape [17]. Recently, Eden et al [13] proposed the synthesis of the AuNPs-BC nanopaper and its application as detection platform for the analyses of thiourea and cyanide. There is some work describes the use of the functionalized-AuNPs solution for the spectrophotometric detection of H_2O_2 [18]. Although the method was highly selective and sensitive, the steps for modification of the AuNPs surface were rather complicated as two ligands, i.e. 1-hexanethiol and lipoic-phenylboronate-mPEG$_{5000}$ were used. 1-Hexanethiol is a hydrophobic ligand with a short length, and it forms a hydrophobic layer around AuNPs. Lipoic-phenylboronate-mPEG$_{5000}$ is the ligand with a long hydrophilic polyethylene glycol tail. The removal of polyethylene glycol chains from the nanoparticle surface under H_2O_2 treatment let to the exposure of inner hydrophobic ligands, causing the nanoparticle aggregation in aqueous medium. Detection procedure of the above work [18] was performed by the ordinary cuvette. In contrast to this work, we prepared the AuNPs-BC nanopaper for employing as the 2D-microcuvette instead of the commercial cuvette. We proposed the method for the embedding of AuNPs onto the nanofibrils of the nanopaper in which the nanopaper, itself was used as a reducing reagent to convert Au (III) to become Au^0. Detection principle for the detection of H_2O_2 is based on the simple redox reaction between the AuNPs (on the nanopaper) and the analyte. By this reaction, wine-red color of the AuNPs-BC nanopaper was decreased correspondingly to the concentration of H_2O_2. The absorbance reading of the nanopaper at 525 nm was monitored by UV-visible spectrophotometer. The developed method was applied to

95 determine the H_2O_2 contents in wound cleaner samples to demonstrate the possibility of the
96 method for real application.

97

98 **2. MATERIALS AND METHOD**

99 **2.1. Reagents and chemicals**

100 All chemicals are analytical reagent grade and deionized-distilled water (18 MΩ·cm)
101 purified by ZENEER UP 900 (Human corporation, Korea) was used throughout. All glassware
102 used were cleaned with aqua regia, rinsed with deionized-distilled water and air dried prior to
103 use. A stock solution of 50 mmol L^{-1} $HAuCl_4$ (100.0 mL) was prepared by dissolving 1.97 g
104 of $HAuCl_4 \cdot 3H_2O$ (Sigma-Aldrich, USA) with water and this solution was kept at 4 °C before
105 use. The precursor solution (0.75 mmol L^{-1} $HAuCl_4$) for the preparation of the AuNPs-BC
106 nanopaper was freshly prepared by pipetting an aliquot of 375 µL of the stock $HAuCl_4$ solution
107 and making to 25.0 mL with water. A 20 mmol L^{-1} citrate buffer solution (pH 6.0) was prepared
108 from sodium citrate dihydrate (UNIVAR, New Zealand) and citric acid (UNIVAR, New
109 Zealand). The working standards of H_2O_2 (1 to 20 % v/v) were freshly prepared by appropriate
110 dilution of the stock solution (35 % v/v) (Carlo Erba, Italy). It is noted that the standard stock
111 solution was standardized with the acidified potassium permanganate solution [12] before use.

112

113 **2.2 Preparation of the bare BC nanopaper**

114 The bare BC nanopaper was prepared using Hestrin-Schramm's culture medium [16].
115 The culture medium was prepared by dissolving the following chemicals: 10 g of glucose
116 (Sigma Aldrich, USA), 2.5 g of peptone (UNIVAR, New Zealand), 2.5 g of yeast extract
117 (Sigma Aldrich, USA), 1.35 g of Na_2HPO_4 (Carlo Erba, Italy) and 0.6 g of citric acid (Ajax
118 Finechem, Australia) in 500 mL of water and the pH value was adjusted to 5.25 using 1.0 mol

119 L^{-1} NaOH (Sigma Aldrich, USA). The medium was separated into five Erlenmeyer flasks. Each
120 flask was covered with cotton balls and then was autoclaved at 121°C for 15 min. Aliquot of
121 5.0 mL of the starter BC from coconut juice was added to each flask and kept growing for six
122 days. The nanopaper was purified by soaking in 5 % w/w NaOH at ambient temperature for 24
123 h and was then bleached with the mixture of 1 % w/w NaOH and 0.2 % w/v H_2O_2 at 80 °C for
124 1 h. Finally, the bare BC nanopaper was cleaned with water until the pH value become 6.0.

125

126 **2.3 Preparation of the AuNPs-BC nanopaper**

127 The AuNPs was prepared based on an ex-situ concept [19] with the following procedures.
128 Briefly, 25.0 mL of 0.75 mmol L^{-1} $HAuCl_4$ (Sigma Aldrich, USA) was boiled until 90 °C.
129 Then, a piece of the purified wet BC nanopaper (30 mm ∅ and 3 mm thickness) was put into
130 the boiled $HAuCl_4$ solution. This solution was continuously heated for 60 min under vigorous
131 stirring. The AuNPs-BC nanopaper was washed with 20 mL water to removed excess $HAuCl_4$
132 before use. The wet as-prepared nanopaper was dried overnight (~ 12 h) at ambient
133 temperature. The dried AuNPs-BC nanopaper was characterized using a V-630 UV-visible
134 spectrophotometer (Jasco, Japan) and a JSM-6610LV Field Emission-Scanning Electron
135 Microscope (FE-SEM) with an Energy Dispersive X-Ray Spectrometer (EDS) from JEOL
136 Ltd., Japan, for evaluation of its absorption spectrum, morphology and Au^0 content,
137 respectively.

138

139 **2.4 Spectrophotometric assay for the determination of H_2O_2 using the AuNPs-BC**
140 **nanopaper**

141 The dried AuNPs-BC nanopaper was cut into a piece with dimension of 10 mm width ×
142 25 mm length ×1 mm thickness. Aliquots of 400 µL of 20 mmol L^{-1} citrate buffer (pH 6.0)

and 100 µL of standard H_2O_2 (or samples) were transferred onto the AuNPs-BC nanopaper. The nanopaper was then put in a plastic zip-lock bag and placed into the thermostat bath (40 °C) for 10 min. Later, the nanopaper was directly attached in front of the sample holder inside a V-630 UV-visible spectrophotometer (Jasco, Japan). The absorbance readings at 525 nm of each nanopaper before and after dropping of the standard H_2O_2 (or sample) solution were recorded. Difference in the absorbances between before and after dropping of standard/sample ($\triangle Abs_{525nm}$) was evaluated. Calibration was constructed by plotting the $\triangle Abs_{525nm}$ against the concentrations of the standard solutions of H_2O_2 (1 to 20 % v/v). Note that all samples were directly analyzed without any prior pre-treatment process.

3. RESULTS AND DISCUSSIONS

3.1 Characterization of the AuNPs-BC nanopaper

The bare BC nanopaper exploited throughout this work was obtained using a bottom-up approach where the nanofibers were created by *Acetobactor xylinuim*, which synthesized cellulose and subsequently assembled bundles of cellulose nanofibrils. The bare BC nanopaper was used as both a reducing agent and a template for the preparation of the AuNPs-BC nanopaper. By this preparation, the penetrated Au (III) ions into the BC network were gradually reduced to the Au^0 nanoparticles due to the presence of hydroxyl groups on the surface of the bare BC nanopaper [13].

Figure 1A and 1B illustrate the photographic images of the wet bare BC nanopaper (after bleaching) and the dried AuNPs-BC nanopaper, prepared by this work, respectively. The color of the nanopaper is changed from milky-white to wine-red after the embedding process. The absorption spectra of these nanopapers were recorded by UV-visible spectrophotometer and were compared to the absorption spectrum of the colloidal AuNPs solution. Results in Figure

1C show that a shoulder peak at 525 nm is obtained by the AuNPs-BC while this shoulder is not appeared by the bare BC. This wavelength is the maximum absorption wavelength of the colloidal gold solution. The nanopapers were further characterized by FE-SEM and EDS. The SEM images of the bare BC and the as-prepared AuNPs-BC nanopapers are presented in Figure 2A and 2B, respectively. Figure 2A shows that bundles of cellulose nanofibrils are observed. It is also clearly demonstrated in Figure 2B that Au^{o} is occurred and is deposited onto the fibril of the nanopaper. Results by EDS in Figure 3 also reveal that the EDS line of Au^{0} is existed and the Au^{0} content of 97.3 weight % is found. These results confirm that the AuNPs-BC nanopaper was successfully prepared. However, the observed content of Au(0) is moderately high and is not represented for the Au(0) content of the whole nanopaper sheet. It is because the image of the as-prepared nanopaper was captured and then was focused especially on the area that there were a larger numbers of Au(0) nanoparticles, deposited in the BC nanopaper.

3.2 Study on detection principle

Detection principle for the spectrophotometric determination of H_2O_2 was studied by UV-visible spectrophotometer using the ordinary cuvette for the measurement of the AuNPs solution. The principle is based on the simple redox reaction between Au^{0} and H_2O_2 in the acidic medium as written in the following equation:

$$2\,Au^{0}\,(s) + 3\,H_2O_2\,(l) + 6\,H^{+}\,(aq) \longrightarrow 2\,Au^{3+}(aq) + 6\,H_2O\,(l) \quad \text{..... (1)}$$

wine-red pale yellow

In the presence of H_2O_2, the wine-red color of the AuNPs solution is decreased as Au^{0} is oxidized to become Au (III). It is observed in the inset photographic images of Figure 4 that the wine-red color of the AuNPs is slightly diminished when the concentration of the standard H_2O_2 is increased. However, by the spectrophotometer, it is clearly observed that the

absorbency at 525 nm (Abs $_{525nm}$) is decreased proportionally to the concentration of standard H_2O_2 solution (Figure 4). Therefore, this chemical reaction can be applied for the quantitative analysis of H_2O_2.

3.3 Optimization study for the detection of H_2O_2 by the AuNPs-BC

Parameters affecting the sensitivity of the detection of H_2O_2 were optimized. Each effect is discussed in the following details. Summary of the studied ranges and the selected values are presented in Table 1.

3.3.1 Effect of pH of citrate buffer

The effect of pH of the citrate buffer solution was studied from the values of 3.0 to 6.0 when the concentration of the buffer was kept at 20 mmol L^{-1}. A concentration of 30 % (v/v) H_2O_2 was studied. The △Abs of the nanopaper at 525 nm (Abs $_{before\ dropping\ hydrogen\ peroxide}$ − Abs $_{after\ dropping\ hydrogen\ peroxide}$) was calculated and was plotted against the investigated pH value. Results are shown in Figure 5A. The $\triangle Abs_{525nm}$ is faintly increased when the pH value is increased. The low pH value can induce aggregation of gold nanoparticles which results in red shift of plasmonic absorption peak and decreasing in the absorbance reading at 525 nm [20, 21]. As the pH value of 6.0 provides the highest signal, this value is selected as the optimal pH value. Note that we also investigated the effect of the pH values from 7.0 to 9.0 using ammonium buffer (20 mmol L^{-1}). It was found that after dropping the buffer solution, the color of the AuNPs-BC nanopaper turned to dark purple. It might be because of the precipitation of colloidal gold nanoparticles at higher pH values [22].

3.3.2 Effect of citrate buffer concentration

The effect of the concentration of citrate buffer was studied from 1 to 40 mmol L^{-1} when pH of the buffer was fixed at 6.0. A concentration of 30 % (v/v) H_2O_2 was investigated. Results in Figure 5B indicate that when the concentration of the buffer is increase from 1 to 20 mmol L^{-1}, the $\triangle Abs_{525nm}$ is also increased. At higher concentration, the $\triangle Abs_{525nm}$ is decreased. It was due to the self-aggregation effect of the AuNPs, induced by salt ions, existed in the buffer solution [23]. The concentration of 20 mmol L^{-1} is chosen as the highest signal is achieved.

3.3.3 Effect of incubation temperature

The effect of the incubation temperature was investigated from the ambient temperature (~ 25 °C) to 50 °C by using 20 mmol L^{-1} citrate buffer (pH 6.0). Results in Figure 5C show that when the temperature is risen, the $\triangle Abs_{525nm}$ is increased up to 40 °C. At higher temperature, the signal is decreased accordingly to the decomposition of H_2O_2 under too high temperature. Therefore, 40 °C is selected.

3.3.4 Effect of incubation time

The effect of incubation time was evaluated from 5 to 50 min when 20 mmol L^{-1} citrate buffer (pH 6.0) was exploited. Results in Figure 5D show that when the incubation time is increased to 10 min, the $\triangle Abs$ is dramatically increased. This implies that longer incubation time can result in higher sensitivity. However, the $\triangle Abs$ becomes stable and reaches its plateau after 10 min. As compromising between the sensitivity and the analysis time, the incubation time of 10 min is chosen as the optimal condition.

4. Analytical performances

Analytical performances of the developed method, in term of, linearity range, recovery, precision and detection limit, were studied. Recovery study was carried out by spiking of the standard H_2O_2 solutions of 3 % (v/v) into wound cleaner samples, respectively. Summary of the results is presented in Table 2. It is found that the recovery is ranging from 90.2 to 97.2 %. This suggests that the developed method is free from the sample matrix effect. Precision of the developed method was studied by pipetting an aliquot of 100 µL of standard H_2O_2 (10 % v/v) onto 10 different sheets of the AuNPs-BC nanopapers. The RSD was calculated based on using the absorbance reading obtained by each nanopaper. RSD of 3.3 % is obtained and this implies that the method provides high precision. Detection limit ($LOD = y_B + 3S_B$) [24] of 0.79 % (v/v) H_2O_2 is achieved. This value is sufficient sensitive to apply the proposed method for the quantitative analysis of H_2O_2 in wound cleaner samples.

5. Spectrophotometric determination of H_2O_2 by the AuNPs-BC nanopaper

The optimal conditions as summarized in Table 1 was adapted for the spectrophotometric determination of H_2O_2 using the AuNPs-BC nanopaper as the analytical platform and the 2D-microcuvette. When the concentration of H_2O_2 is increased, the wine-red color of the nanopaper is decreased as presented in Figure 6A. This result is clearly observed by naked eye. An example of the calibration plot between the $\triangle Abs_{525nm}$ ($Abs_{\textit{before dropping hydrogen peroxide}} - Abs_{\textit{after dropping hydrogen peroxide}}$) and the concentrations of the standard H_2O_2 solutions is presented in Figure 6B. The $\triangle Abs_{525nm}$ is increased when the concentration of the standard H_2O_2 is increased. The working range was observed from 1 to 20 % (v/v) with good linearity (r^2 = 0.984). In order to demonstrate that the developed method was viable for real usage, it was applied for the spectrophotometric determination of H_2O_2 in four wound cleaner samples,

commercially available in the local supermarket in Bangkok, Thailand. The samples were directly analyzed without requirement of any sample pre-treatment. Results are summarized in Table 2. It is found that the calculated H_2O_2 concentrations in all samples are agreed well with the label concentrations with the relative error below than 8 %. This result indicates that the AuNPs-BC nanopaper provides high possibility to be applied as the 2D-microcuvette for the spectrophotometric determination of H_2O_2. From results in Table 2, the negative and positive errors mean the calculated concentrations of H_2O_2 are lower and higher than the label concentrations, respectively.

CONCLUSIONS

The AuNPs-BC nanopaper was successfully prepared. The bare BC nanopaper was exploited as both the reducing agent for conversion of Au (III) to become the gold nanoparticles (Au^0) and as the scaffold for Au^0. The AuNPs-BC nanopaper showed the characteristic absorption peak at 525 nm, similar to the characteristic peak obtained by the colloidal AuNPs solution. By the FE-SEM and EDS results, the Au^0 content was observed at 97.3 weight % in the as-prepared nanopaper. The AuNPs-BC nanopaper was effectively applied as the sensing platform and the 2D-microcuvette for the spectrophotometric measurement of H_2O_2 based on the simple redox reaction between the analyte and the embedded AuNPs in the nanopaper. The linear calibration plot between the $\triangle Abs_{525nm}$ ($Abs_{\textit{before dropping hydrogen peroxide}} - Abs_{\textit{after dropping hydrogen peroxide}}$) and the concentration of the standard H_2O_2 solutions was achieved up to 20 % (v/v). The developed method was successfully applied to determine the H_2O_2 contents in wound cleaner samples with high accurate and precise results.

ACKNOWLEDGEMENTS

The authors would like to thank the financial supports form Faculty of Science, King Mongkut's Institute of Technology Ladkrabang (KMITL), Grant no. 2563-01-05-72 to NC and the scholarship for research assistance and teaching assistance (RA&TA) to PS. The authors would also like to thank A. Mathaweesansurn, K. Khongpetch and J. Jindanom for their contributions for preliminary experiments. We also thank Prof. John Morris, KMITL Research and Innovation Services, for his assistance with English.

REFERENCES

[1] Sophia J. and Muralidharan G., *J. Appl. Electrochem*., 2015; **9**: 963-971. DOI 10.1007/s10800- 015-0862-8

[2] Li C., Hu J., Liu T. and Liu S., *Macromolecules*, 2011; **44**: 429-431. DOI org/10.1021/ma102608a.

[3] Meng F., Yan X., Liu J., Gu J. and Zho Z., *Electrochim. Acta,* 2011; **56**: 4657-4662. DOI org/10.1016/j.electacta.2011.02.105

[4] Wang D. Y., Qiu S. Y., Wang M. Y., Pan S. W., Ma H. F. and Zou J., *Spectrochim. Acta. A*, 2019; **221**: 117138. DOI org/10.1016/j.saa.2019.117138

[5] Nogueira R. F. P., Oliveira M. C. and Paterlini W.C., *Talanta*, 2005; **66**: 86-91. DOI 10.1016/j.talanta.2004.10.001.

[6] Sellers R.M., *Analyst*, 1980;**105**: 950-954. DOI org/10.1039/AN9800500950.

[7] Luo W., Abbas M. E., Zhu L., Deng K. and Tang H., *Anal. Chim. Acta*, 2008; **629**: 1-5. DOI 10.1016/j.aca.2008.09.009.

[8] Schick R., Strasser I. and Stabel H., *Water Res.*, 1997; **6**: 1371-1378. DOI org/10.1016/S0043-1354(96)00410-1.

[9] Xie Y., Cheng W., Jin B., Liang C., Ding Y. and Zhang W., *Analyst*, 2018; **143**: 5583-5588. DOI 10.1039/c8an01736k.

[10] Hu Y., Zhang Z. and Yang C., *Anal. Chim. Acta*, 2007; **601**: 95-100. DOI org/10.1016/j.aca.2007.08.018.

[11] Razmi H., Mohammad-Rezaei R. and Heidari H., *Electroanal.*, 2009; **21**: 2355-2362. DOI org/10.1002/elan.200904687.

[12] Klassen N. V., Marchington D. and McGowan H. C. E., *Anal. Chem.*, 1994; **66**: 2921-2925. DOI org/10.1021/ac00090a020.

[13] Eden M. N., Hamed G., Tina N., Hossein Y., Uliana K., Daniel H., Nahid P. and Arben M., *ACS Nano.,* 2015; **9**: 7296 - 7305. DOI org/10.1021/acsnano.5b03097.

[14] Naghdi T., Golmohammadi H., Vosough M., Atashi M., Saeedi I. and Maghsoudi M. T., *Anal. Chim. Acta*, 2019; **1070**: 104-111. DOI 10.1016/j.aca.2019.04.037.

[15] Erhan Z., *Talanta,* 2018; **184:** 149 - 155. DOI org/10.1016/j.talanta.2018.02.096.

[16] Erhan Z., Alpaydin S., Arici A., Saglam M. E. and Bingol H., *Sens. Actuators B Chem.*, 2018; **254**: 1216-1224. DOI org/10.1016/j.snb.2017.07.208

[17] Ng S.M., Koneswaran M. and Narayanaswamy, R., *RSC Adv*., 2016; **6**: 21624-21661. DOI org/10.1039/C5RA24987B.

[18] Wu S., Tan S. Y., Ang C. Y., Luo Z. and Zhao Y., *Chem. Commun.*, 2016; **52(17)**: 3508-3511. DOI org/10.1039/C5CC09447J.

[19] Urbina L., Guaresti O., Requies J., Gabilondo N., Eceiza A., Corcuera M. A. and Retegi A., *Carbohydr. Polym.*, 2018; 193: 362-372. DOI.org/10.1016/j.carbpol.2018.04.007

[20] Park S. H., Lee W. J., Park S. M, Choi D. W., Kim S. J. and Park N. Y., *Sci. Rep.*, 2019; **9**: 1-9. DOI.org/10.1038/s41598-019-56754-8.

[21] Zhu J., Li W. B., Zhu M., Zhang W., Niu W. C. and Liu G. H., *AIP Adv.*, 2014; **4**: 1-5. DOI.org/10.1063/1.4869615.

[22] Polyakov A.Y., Lebedev V.A., Shirshin E.A., Rumyantsev A.M., Volikov A.B., Zherebker A., Garshev A.V., Goodilin E.A. and Perminova I.V., *Cryst. Eng. Comm.,* 2017; **19**: 876-886. DOI 10.1039/C6CE02149B.

[23] Kumar S., Gandhi K.S. and Kumar R, *Ind. Eng. Chem. Res.,* 2007; **46**: 3128-3136. DOI org/10.1021/ie060672j.

[24] Miller J.N., Miller J.C., Statistics and chemometrics for analytical chemistry, 4th edn., Pearson Education, 1993.

Figure captions

Figure 1. The photographic images of: (A) the wet bare BC nanopaper and (B) the dried AuNPs-BC nanopaper, synthesized using 0.75 mmol L^{-1} $HAuCl_4$ as the precursor solution. (C) The overlaid absorption spectra of 1.03 nmol L^{-1} of AuNPs solution, the dried AuNPs-BC nanopaper and the dried bare BC nanopaper.

Figure 2. The SEM images of: (A) the dried bare BC nanopaper and the dried AuNPs-BC nanopaper, prepared when 0.75 mmol L^{-1} $HAuCl_4$ was used as the precursor. Conditions for the SEM images are listed as: (A) SU8000, 10.0 kV, 13.0 mm × 10.0 k SE (U) and (B) SU8000, 10.0 kV, 13.0 mm × 40.0 k SE (U). Inset of Figure 2(A) and (B) are the photographic images of the dried bare BC nanopaper and the dried AuNPs-BC nanopaper, respectively.

Figure 3. The EDS spectrum of the dried AuNPs-BC nanopaper (using 0.75 mmol L^{-1} $HAuCl_4$ as the precursor) and its corresponded Au^0 content obtained by the elemental analysis.

Figure 4. The linear correlation between the absorbance reading of the AuNPs solution (0.506 nmol L^{-1}) at 525 nm and the concentrations of standard H_2O_2. Inset photographic images are the AuNPs solutions in the presence of various concentrations of standard H_2O_2.

Figure 5. Summary of the results of the optimization study for the determination of H_2O_2 by the AuNPs-BC nanopaper. (A) Effect of the pH solution of 20 mmol L^{-1} citrate buffer, (B) Effect of the concentration of the citrate buffer at pH 6.0, (C) Effect of incubation temperature and (D) Effect of incubation time.

Figure 6. (A) The photographic images of the AuNPs-BC nanopaper in the presence of various concentrations of the standard H_2O_2. (B) An example of the linear calibration plot between the $\triangle Abs_{525nm}$ of the AuNPs-BC nanopaper and the concentrations of standard H_2O_2.

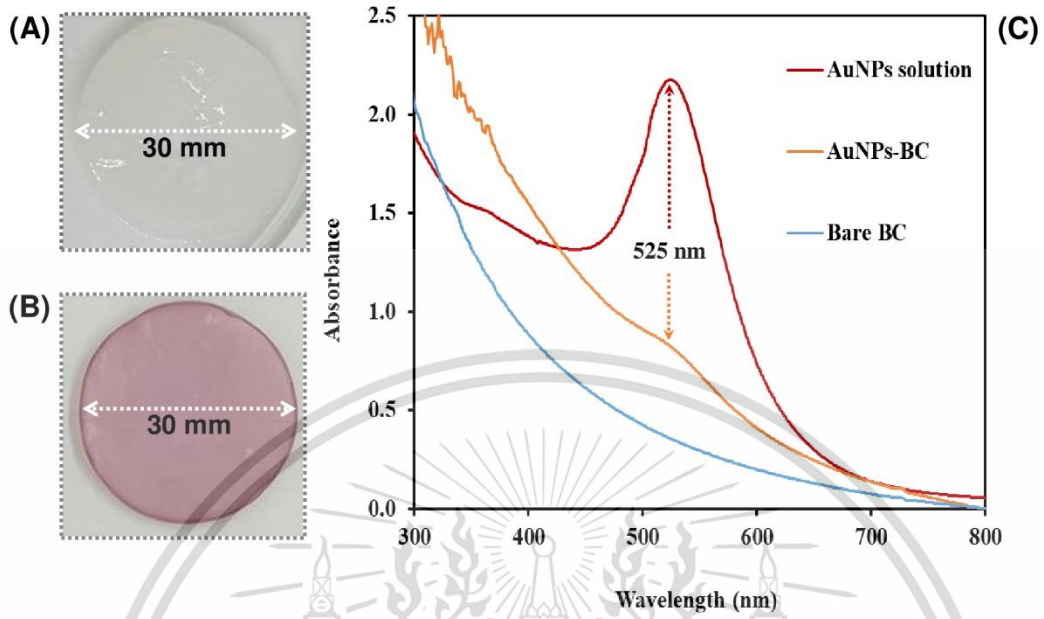

Figure 1

374

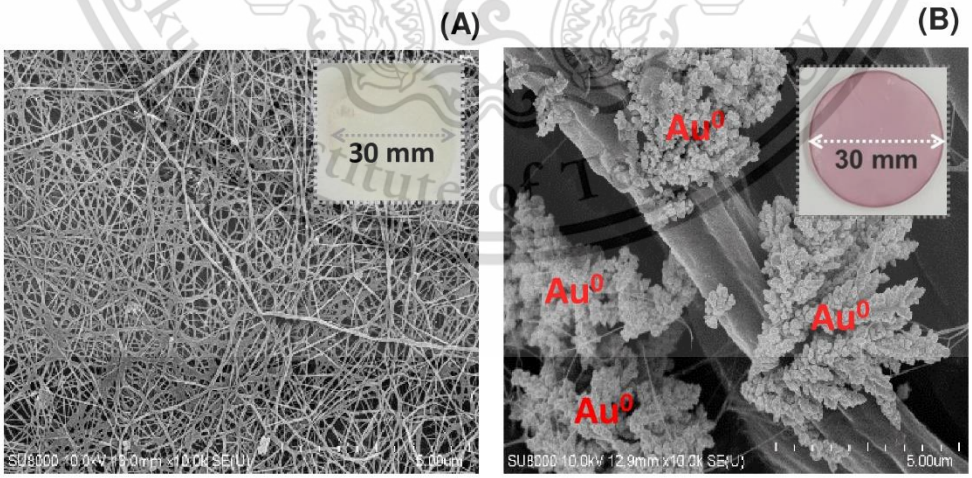

Figure 2

375

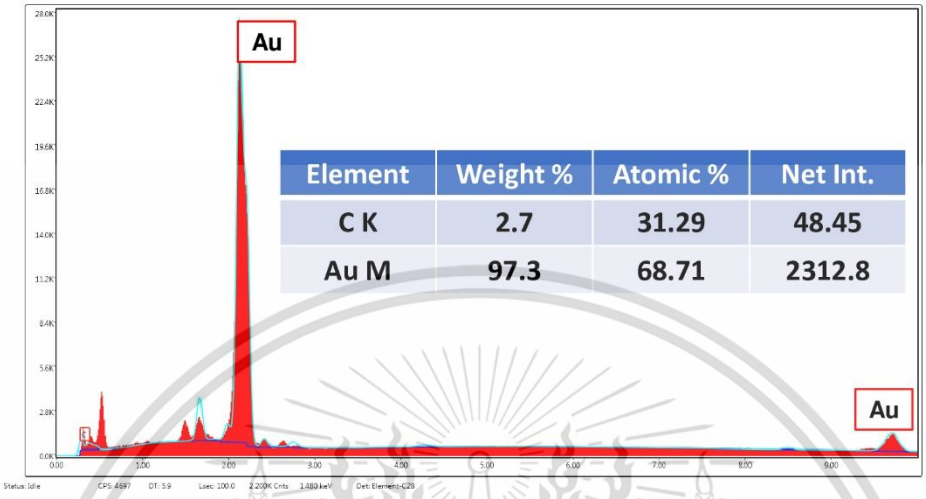

Figure 3

376

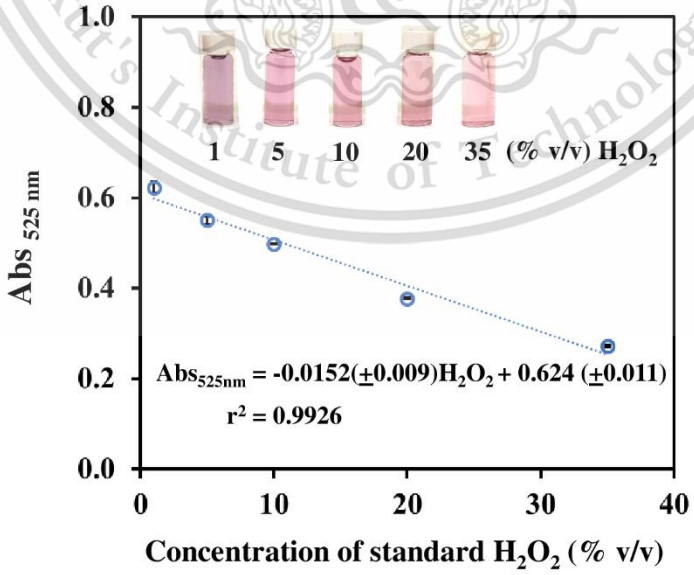

Figure 4

377

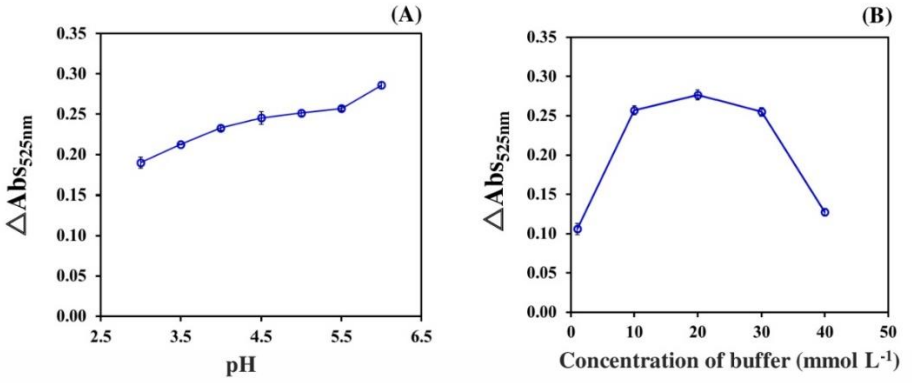

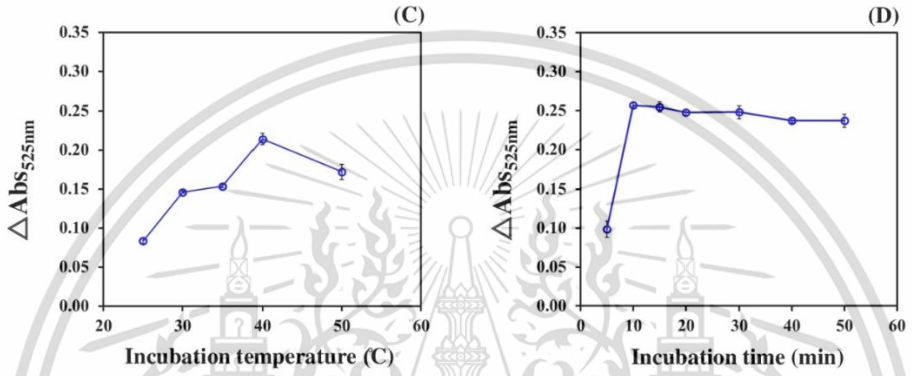

Figure 5

378

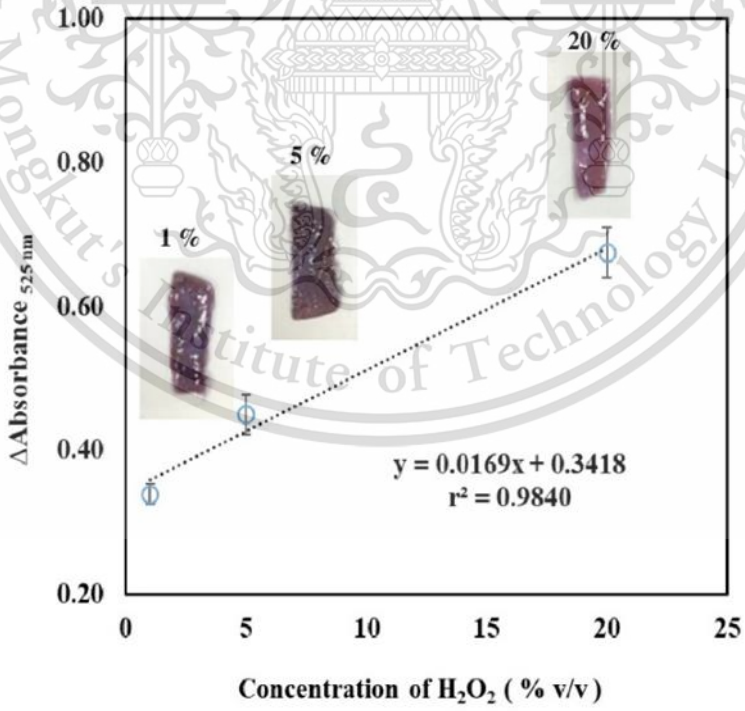

379

380 **Figure 6**

381 **Table 1.** Summary of the optimization study for the spectrophotometric detection of H_2O_2 by
382 the AuNPs-BC.

Parameters	Studied range	Selected value
pH of citrate buffer	3-6	6
Citrate buffer concentration (mmol L^{-1})	1-40	20
Incubation temperature (°C)	Ambient temperature to 50	40
Incubation time (min)	5-50	10

383

384 **Table 2.** Comparison of the H_2O_2 concentrations (% v/v) in samples, determined by this work
385 with the label values and the results by the recovery study.

Sample	H_2O_2 concentration (% v/v)		Relative error [a] (%)	Recovery (%)
	Label	This work (Mean ± SD)		
1	3	3.14 ± 0.03	4.6	97.0
2	3	2.84 ± 0.04	-5.4	95.1
3	3	2.78 ± 0.09	-7.2	90.2
4	3	2.79 ± 0.07	-6.9	97.2

386 **Note**: [a] Relative error was calculated as the following equation;

387 $$\text{Relative error (\%)} = ((\text{Calculated value} - \text{Label value}) / \text{Label value}) \times 100$$

CHEMISTRY TOWARD A SUSTAINABLE FUTURE

Proceedings

February 7-9, 2018

The 60th Anniversary of His Majesty the King's Accession to the Throne International Convention Center, Hat Yai, Songkhla, Thailand

PACCON
PURE AND APPLIED CHEMISTRY INTERNATIONAL CONFERENCE 2018

PACCON 2018
Pure and Applied Chemistry International Conference

Facile immunoassay for colorimetric detection of parathyroid hormone based on aggregation of gold nanoparticles

Aurachat Lert-itthiporn[1,2]*, Tipachai Vatanavicharn[2,3], Nathawut Choengchan[1,2]*
[1]*Flow Innovation-Research for Science and Technology Laboratories (FIRST Labs)*,
[2]*Applied Analytical Chemistry Research Unit, Department of Chemistry, Faculty of Science, King Mongkut's Institute of Technology Ladkrabang, Bangkok 10520, Thailand*
[3]*Department of Applied Biology, Faculty of Science, King Mongkut's Institute of Technology Ladkrabang, Bangkok 10520, Thailand*
**E-mail: aurachat.l@gmail.com, nchoengchan@gmail.com*

Abstract:

This work presents the immunoassay based on using gold nanoparticles (AuNPs) for facile colorimetric detection of parathyroid hormone. AuNPs were synthesized accordingly to Turkevich's method and were then conjugated with anti-parathyroid hormone antibody by incubation for 1 hr at 25 °C. Conjugated AuNPs were applied to detection of parathyroid hormone based on aggregation of AuNPs in the presence of the hormone. Color of the solution was changed from red wine to purple and the characteristic surface plasmon peak was shifted from 521 nm to 542 nm. Under the optimized conditions, the level of parathyroid hormone can be detected in the range of 10 – 1,000 pg mL^{-1} with good linearity (r^2 = 0.997). This method was applicable for the parathyroid hormone determination with good recovery (106.3 – 113.6%).

1. Introduction

Parathyroid hormone (PTH) is a hormone containing 84 amino acids secreted by the parathyroid glands to maintain normal amount of blood calcium.[1] An amount of PTH for normal people is 10 - 65 pg mL^{-1}.[2] Abnormal excretion of PTH can cause hypo-parathyroidism and hyper parathyroidism. Hypoparathyroidism occur when not enough PTH is produced result in low blood calcium.[3] Hyperparathyroidism is caused by secretion of PTH is exorbitant occur with fragile bones and kidney stones.[4] Curing of this symptom is parathyroid surgery.[5] Therefore detection of the blood PTH level is required for close monitoring.

The most widely used analytical methods for quantitative analysis of blood PTH level are chromatography and immunoassay. For chromatographic method,[6-8] high accuracy and precision are achieved. However, it was found that large volume of organic solvent was employed. In addition, the instrument and its operation procedures are complicated. The immunoassays have been also developed for the PTH determination. There have been both manual[1] and automatic methods.[9-11] Although these methods provided high selectivity but sensor preparation steps were sophisticated.

To date, applications of nanoparticles are widely used due to a variety of potential applications in biomedical, optical and electronic fields.[12] For examples, W.D. Dittmer *et al.*[13] presented labeling magnetic particles for quantification of the amount of PTH. V. Jarrige *et al.*[14] developed a point of care (POC) device based on magnetically controlled movement of superparamagnetic nanoparticles for measurement of PTH. Amongst the reported nanoparticles mentioned above, AuNPs are the most attractive metallic nanoparticles because of their high capability for functionalization with biomolecules.[15] This leads to their application for determination of various proteins and hormones.[16-18] However, to the best of our literacy, there has not been any work reported on the analysis of PTH in blood using the AuNPs so far.

This work, we consequently develop a simple method for PTH detection based on immunoassay by aggregation of AuNPs. The AuNPs were preliminarily conjugated with anti PTH antibody. In the presence of PTH, aggregation of conjugated AuNPs was occurred and color of the solution was changed from red wine to purple. The corresponding surface plasmon peak was also shifted (521 to 542 nm). Possibility of develop assay for applying to rat blood samples are investigated.

2. Materials and Methods

2.1 Reagents and materials

AuNPs were prepared from $HAuCl_4 \cdot 3H_2O$ (Sigma-Aldrich, USA) by using sodium citrate tribasic dehydrates (Sigma-Aldrich, USA) as reducing agent. Anti-PTH antibody (ab53040, Abcam, UK), was used for conjugation of AuNPs. Standard PTH was prepared in phosphate buffer saline, pH 7.4 (PBS, Sigma-Aldrich, Switzerland). Working standard solutions were appropriate dilution of this stock solution. Autoclaved deionized-distilled water was used throughout the experiment.

2.2 Synthesis of AuNPs

Colloidal AuNPs were prepared accordingly to Y. Wang *et. al.*[19] Briefly, 100 mL of 0.01% w/v $HAuCl_4$ was heated to boil, followed by adding 2 mL of 1.0% w/v sodium citrate and simultaneously stirred for 15 min. The solution was kept stand to ambient temperature and stored at 4°C. The particles were characterized by a transmission electron microscope (TEM) a TECNAI-10 (Netherlands) and a UV- Vis spectrophotometer (JASCO V-630).

2.3 Conjugation of antibody and colloidal AuNPs

A 15 µL of 0.1 mg mL^{-1} antibody was added to 100 µL of the adjusted pH 7.0 AuNPs. After 5 min, 15 µL of 10% w/v NaCl was added. The solution was incubated at 25 °C for 1 hr. The conjugated AuNPs solution was used without any purification.

2.4 Procedure for PTH determination

A 10 µL of each concentration of standard PTH was added to the conjugated AuNPs and incubated for 1 hr at 25 °C. The surface plasmon bands of the AuNPs were recorded from 400 – 800 nm using UV – Vis spectrophotometer.

3. Results and Discussion

3.1 Characterization of the prepared AuNPs

Results in Figure 1(a) and (b) reveal that the surface plasmon peak is located at 521 nm with red wine colored solution. Results by TEM image show that shape of the nanoparticles are spherical with the average size of 25.0 ± 11.4 nm. (Figure 1(c) and (d)).

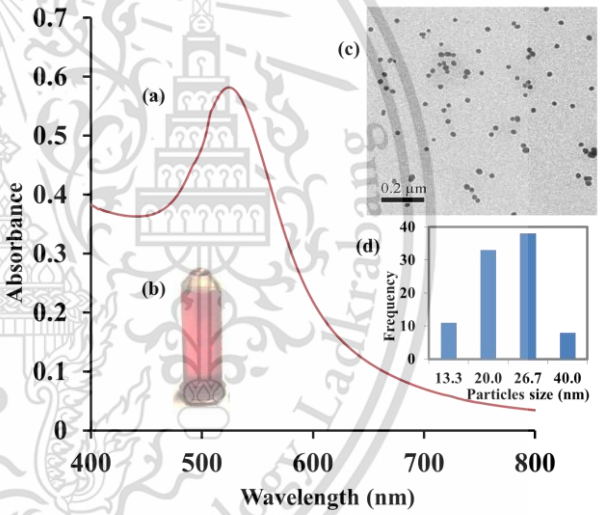

Figure 1. (a) surface plasmon peak, (b) red wine color solution, (c) TEM image and (d) size distribution chart of the as-prepared AuNPs (4.84 x 10^{-3} nM)

3.2 Detection principle

Schematic illustration for the detection principle of PTH using the conjugated AuNPs is shown as Schematic 1.

The reaction detection for PTH is based on aggregation of conjugated AuNPs by adding PTH. The surface plasmon peaks were changed from 521 to 542 nm (Figure 2(a)). This results in changing of solution color from red wine to purple (Figure 2(b)). Aggregation of the conjugated

AuNPs was found proportional to the PTH concentration (Figure 2(c)).

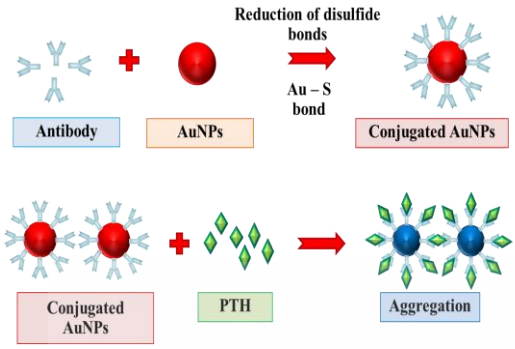

Schematic 1. Schematic illustration for the detection principle of PTH using the conjugated AuNPs

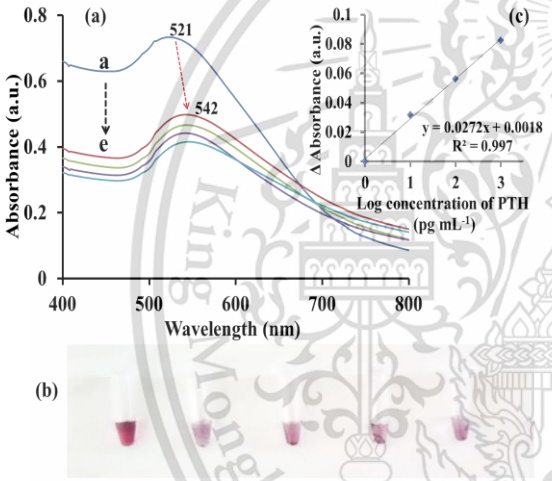

Figure 2. (a) surface plasmon peaks of AuNPs with different concentrations of PTH ((a) – (e) are the AuNPs in the presence of 0, 10, 100 and 1,000 pg mL^{-1}, respectively), (b) red wine to purple- colored solution of AuNPs and (c) linear calibration for PTH detection

3.3 Effect of pH of AuNPs on conjugation of antibody

pH of AuNPs were adjusted using 0.05 mM NaOH to the final pH of 5-9 before conjugated with antibody. Results are presented in Figure 3.

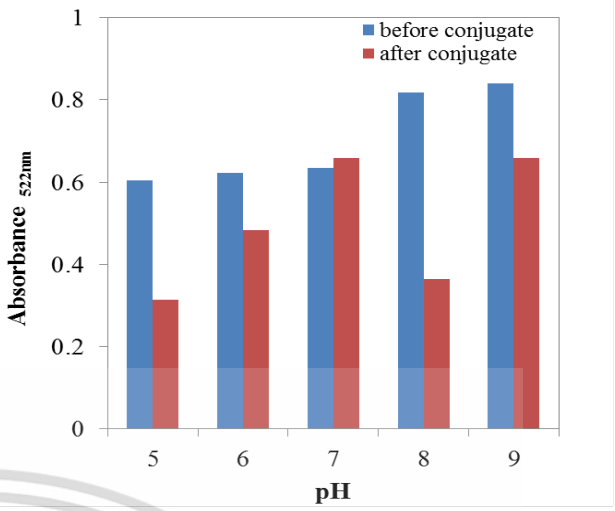

Figure 3. Absorbance of AuNPs at difference pH

Results in Figure 3 demonstrate that absorbance of the particles were deviated after conjugation for most of the studied pH values, excepting pH 7.0. This is due to inappropriate pH results in both self-aggregation of the AuNPs after conjugation and the denatured protein effect. Therefore, pH 7 was selected for further study.

3.4 Effect of reaction time.

Effect of reaction time was studied from 30 min to 2 hr. Poor linearity (r^2 = 0.554) at 30 min reaction time was observed. It is due to incomplete reaction. In contrast to 1 and 2 hr, they both provided good linearity (r^2 > 0.98) with no significant difference in sensitivity. It is because the reactions reached the equilibrium. Reaction time at 1 hr was therefore chosen.

3.5 Application to blood sample

The aggregation reaction of AuNPs was applied as detection principle of the method for colorimetric determination of PTH in blood samples. Rat blood samples were received from National Laboratory Animal Center, Thailand. They were centrifuged at 13,000 rpm for 40 min and filtered through a 0.22 µm Nylon membrane filter prior to analysis. Results as analytical recovery are summarized in Table 1.

Table 1. Analytical recovery of spiked blood samples

No.	Concentration of PTH (pg mL^{-1})			Recovery (%)
	Original	Added	Found	
1	16.6	53.7	77.6	113.6
2	288.4	89.1	389.0	112.9
3	33.88	1023.3	1122.0	106.3

Results in Table 1 reveal that the satisfied recovery was achieved. However, the relatively high recoveries are obtained for some samples. Prior pre-treatment of sample is required and is now under investigation.

4. Conclusion

A facile immunoassay for colorimetric detection of PTH was developed. The developed method provided a good linearity. The very low concentration of PTH (~ 10 pg mL^{-1}) were detectable. The method showed the potential for applying to determine the blood PTH. However, sample pretreatment prior to analysis is necessary.

Acknowledgements

Applied Analytical Chemistry Research Unit, Department of Chemistry, Faculty of Science, King Mongkut's Institute of Technology Ladkrabang is grateful acknowledged for equipments and financial support.

References

1. Çiğdem, S. S.; Münteha, N. S. K.; Mustafa, K. S. *Talanta*. **2015**, *144*, 210-218.
2. Benjamin, D. L. Department of Otolaryngology, University of Missouri-Columbia School of Medicine **2014**.
3. Ejigayehu, G. A.; Bart, L. C. *Front. Endocrinol.* **2017**, *7* (172*)*, 1-7.
4. Henry, G. B.; William, H. S.; Charles, Y. C. P. *Ann. Rev. Med.* **1977**, *28*, 111-117.
5. Edna, D. T. *Am. Fam. Physician*. **2004**, *69*, 333-339.
6. Marika, K.; Paul, C.; Richard, D. V.; Lily, L.; Zengji, L.; Xiaoyan, M.; Steven, F.; Christopher, M. R. *J. Chromatogr. B* **2004**, 810**,** 151–155.
7. Shaligram, S. R.; Alkesh, A.; Rustom, M.; Padmaja P. *J. Pharm. Analysis* **2012**, *2* (2), 136-142.
8. Erin, E. C.; Mary, E. L.; Jon, B.; Sally, H.; Cristina, L. Q.; Norman, S.; Kenneth, J. F.; Eileen, C.; Elizabeth, T. *J. Chromatogr. B* **2013**, 938, 96-104.
9. María, T. J.; Jose, M. B.; María, L. G.; Pau, M.; Antonio, A.; Manel, P. D.; Anna, L. *Am. J. Surg.* **2013**, *206,* 783-789.
10. Esther, P. G. S.; Jesús, M. F.; Aurora, G. R.; Bruno, M, T.; Fernando, M. P.; Carmen, M. C.; Virginia, M. A.; Susana, S. G. *Endocrinol Nutr*. **2014**, *61* (1), 3-8.
11. Valerie, C.; Noah, S.; Michael, P. H.; Martin, J. B.; Michae,l T. Elizabeth, M.; Xun, Z.; Richard, J. P. *Otolaryngol. Head Neck Surg*. **2008**, 138, 204-208.
12. Abhilash, M. *Int. J. Pharma Bio. Sci.* **2010**, *1*, 1-12.
13. Dittmer, W. U.; Kievit, P.; Prins, M. W. J.; Vissers, J. L. M.; Mersch, M. E. C.; Martens, M. F. W. C. *J. Immunol. Methods*. **2008**, *338*, 40-46.
14. Veronique, J.; Jeroen, H. N.; Jacco, P. H. F. V. S.; Mike, F. W. C. M.; Joost, L. M. V. *Langenbecks Arch Surg*. **2011**, *396*, 337-343.
15. Ralph, A. S.; Pilar, R. G.; Feng, Z.; Marco, Z.; Wolfgang, J. P. *Chem. Soc. Rev.* **2008**, *37*, 1896–1908.
16. Bing, Z.; Dianping, T.; Bingqian, L.; Yuling, C.; Huafeng, C.; Guonan, C. *Anal. Chim. Acta* **2012**, *711*, 17-23.
17. Afsaneh, S.; Mohamad, M.; Masoud, T. M.; Reza, A. *Anal. Biochem.* **2017**, *516*, 1-5.
18. Sánchez, M.; Aguilar, C.; Gómez, H. *Anal. Chim. Acta* **2009**, *636*, 58-62.
19. Ying, W.; Lifang, W.; Jianwei, Z.; Guangxi, W.; Wenbi, C.; Lin, C.; Xilin, Z. *PLOS ONE* **2014**, 9, 1-6.

PACCON 2019
Pure and Applied Chemistry International Conference
TOGETHER FOR THE BENEFIT OF MANKIND
February 7 - 8, 2019 | BITEC, Bangkok, Thailand

A paper-based analytical device for determination of iodate based on redox reaction of tri-iodide and gold nanoclusters

Aurachat Lert-itthiporn[1, 2]*, Natnicha Luekijna[1, 2], Thanyaphon Kamenmai[1, 2], Thichakorn Seenamngoen[1, 2], Pongpichet Srikritsadawong[1, 2] and Nathawut Choengchan[1, 2]

[1] *Flow Innovation-Research for Science and Technology Laboratories (FIRST Labs),*

[2]*Department of Chemistry and Applied Analytical Chemistry Research Unit, Faculty of Science, King Mongkut's Institute of Technology Ladkrabang, Bangkok, 10520, Thailand*

**E-mail: Aurachat.l@gmail.com)*

Abstract:

A method development for determination of iodate using a paper-based analytical device (PAD) is presented. Detection principle was based on the reaction of tri-iodide and gold nanoclusters (AuNCs). Gold nanocluters were synthesized by the reduction of Au (III) using bovine serum albumin in alkaline solution as a reducing agent. By exploiting microwave as a heating source for AuNCs synthesis, the process was completed within 10 min. The as-prepared AuNCs provided yellowish-brown color under the white light and they were changed to red emission under UV excitation. This red color of AuNCs was further altered to purple when tri-iodide was present. By means of this method, the hydrophobic barrier of circular shaped PAD (i.d. 20 mm) was fabricated by painting with a permanent pen. Aliquot of the nanocluster solution was dropped onto circular reaction reservoir. Later, small portions of the iodate, iodide and sulfuric acid were added and then waiting for 20 min. During this time, iodate was prior converted to tri-iodide which was further reacted with AuNCs. The image of the reaction reservoir was taken by a mobile phone under UV irradiation and intensity of color was evaluated by using Image J^{TM} software. The calibration graph was plotted between the intensity ratio of Red/Blue and the concentration, it was linear in the range of 0.01 to 1.00 mM IO_3^- ($R^2 > 0.99$). The developed method was successfully validated against the iodometric titration and the results were not significant difference from titration method.

1. Introduction

Iodine deficiency disorder (IDD) is an abnormal iodine concentration in human body which can cause some symptoms such as increasing in size of thyroid gland and cause preventable mental retardation in new-born babies and infants for pregnant woman. This situation still widely spread in some developing countries, including Thailand.[1] One campaign to prevent IDD is to add iodine as KIO_3 into table salt.[2] Thus, quantitative analysis of iodate content in salt is necessary. Iodometry[3] is used as a gold standard method for determination of iodate in salt. Various instrumental methods, such as, chromatography[4], electrochemistry[5,6] and spectrometry[7,8] have been also developed for accurate determination of iodate. However, these above mentioned methods still suffer from complicated analytical workflow which is not suitable for real routine uses. Some group then proposed the simple method using flow injection[9] for determination of iodate in table salts.[10, 11]

Nowadays, a paper-based analytical device (PAD) is widely used as a sensing platform in various analytical applications due to its simple fabrication, low-cost, portable and viable for test kit application. Nevertheless, there are still less publications concerning development of the PAD for quantitative analysis of iodate.[12,13]

In this work, we therefore aim to explore and to demonstrate use of the PAD for determination of iodate. The circular-shaped PAD was fabricated and the

hydrophobic barrier was patterned through painting with the indelible ink. We interested in applying gold nanoclusters (AuNCs) as the chemical sensor for the iodate detection as, recently, the fluorescence properties of the AuNCs receive extremely attention in sensing.[14-17] Detection principle is based on quenching of the AuNCs by tri-iodide ions which result in the color change from pink to purple. The developed device was applied to determine the iodate content in iodized-table salt samples.

2. Materials and Methods

2.1 Reagents and materials

All chemicals are analytical reagent grade and deionized-distilled water from Zeneer up 900 (Human corporation, USA) was used throughout. Bovine serum albumin (BSA) was obtained from Acros Organics, USA. Tetrachloroaurate trihydrate ($HAuCl_4 \cdot 3H_2O$) and potassium iodide were purchased from Sigma Aldrich, USA. Sodium hydroxide and di-sodium hydrogen phosphate were obtained from Carlo Erba, Spain. Potassium iodate and citric acid were bought from Ajax Finechem, Australia. Sulfuric acid was purchased from Fisher Chemical, UK.

2.2 Fabrication of the PAD

The PAD was made of a No. 2-filter paper (Advantec, Taiwan). The circular pattern of i.d. of 20 mm was fabricated by painting with indelible ink of a permanent pen (1225 Faber-Castel^{TM}). The fabricated PAD is shown in Figure 1.

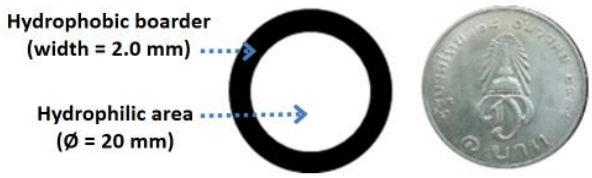

Figure 1. Dimension of the fabricated PAD for determination of iodate.

2.3 Synthesis of AuNCs

AuNCs were synthesized with some modification from Lei Y. *et al*.[18] At first, 2.0 mL of 10 mM $HAuCl_4$ was pipetted into a dark vial, followed by adding 2.0 mL of 50 mg mL^{-1} BSA and 0.2 mL of 1.0 M NaOH. The solution was heated at 100 watt for 9 min using a microwave oven (Samsung ME81 KS-1, Korea). The suspended AuNCs were kept in under 4 °C and were optical characterized by a 630-UV-visible spectrophotometer and a FP6300-spectrofluorometer (Jasco, USA).

2.4 Samples preparation

All sample solutions were prepared by weighing of approximate mass 10 g for exact amount of iodized-table salt, commercially available at local supermarket in Bangkok. The samples were dissolved and adjusted to 100.00 mL with water. This sample solution was analyzed directly without further sample pretreatment step.

2.5 Analytical procedure for determination of iodate in iodized-table salt

An aliquot of 60 µL of the AuNCs was dropped onto the PAD. Followed by transferring of 10 µL of standard (or sample) solution, 10 µL of 0.1 M KI. 1 min later, 10 µL of 1M H_2SO_4 was introduced and mixed for 1 min. Finally, 150 µL of 200 mM citric-phosphate buffer (pH 7.0) were added since it was found that at the greatest quenching was obtained at this pH due to neutral pH make it compatible with the nanocluster quenching.[19] The paper-based device was incubated in dark (20 min). Finally, the optical image of the device was captured by a smart mobile phone (Samsung Galaxy S5, Korea) under UV irradiation in a lighting control box (King lamp T5 SOAV-V5 UV Black Light 8 Watt, China) and was evaluated using Image J^{TM} software.

3. Results & Discussion

3.1 Optical characteristics of the as-prepared AuNCs

A conventional method for synthesis of the AuNCs requires continuously and vigorously stirring of the precursor on a hot plate for at least 12 h.[19] In this work, we therefore intend to shorten the synthesis time by using the microwave-assisted approach[18] as an alternative heating source to accelerate the reaction. We found that, under the optimal heating conditions, the process for synthesis of the AuNCs was completed within 10 min. The AuNCs solution provides yellowish-brown and emits red color under UV light as illustrated in the inset photo in Figure 2.

Optical properties of the AuNCs were characterized by spectrofluorometer. Result in Figure 2 reveals that the excitation and emission wavelengths are situated at 492 and 625 nm, respectively. This is also corresponded to literature[18].

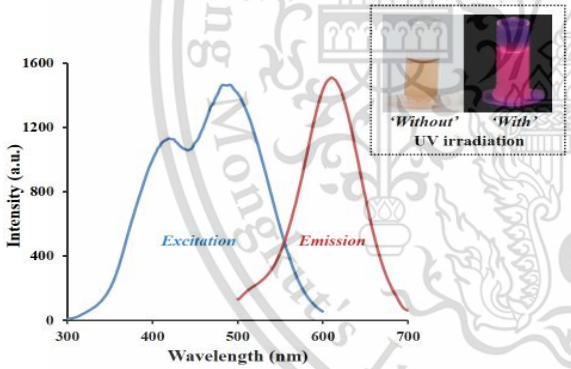

Figure 2. Excitation and emission spectra of the prepared AuNCs. Inset picture was *'without'* and *'with'* UV light irradiation.

3.2 Study on detection principle

Detection principle was studied using fluorometer. Mechanism of the detection reaction was proposed by Ruiping, L. *et al* .[20] Iodate is reduced to form iodine. In the presence of excessive amount of iodide, tri-iodide (I_3^-) is obtained. Au^0 is converted by I_3^- to become Au (I) and Au (III) species. This results in decreasing in the fluorescent intensity of the AuNCs[18] and color of the AuNCs solution obviously changes from pink to purple under UV light irradiation.

3.3 Effect of incubation time

Incubation time is defined as the interval time for mixing all reagents with standard iodate on the paper-based device. Incubation times were studied from 10 - 20 min. Sensitivity, which is slope of each linear calibration plot between the color intensity as red to blue ratio (R/B) and the iodate concentration (0.01 to 1.0 mM) is compared. Results in Figure 3 demonstrate that the sensitivity is dramatically increased when incubation time is prolonged to 20 min. This time is therefore selected as the highest sensitivity is achieved.

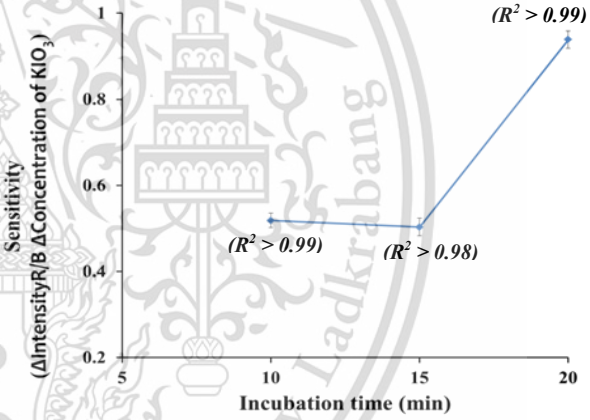

Figure 3. Effect of the incubation time on sensitivity for the iodate detection by the developed paper-based device.

3.4 Selectivity study

The investigated foreign ions are the anions which can be co-existed in salt sample. Effect of the foreign ion was studied by spiking either standard iodate or the other anion solutions (at equivalent concentration) onto the Au NCs-paper-based device. Optical image of each platform was captured. The color intensity was then evaluated and compared. Results are displayed in Figure 4.

The R/B intensity was significantly decreased in the presence of iodate ion. This implies that the AuNCs-paper-based device

is more selective to the iodate measurement than the other investigated foreign ions. As in this work, 10 % (w/v) of iodized-table salt was prepared, we therefore also examined the influence of 10 % (w/v) NaCl on the analysis of iodate. We found that the R/B intensity obtained by 10 % (w/v) NaCl (R/B = 1.48) was not significant difference from that of the control (R/B = 1.41). This implies that 10 % (w/v) NaCl is not interfered the iodate determination.

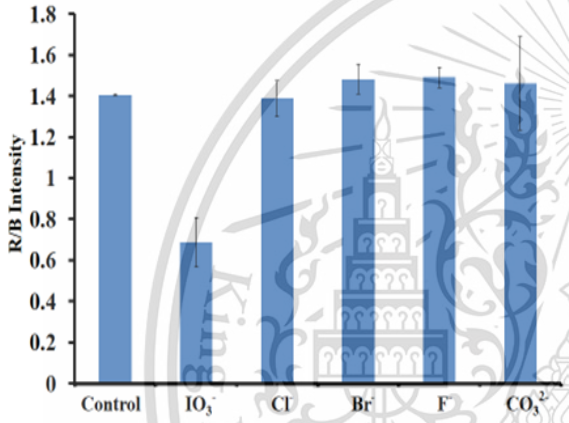

Figure 4. Comparison of the R/B intensities, derived from adding of either 0.5 mM iodate or 0.5 mM foreign ions onto the AuNCs-paper-based device.

3.5 Analytical performances

We have found that the color changes from pink to purple is obviously noticed by naked-eye under UV irradiation (Figure 5A). The correlation between the R/B intensity and the concentration of the standard iodate is also in good linearity up to 0.10 mM (Figure 5B). The developed method provides high precision with %RSD = 0.39 (n = 10 replicate detection of 0.5 mM iodate) and good analytical recoveries in the range of 96.7 – 102 %. Limit of detection was observed at 0.02 mM which is enough sensitive to apply the method to the commercially available iodized-table salt.

3.6 Application to iodized salt samples

The developed method was applied to determination of IO_3^- in iodized-table salt samples. The results were validated against the contents determined by iodometric titration method. Results are shown in Figure 6.

By mean of paired *t*-test[21], the results were not significant difference at 95 % confidence (t_{cal} = 1.57, t_{cri} = 3.18). This means that the developed method was successfully validated.

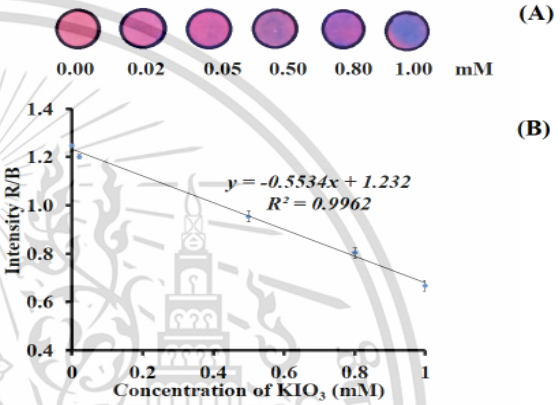

Figure 5. (A) The optical image (under UV irradiation) of the developed PAD and **(B)** its corresponded linear calibration plot between the R/B intensity and the standard KIO_3 concentration.

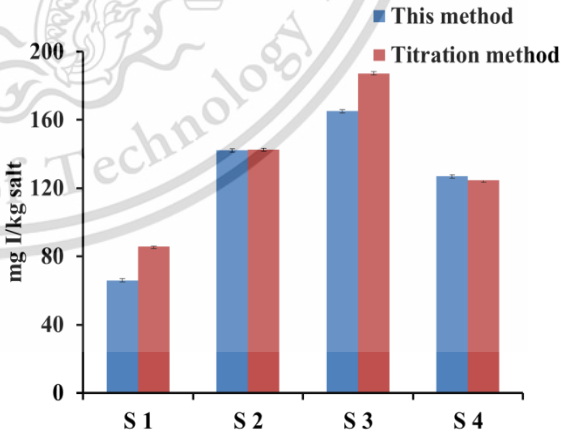

Figure 6. The iodate content (as mg I / kg salt, mean ± SD, n = 3)) in iodized-table salt samples obtained by the proposed method and the iodometric titration. Samples were analyzed as produced by manufacturers. Any further pretreatment is not essential.

4. Conclusion

A simple method for quantitative analysis of iodate based on using the PAD as the analytical platform and the redox reaction of tri-iodide and AuNCs as the detection principle was successfully developed. The method provided high precision and high accuracy. The method is also possible to be applied to the iodized-table salt for quality control of iodate content. However, long reaction time is still necessary. In the next study, the attempt to shorten the reaction time will be carried out.

Acknowledgements

Financial support from Faculty of Science, King Mongkut's Institute of Technology Ladkrabang (KMITL) is gratefully acknowledged. The author would also like to thank Department of Chemistry and Applied Analytical Chemistry Research Unit and FIRST lab@KMITL for some device and instrument.

References

1. Zihao, L.; Ruiyi, L.; Guofeng, X.; Tong, W.; Siyu L. *Biosens. Bioelectron*. **2017,** *96*, 44-48.
2. Venkatesh M. G. M.; John T. D. *International Council for Control of Iodine Deficiency Disorders*. **1995,** 19-25.
3. Assessment of iodine deficiency disorders and monitoring their elimination: A guide for programme managers, Third ed., *World Health Organization*. **2007**, 57-61.
4. Kumar, S.D.; Maiti, B.; Mathur, P. K. *Talanta*. **2001**, *53*, 701-705.
5. Abdollah, S.; Abdollah, N.; Mohammad, G. *Sens. Actuator B.* **2007**, *123*, 530-537.
6. Wang, H.; Cheng, N.; Yang, X.; Li, X.; Zhu, L. *Chem. Res. Chin. Univ.* **2013**, *29(1)*, 132-138.
7. Narayana, B.; Chand, P.; Tom, C.; Mendalin, M. *Bull. Chem. Soc. Ethiop.* **2006**, *20(1)*, 143-147.
8. Ai, H.; Zhi, L.; Biao, M.; Qing, Y.; Jie, L.; Xi, L. *Anal. Chim. Acta*. **2005**, *530*, 131-134.
9. Jaromír, R.; Elo, H. H. *Flow Injection Analysis Second Edition.* **1987.**
10. Choengchan, N.; Uraisin, K.; Choden, K.; Veerasai, W.; Grudpan, K.; Nacapricha, D. *Talanta.* **2002**, *58*, 1195-1201.
11. Choengchan, N.; Lukkanakul, K.; Ratanawimarnwong, N.; Waiyawat, W.; Wilairat, P.; Nacapricha, D. *Anal. Chim. Acta.* **2003**, *499*, 115-122.
12. Nicholas, M. M.; Emalee, N. K.; Marya, L. *Anal. Chem.* **2015**, *87*, 3764-3770.
13. Marina, O. G.; Anastasiya, A. B.; Margarita, S. K.; Vladimir, V. A.; Aleksei, A. F.; Alexey, V. G.; Stanislava, G. D. *Microchem. J.* **2019**, *145*, 729-736.
14. Yongming, G.; Zhuo, W.; Huawu, S.; Xingyu, J. *Analyst*. **2012**, *137*, 301-304.
15. Xianxiang W.; Peng, W.; Xiandeng, H.; Yi, L. *Analyst*. **2013**, *138*, 229-233.
16. Lihua, J.; Li, S.; Shaojun, G.; Youxing, F.; Dan, W.; Li, W.; Jianyuan, Y.; Shaojun, D. *Biosens. Bioelectron*. **2011**, *26*, 1965-1969.
17. Lianzhe, H.; Shuang, H.; Saima, P.; Yali, Y.; Ling, Z.; Guobao, X. *Biosens. Bioelectron*. **2012**, *32*, 297-299.
18. Lei, Y.; Yuqing, C.; Baozhan, Z.; Hongyan, Y.; Yong, G.; Dan, X.; Martin, M.F.C. *J. Mater. Chem*. **2012**, *22*, 1000-1005.
19. Ruiping, L.; Pingping, X.; Yifeng, T.; Jilin, Y. *Miocrochim. Acta*. **2016**, *183*, 497-502.
20. Ruiping, L.; Pingping, X.;Jun, F.; Junwei, D.;Yifeng, T.; Jilin, Y. *Anal. Chim. Acta*. **2014**, *827*, 80-85.
21. Irwin, M.; Marylees, M. *John E. Freund's Mathematical Statistics with Applications, 8th Edition.* **2014.**

Author Biography

Name	Miss Aurachat Lert-itthiporn
Date of Birth	22 July 1988
Address	156 Soi On-nut 50, Sukumvit 77 Road, Suanlaung District, Bangkok, 10250 Thailand
Education	(2009) Bachelor of Science in Industrial Chemistry - Analytical Instrumentation, GPA 2.84 King Mongkut's Institute of Technology Ladkrabang. (2013) Master of Science in Analytical Chemistry, GPA 3.50 King Mongkut's Institute of Technology Ladkrabang.

International Publications

1. **A. Lert-itthiporn**, S. Phunpruch, M. Prommajun, P. Srikritsadawong and N. Choengchan. *Preparation of gold nanoparticles-bacterial vellulose nanopaper and its application as 2D-microcuvette for spectrophotometric determination of hydrogen peroxide,* Chiang Mai Journal of Science, In Press.

Conference Proceedings

1. **A. Lert-itthiporn**, T. Vatanavicharn and N. Choengchan. *Facile immunaoassay for colorimetric determination of parathyroid hormone based on aggregation of gold nanoparticles*, Proceedings of Pure and Applied Chemistry International Conference, pp. 74-77, 2018.
2. **A. Lert-itthiporn**, N, Luekijna, T. Kamenmai, T. Seenamngoen, P. Srikritsadawong and N. Choengchan. *A paper-based analytical device for determination of iodate based on redox reaction of tri-iodide and gold nanoclusters,* Proceedings of Pure and Applied Chemistry International Conference, pp. 51-55, 2019.

3. P. Srikritsadawong, M. Prommajun, **A. Lert-itthiporn**, S.Phunpruch and N. Choengchan. *Synthesis of gold nanoparticles-embedded bacterial cellulose nanopaper for colorimetric detection of hydrogen peroxide.* Proceedings of Pure and Applied Chemistry International Conference, pp. 102-107, 2020.